

AFOSR-TR- 81 -0588

LEVEL

(B)

FLUID, THERMAL AND AEROSPACE SCIENCES

AD A102072

Approved for public release;
distribution unlimited.

DTIC
ELECTED
S JUL 28 1981 D

412458

DEPARTMENT OF MECHANICAL AND AEROSPACE ENGINEERING
CASE INSTITUTE OF TECHNOLOGY

CASE WESTERN RESERVE UNIVERSITY

UNIVERSITY CIRCLE • CLEVELAND, OHIO 44106

8 1 7 24 051

Approved for public release;
distribution unlimited.

FILE COPY

FTAS/TR-81-155

13

Accession For		
NTIS GRA&I	<input checked="" type="checkbox"/>	
DTIC TAB	<input type="checkbox"/>	
Unannounced	<input type="checkbox"/>	
Justification		
By		
Distribution/		
Availability Codes		
Avail and/or		
Dist : Special		
A		

PRELIMINARY EXPERIMENTAL STUDY OF DISTURBANCES IN A
LAMINAR BOUNDARY-LAYER DUE TO
DISTRIBUTED SURFACE ROUGHNESS

by

Leon Leventhal and Eli Reshotko

Department of Mechanical and Aerospace Engineering
CASE WESTERN RESERVE UNIVERSITY

May 1981

STIC
S
JUL 23 1981

Approved for public release; distribution unlimited

D

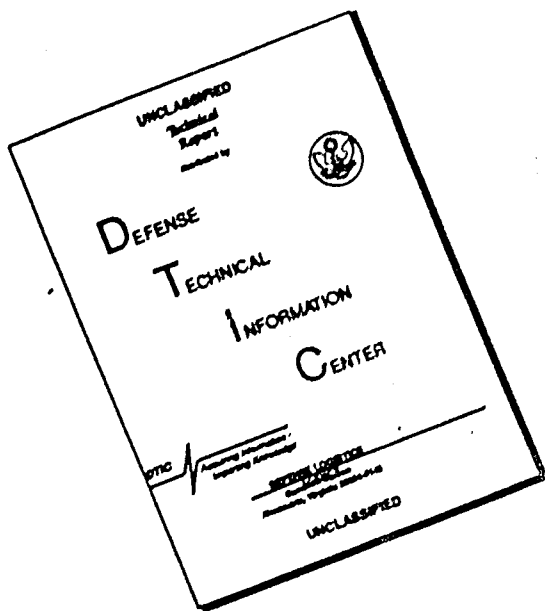
EL

Qualified requestors may obtain additional copies from the Defense Technical Information Service.

Conditions of Reproduction

Reproduction, translation, publication, use and disposal in whole or in part by or for the United States Government is permitted.

DISCLAIMER NOTICE



**THIS DOCUMENT IS BEST
QUALITY AVAILABLE. THE COPY
FURNISHED TO DTIC CONTAINED
A SIGNIFICANT NUMBER OF
PAGES WHICH DO NOT
REPRODUCE LEGIBLY.**

UNCLASSIFIED

SECURITY CLASSIFICATION OF THIS PAGE (When Data Entered)

REPORT DOCUMENTATION PAGE			READ INSTRUCTIONS BEFORE COMPLETING FORM	
1. REPORT NUMBER AFOSR-TR-81-0588	2. GOVT ACCESSION NO. AD-A202 072	3. RECIPIENT'S CATALOG NUMBER		
4. TITLE (and Subtitle) PRELIMINARY EXPERIMENTAL STUDY OF DISTURBANCES IN A LAMINAR BOUNDARY-LAYER DUE TO DISTRIBUTED SURFACE ROUGHNESS			5. TYPE OF REPORT & PERIOD COVERED Final	
7. AUTHOR(S) LEON LEVENTHAL ELI RÉSHOTKO			6. PERFORMING ORG. REPORT NUMBER AFOSR-78-3562	
9. PERFORMING ORGANIZATION NAME AND ADDRESS CASE WESTERN RESERVE UNIVERSITY DEPARTMENT OF MECHANICAL & AEROSPACE ENGINEERING CLEVELAND, OH 44106			10. PROGRAM ELEMENT, PROJECT, TASK AREA & WORK UNIT NUMBERS 2307/A2 61102F	
11. CONTROLLING OFFICE NAME AND ADDRESS AIR FORCE OFFICE OF SCIENTIFIC RESEARCH/NA BOLLING AFB, DC 20332			12. REPORT DATE May 1981	
14. MONITORING AGENCY NAME & ADDRESS (if different from Controlling Office) 9 Final rept.			13. NUMBER OF PAGES 101	
16. DISTRIBUTION STATEMENT (of this Report) Approved for public release; distribution unlimited.			15. SECURITY CLASS. (of this report) UNCLASSIFIED	
17. DISTRIBUTION STATEMENT (of the abstract entered in Block 2a, if different from Report)				
18. SUPPLEMENTARY NOTES Key words (Check one or more boxes that apply to this report) BOUNDARY-LAYER TRANSITION BOUNDARY-LAYER ROUGHNESS				
19. ADDITIONAL COMMENTS (If necessary, indicate by block number) Mean flow and disturbance measurements have been made on a flat plate model, one meter long in the CWRU low speed wind tunnel using hot-wire anemometry. Tests were conducted on a smooth plate and with two different grades of sandpaper covering; first with a sandpaper covering giving Re_k values centered around 10 and then with a coarser sandpaper having Re_k values of about 150. The mean flow measurements indicated Blasius profiles for the smooth plate and with the finer roughness. With the coarser roughness, the profile was best approximated by a Blasius profile at the early stations but then progressed				

UNCLASSIFIED

SECURITY CLASSIFICATION OF THIS PAGE(When Data Entered)

toward a turbulent profile. The finer surface roughness ($Re_k \approx 10$) had only a very slight effect on the u'^{rms} distributions relative to those for a smooth plate. This showed up primarily through examination of the distribution of local turbulence intensity, u'^{rms}/\bar{u} , which proved to be a much more sensitive indicator than dimensionless turbulent energy, $u'^2/rms^2/U_e^2$. For the coarser roughness ($Re_k \approx 150$), local u'^{rms} intensities in the boundary layer of the order of 5% were observed before the mean profile departed from a Blasius shape. The progression toward turbulent mean velocity profiles was accompanied by large increases in turbulent intensities over the whole boundary layer but especially near the wall. A study of disturbance spectra for this case shows largest amplitudes and amplifications at frequencies well below the Blasius neutral curve. The maximum amplification rates are about three times those for Tollmien-Schlichting instability over a smooth plate. Transition occurs at $Re_X \approx 350,000$ which is much below that for a smooth plate.

UNCLASSIFIED

SECURITY CLASSIFICATION OF THIS PAGE(When Data Entered)

ABSTRACT

Mean flow and disturbance measurements have been made on a flat plate model, one meter long in the CWRU low speed wind tunnel using hot-wire anemometry. Tests were conducted on a smooth plate and with two different grades of sandpaper covering; first with a sandpaper covering giving Re_k values centered around 10 and then with a coarser sandpaper having Re_k values of about 150.

The mean flow measurements indicated Blasius profiles for the smooth plate and with the finer roughness. With the coarser roughness, the profile was best approximated by a Blasius profile at the early stations but then progressed toward a turbulent profile.

The finer surface roughness ($Re_k \approx 10$) had only a very slight effect on the u'_{rms} distributions relative to those for a smooth plate. This showed up primarily through examination of the distribution of local turbulence intensity, u'_{rms}/\bar{u} , which proved to be a much more sensitive indicator than dimensionless turbulent energy, u'^2_{rms}/\bar{u}^2 . For the coarser roughness ($Re_k \approx 150$), local u'_{rms} intensities in the boundary layer of the order of 5% were observed before the mean profile departed from a Blasius shape. The progression toward turbulent mean velocity profiles was accompanied by large increases in turbulent intensities over the whole boundary layer but especially near the wall. A study of disturbance spectra for this

case shows largest amplitudes and amplifications at frequencies well below the Blasius neutral curve. The maximum amplification rates are about three times those for Tollmien-Schlichting instability over a smooth plate. Transition occurs at $Re_x \approx 350,000$ which is much below that for a smooth surface.

ACKNOWLEDGEMENTS

The authors wish to thank Dr. Yasuhiro Kamotani for his very important help with the hot-wire instrumentation. Special thanks are also due to Mr. Mike Marhefka for his help concerning equipment design and maintenance, and to Mrs. Helena Mencl for typing this report.

This work was supported by the U.S. Air Force Office of Scientific Research.

TABLE OF CONTENTS

	Page
ABSTRACT	ii
ACKNOWLEDGEMENTS	iv
TABLE OF CONTENTS	v
LIST OF FIGURES	vii
CHAPTER I - INTRODUCTION	1
CHAPTER II - TEST FACILITIES	6
2.1 Low Speed Wind Tunnel	6
2.1.1 Physical Description	6
2.1.2 Calibration	6
2.2 Flat Plate Model	6
2.2.1 The Plate	6
2.2.2 The Mounting	7
2.2.3 Roughness	8
2.3 Measuring Equipment	9
2.3.1 Pitot-Static Tube	9
2.3.2 Hot Wire	10
2.3.3 Traverse Mechanism	13
2.3.4 Spectrum Analyzer	14
CHAPTER III - EXPERIMENTAL PROCEDURE	15
3.1 Calibration	15
3.2 Smooth Plate	15
3.2.1 Adjustment of Zero Pressure Gradient	15
3.2.2 Measurement of Mean and Fluctuating Information	17
3.3. Rough Plate	18

	Page
3.3.1 Additional Adjustments	18
3.3.2 Measurements Taken with Each of the Two Sandpapers	19
CHAPTER IV - RESULTS AND DISCUSSION	21
4.1 Smooth Plate	21
4.2 Distributed Roughness of Re_k ($X = 30$ cm) = 10.6	22
4.3 Distributed Roughness of Re_k ($X = 30$ cm) = 155	24
4.3.1 Mean and Fluctuation Measurements	24
4.3.2 The Spectrum	29
4.3.3 Filtering	31
4.4 Leading Edge of the Distributed Roughness	32
CHAPTER V - SUMMARY AND CONCLUSIONS	34
REFERENCES	36
FIGURES	38

AIR FORCE OFFICE OF SCIENTIFIC RESEARCH (AFSC)
 NOTICE OF TRANSMITTAL TO DDC
 This technical report has been reviewed and is
 approved for public release IAW AFR 190-12 (7b).
 vi Distribution is unlimited.
 A. D. BLOM
 Technical Information Officer

LIST OF FIGURES

Figure		Page
1	Schematic diagram of effect of distributed roughness on transition on a flat plate	38
2	The mean velocity distortion due to 2-D roughness element	38
3	View of wind tunnel looking upstream toward entrance	39
4	Side view of test section with plate installed	39
5	Turbulence intensity profile in Z direction $X = 49.25"$, $Y = 17.5"$, $U_e = 6 \text{ m/sec.}$	40
6	Turbulence intensity profile in Y direction $X = 49.25"$, $Z = -14.0"$, $U_e = 6 \text{ m/sec.}$	41
7	Turbulence intensity profile in X-direction $Z = -14.0"$, $Y = 17.5"$, $U_e = 6 \text{ m/sec.}$	42
8	The front view of the model	43
9	General view of the model with sandpaper	44
10	Hot-wire probe and pitot tube over smooth plate	44
11	Plate vibrations at $U_e = 6 \text{ m/sec.}$	45
12	The Prandtl type pitot-static tube, Sensor United model PAC-12 KL	46
13	Hot-wire probe and pitot tube above a rough surface	46
14	Flow regimes about unheated circular cylinders of high length-to-diameter ratio versus Reynolds number	47
15	The hot-wire anemometer (Shapiro & Edwards, model 50), and Meriam manometer	48

Figure		Page
16	A close up of the hot-wire probe during the etching process	48
17	The hot-wire probe in the process of the hot-wire etching	49
18	The top view of the test section with the traversing mechanism	49
19	Hot-wire calibration curve	50
20	Pressure coefficient for the plate at 0° angle of attack	51
21	Mean velocity profiles for the plate at 0° of attack	52
22	Pressure coefficient for the plate tilted at 1° angle of attack	53
23	Mean velocity profiles for the plate tilted at 1° angle of attack	54
24a	Mean velocity profile for a smooth plate, $X = 30 \text{ cm}$	55
24b	Mean velocity profile for a smooth plate, $X = 40 \text{ cm}$	56
24c	Mean velocity profile for a smooth plate, $X = 50 \text{ cm}$	57
24d	Mean velocity profile for a smooth plate $X = 60 \text{ cm}$	58
25a	Energy profiles for a smooth plate, $U_e = 6.1 \text{ m/sec.}$	59
25b	Energy profiles for a smooth plate, $U_e = 6.1 \text{ m/sec.}$	60
26	Local intensity profiles along a smooth plate, $U_e = 6.1 \text{ m/sec.}$	61
27a	Mean velocity profile for a rough plate, $Re_k (X = 30 \text{ cm}) = 10.6; X = 30 \text{ cm}$	62

Figure		Page
27b	Mean velocity profile for a rough plate $Re_k (X = 30 \text{ cm}) = 10.6; X = 40 \text{ cm}$	63
27c	Mean velocity profile for a rough plate, $Re_k (X = 30 \text{ cm}) = 10.6; X = 50 \text{ cm}$	64
27d	Mean velocity profile for a rough plate, $Re_k (X = 30 \text{ cm}) = 10.6; X = 60 \text{ cm}$	65
28a	Energy profiles for a rough plate, $Re_k (X = 30 \text{ cm}) = 10.6; U_e = 5.9 \text{ m/sec.}$	66
28b	Energy profiles for a rough plate, $Re_k (X = 30 \text{ cm}) = 10.6; U_e = 5.9 \text{ m/sec.}$	67
29	Local turbulence intensity profile along a rough plate, $Re_k (X = 30 \text{ cm}) = 10.6; U_e = 5.9 \text{ cm/sec.}$	68
30a	Mean velocity profile for a rough plate, $Re_k (X = 30 \text{ cm}) \approx 155; X = 30 \text{ cm}$	69
30b	Mean velocity profile for a rough plate, $Re_k (X = 30 \text{ cm}) \approx 155; X = 40 \text{ cm}$	70
30c	Mean velocity profile for a rough plate, $Re_k (X = 30 \text{ cm}) \approx 155; X = 50 \text{ cm}$	71
30d	Mean velocity profile for a rough plate, $Re_k (X = 30 \text{ cm}) \approx 155; X = 60 \text{ cm}$	72
31a	Test I - Energy profiles for a rough plate $Re_k (X = 30 \text{ cm}) \approx 155$	73
31b	Test II - Energy profiles for a rough plate, $Re_k (X = 30 \text{ cm}) \approx 155$	74
32a	Test I - Local turbulence intensity profiles for a rough plate, $Re_k (X = 30 \text{ cm}) = 155$	75
32b	Test II - Turbulence intensity profiles for a rough plate, $Re_k (X = 30 \text{ cm}) = 155$	76
33	Test II - Local turbulence intensity due to roughness only, $Re_k (X = 30 \text{ cm}) = 155$	77

Figure	Page
34 $(u'_{rms})_{max}/U_e$ and $(u'_{rms}/\bar{u})_{max}$ versus Re_X for Test I and II, Re_k ($X = 30$ cm) = 155	78
35 Spectrum at $X = 20$ cm, $Y = 1.0$ mm, Re_k ($X = 30$ cm) = 155	79
36 Spectrum at $X = 30$ cm, $Y = 1.5$ mm, Re_k ($X = 30$ cm) = 155	79
37 Spectrum at $X = 40$ cm, $Y = 1.7$ mm, Re_k ($X = 30$ cm) = 155	80
38 Spectrum at $X = 50$ cm, $Y = 1.75$ mm, Re_k ($X = 30$ cm) = 155	81
39 Spectrum at $X = 60$ cm, $Y = 1.25$ mm, Re_k ($X = 30$ cm) = 155	81
40 Amplitudes of disturbances with frequencies from 4.3 Hz to 17.2 Hz versus X . Re_k ($X = 30$ cm) = 155	82
41 Amplification rates versus X , for disturbances with frequencies from 4.3 Hz to 17.2 Hz; Re_k ($X = 30$ cm) = 155	83
42 Amplification rate versus frequency for a con- stant Re_{δ^*} in the 4.3 Hz to 17.2 Hz band; Re_k ($X = 30$ cm) = 155	84
43 The highest amplification rate versus X . Re_k ($X = 30$ cm) = 155	85
44 Amplification rate versus frequency for $Re_{\delta^*} = 764$, $X = 50$ cm, Re_k ($X = 30$ cm) = 155	86
45 Neutral stability results	87
46 Energy content for three frequency bands at the location of the maximum total energy, Re_k ($X = 30$ cm) = 155	88

CHAPTER I

INTRODUCTION

On a smooth surface, transition of the boundary layer presumably occurs as the result of the amplification of the disturbances initially present in the flow. In this model of the transition process, the disturbances amplified are those whose frequencies lie within the neutral curve for Tollmien-Schlichting waves and are dependent on the Reynolds number of the boundary layer. If transition on a smooth plate occurs at distance X_{t_0} downstream of the leading edge (with corresponding Reynolds number, $Re_{t_0} = UX_{t_0}/v$), then for roughness, transition occurs at some location X_t less than X_{t_0} , corresponding to a transition Reynolds number, $Re_t = UX_t/v$, which is smaller than Re_{t_0} (Fig. 1). Roughness enhances friction and drag, and also increases the momentum thickness of the boundary layer. A minimum critical roughness is sometimes defined as one for which Re_t is approximately 0.95 Re_{t_0} [1].

The treatment of roughness is divided into consideration of single roughness elements, both two-dimensional and three-dimensional, and of distributed roughness which is considered to be a collection of three-dimensional protuberances with statistical distribution of height, k , and distributed over the plane of the surface.

There are many experimental results for single roughness elements and there is even a basic understanding of the destabilizing

mechanism. On the other hand, much less has been determined about distributed roughness and there is no understanding of its destabilizing mechanism.

For single two-dimensional roughness elements, Dryden [1] presents a curve of Re_t/Re_{t_0} vs. $\frac{k}{\delta^*}$ as the best correlation of the body of data to that time. Smith and Clutter [2] argue that this is too simplistic a description since there are also effects of the shape of the element and the length of laminar flow ahead of the element. They argue that a more fundamental parameter for effects in the vicinity of a roughness element is $Re_k = \frac{u_k k}{v}$. They found that for a given shape of roughness, $Re_{k,critical}$ was found to be relatively constant and independent of roughness height and location, pressure distribution and free-stream turbulence level. There was, however, a major effect of roughness shape.

A most convincing argument on the mechanism by which a two-dimensional roughness element destabilizes a laminar boundary layer is by Klebanoff and Tidstrom [3]. They show, based on their experiments, that the basic mechanism by which a roughness element induces earlier transition is through the destabilizing influence of the wake-like recovery zone of the element (Fig. 2). Disturbances in the boundary layer are greatly amplified in the recovery zone. The growth rates are many times those of the unaffected Blasius layer. The fact that the local profiles in the recovery zone depend primarily on the nature of the roughness element establishes Re_k as the primary parameter of the phenomenon, and the dependence on the pro-

perties of the parent flow is very weak.

For three-dimensional roughness elements, the critical values of Re_k are higher than for two-dimensional roughness but the destabilizing mechanism may be similar in that disturbances can be greatly amplified by the wake-like unstable profiles downstream of the elements.

In view of the results for single roughness elements and the known sensitivity of boundary layer stability to small profile changes, the analytic investigations to date of distributed roughness are all based on the premise that distortion of the mean flow by the roughness enhances instability and leads to earlier transition.

Singh and Lumley [4] made calculations to find the roughness induced mean velocity profile which they expressed in terms of the spectral density of the roughness and an influence function. The resulting profile had an inflection point deep in the inner viscous region and in their opinion does not contribute to instability. Outside the wall region, the profile they obtained is more stable since the curvature in the vicinity of the critical layer has been increased. Since experimentally, roughness leads to earlier transition, Singh and Lumley argue that even if the profile is more stable, the roughness also introduces disturbances with energy at wavenumbers to which the profile is unstable.

Lessen and Gangwani [5] model the problem by introducing a wavy wall to represent one component of the roughness spectrum. The equation for this roughness induced disturbance is the Orr-Sommerfeld

equation with phase velocity equal to zero, but with a non-homogeneous boundary condition at $y = 0$. They retained the Reynolds stress term in their mean flow equation and so calculated the distorted mean flow. Once this distorted profile was found, the stability of this new profile was examined and its critical Reynolds number calculated. The new profile displayed a point of inflection near the wall. The new profile was found to be slightly less stable than the original Blasius profile. The minimum critical Reynolds number is reduced by about 5% in the example presented by Lessen and Gangwani. This amount of change is probably not very significant experimentally.

Merkle, Tzou and Kubota [6] assumed that roughness enhances momentum and heat transfer near the surface and modeled this using a turbulent eddy viscosity in the vicinity of the roughness, in a region they called the roughness sublayer. They concluded that the roughness sublayer alters the mean velocity and temperature profiles within the laminar portion of the boundary layer. They obtained an increase in shape factor primarily through increase in displacement thickness. Stability calculations for this distorted mean profile indicated reduced stability. An attempt by the authors to validate their results by comparison with Achenbach's experimental results for a circular cylinder [7] resulted only in qualitative agreement.

Experimentally, there is as yet no demonstration that for distributed roughness, a profile change is responsible for enhanced instability. The present work intends giving a definitive experi-

mental look at this question. Accordingly, the mean velocity profiles, disturbance energy distributions and their spectral development are studied in order to help understand the mechanism by which distributed roughness influences transition. The investigation is conducted on a flat plate model with two roughness sizes in addition to the reference case of a smooth surface.

CHAPTER II

TEST FACILITIES

2.1 Low Speed Wind Tunnel

2.1.1 Physical Description

The low speed tunnel is of the open circuit type, with a contraction ratio of 10.4:1 (Fig. 3). There are two screens ahead of the contraction, each with an openness of 65%. The tunnel is operated by a 53 HP DC axial fan. The test section is 7.5' long and its cross-section is 28" x 28" (Fig. 4). Except for the bottom wall, the rest of the test section walls are made of transparent plastic (plexiglas).

2.1.2 Calibration

The inside of the tunnel was cleaned and sealed to achieve as low a free-stream turbulence as possible. At the plate location, values of free-stream turbulence intensity below 0.03% at a test speed of 6 m/sec were obtained as shown in Figs. 5 to 7. The hot-wire readings are affected by the velocity components which are perpendicular to the wire; thus the measured turbulence intensity is:

$$T.I. = \sqrt{\frac{(u')^2}{\bar{u}}} \quad (2.1)$$

2.2 Flat Plate Model

2.2.1 The Plate

The model is a flat smooth plate, 41.5" long, 25" wide and 3/8" thick (Figs. 8-10). The leading edge has a 1/32" radius fol-

lowed by a smooth taper which blends into the flat plate surface 1.2" behind the leading edge. It is the same leading edge contour used by Strazisar et al. [8, 9] in their experimental study of the stability of heated laminar boundary layers in water. The surface of the plate was polished to a mirror finish using aluminum polish compound Met-All. No. 1187.

2.2.2 The Mounting

The plate is supported by two swept front supports which are at a 70° angle to the plate, and two rear supports perpendicular to the plate. The front supports have a symmetric airfoil cross-section with 2 3/4" chord, 3/4" thickness and the cross-section center at the plate junction is 16.5 cm downstream from the leading edge so as to prevent separation from the supports and generally minimize creation of additional disturbances in the tunnel. The rear supports are 3/4" diameter cylinders. Their center is 80 cm downstream of the leading edge. They are not as important as the front supports because their location is behind the test region.

The choice of plate location was based on the wind tunnel calibration results. Since the longitudinal variation of free-stream turbulence intensity is constant, the leading edge of the plate was located near the door of the test section for convenience in making it easier to clean the plate surface. It was positioned at a 17.5" height above the floor and symmetrically in the horizontal plane.

The natural vibrations of the plate on its supports were measured at a tunnel speed of 6 m/sec. Fig. 11 shows that the highest

amplitude appears near the leading edge and is 0.04 mm and occurs at a frequency of 8 Hz which is below the theoretical critical frequency band for Tollmien-Schlichting waves. Its magnitude is much below the roughness heights tested. The amplitudes at the middle and end of the plate are about half those near the leading edge. A flap at a 5° angle into the test-stream at the end of the plate was used to stabilize the stagnation point near the leading edge, in order to prevent leading edge separation.

2.2.3 Roughness

Two sizes of sandpaper made by the Norton Company were used. They were applied to the plate by using RTV adhesive. The finer sandpaper (80 grit) has a specified nominal average grain size of 266 microns (0.0105 inch). Thus Re_k at $X = 30$ cm at $U_e = 6$ m/sec is 10.6. A filler was applied starting 1 cm upstream of the leading edge of the sandpaper and blending smoothly into the sandpaper leading edge.

The coarser sandpaper (24 grit) had a nominal average grain size of 1035 microns (0.0408 inch) so that Re_k at $X = 30$ cm and $U_e = 6$ m/sec is 155. In this case, the filler began 1 inch ahead of the leading edge of the sandpaper. Because of the different thicknesses of the two sandpapers, the ramp angle of the filler was approximately the same in both cases.

Both sandpapers covered the whole plate surface downstream of their leading edges. For the small roughness, Re_k was calculated using the formula:

$$Re_k = \frac{u_k \cdot k}{v} \approx 0.332 \left(\frac{U_e}{v} \right)^{3/2} k^2 X_k^{-1/2} \quad (2.2)$$

based on the fact that for small heights above the plate

$\frac{du}{dy} = 0.332 U_e \left(\frac{X_k}{U_e} \right)^{-1/2}$ just as at the surface [1]. Re_k could also be obtained by calculating the η corresponding to k , $\eta = k \sqrt{\frac{U_e}{X_v}}$, and then the velocity u_k could be taken from the Blasius curve. This method was applied for the coarser sandpaper where the grains are not small.

2.3 Measuring Equipment

2.3.1 Pitot-Static Tube

The pitot-static tube used was of the Prandtl type made by Sensor United, model PAC-12KL (Fig. 12). It is inserted from the top of the test section 30 cm downstream from the leading edge and displaced laterally from the hot-wire probe by 5 cm to minimize any interference effect. It is insensitive to yaw or pitch angles up to 30° and its quoted error is less than 2%. It has 1/8" outside diameter and is positioned 5 cm above the plate. Thus, the distance from the surface is more than 12 boundary layer thicknesses. Since the probe is also more than 10 probe diameters above the plate, the effect of the plate on the readings is negligible.

The Reynolds Number based on the impact hole diameter (0.5 mm) for 6 m/sec speed is approximately 100. In such a case when it is larger than 30, viscous effects in the internal flow can be neglected. The viscous effects in the external flow are also negligible

when the Reynolds number based on the probe radius is larger than 100, which is the case here.

For T.I. around 0.03% and dynamic pressures of about 0.1 in. H_2O , the fluctuation velocity component dynamic pressure, $\frac{1}{2}\rho(u')^2$ corresponds approximately to 9×10^{-9} in. H_2O . This is negligible relative to 0.1 in. H_2O . Thus, the pitot tube reading is insensitive to small turbulence.

The time constant for the pitot probe is approximately five seconds.

The probe is connected to a Meriam manometer which is able to measure 0.001 in. H_2O (Fig. 15).

2.3.2 Hot Wire

The shape of the hot-wire probe was designed appropriately for boundary layer measurements (Fig. 13). It consists of 1/4" stainless steel tubing in which electrical wires run through, that are connected to the copper prongs. The prongs are insulated one from the other by 5 minute epoxy. The tips of the prongs are connected by Wollaston wire (90% platinum, 10% rhodium) 8 mm long.

The length of the control portion which is the sensor varies depending on the etching procedure during its preparation and is approximately 0.8 mm long. Beneath the joining of the prongs there is a protruding support made of 5 minute epoxy. From cathetometer measurements supported by mean velocity profile results, the wire is 0.2 mm above the support bottom.

The principle of the hot-wire and the factors affecting its operation are described briefly as follows:

The wire is heated by a constant current. It is cooled by the flow causing the temperature to drop and, consequently, the electric resistance to diminish. It is cooled primarily by forced convection and heat conduction. Total amount of heat transferred depends on:

- 1) The flow velocity
- 2) The difference in temperature between the wire and the fluid
- 3) The physical properties of the fluid
- 4) The dimensions and physical properties of the wire

The last three are known and thus the flow velocity can be measured.

The hot-wire anemometer is still a prime instrument for turbulence measurements. Its principal advantage is the separation of the mean velocity from the fluctuating components and the ability to measure them separately at the same time. The other main advantage is in its being thin. The Reynolds number based on wire diameter is 1.54 for a speed of 6 m/sec. This is below 3, which is the limit for smooth flow around the wire without separation even with heating, because Reynolds number decreases with temperature [10] (Fig. 14). The thermal inertia of the thin wire is very small and thus the response for frequencies of interest in this experiment (up to 5 KHz) is practically instantaneous. It catches less dirt than a thick sensor and altogether it is sufficiently strong and rigid to sustain vibrations and stresses caused by turbulence. The measured velocity is in good agreement with the flow velocity as measured using the

pitot-static tube for turbulence intensity smaller than 10%.

The joining of the prongs is 32,000 wire diameters behind the wire and thus there is no real influence of the prongs on the flow around the sensor portion of the wire.

There are two problems with the hot wire. The first is drifting and the second is contamination. Both can be treated properly as will be explained in the next chapter. More about hot wires can be found in ref. [11].

The hot-wire anemometer set is a Shapiro and Edwards model 50 (Fig. 15). It includes an amplifier, a resistance bridge, a potentiometer, a mean square output meter and a square wave generator. The potentiometer allows measurement of wire currents up to 10^{-5} amp. and so enables accurate velocity measurements. A compensation circuit is available but is needed only for frequencies above 5KHz and was not utilized in this experiment.

The preparation of the hot-wire sensor is as follows: First, the wire is soldered to the prongs and then the probe is attached to a positioner. The wire is brought into contact with a small drop of 70% concentrated nitric acid (Figs. 16-17). An electrolyzing current is supplied by a 1 1/2 volt Eveready battery for about one minute. The length of the uncovered (etched) center portion of the wire is a function of the drop size, and is of the order of 0.8 mm. This portion which is the sensor has a diameter of 0.00015 in. The wire is then checked using a microscope which magnifies 60 times. It is important to have a straight and clean wire.

The soldering of the wire to the prongs with a soft solder had to be done quickly in order not to create excessive heat in the wire and thus avoid any elongation. If overheated, the uncovered portion of the wire could not sustain as much stress as the rest of the wire, and at the end of the etching process would become deformed.

The other factor which affects wire shape is the surface tension of the drop. To avoid any adverse effect, the wire has to be taken out of the drop very carefully.

2.3.3 Traverse Mechanism

The traverse mechanism (Fig. 18) was designed to give accurate vertical readings of the probe position. It has a metric Mitutoyo micrometer which can be moved longitudinally with the help of a motor. There is an error of ± 0.2 mm in longitudinal positioning. The micrometer enables vertical precision to ± 0.01 mm and so this is the accuracy of the hot-wire probe position because it is attached to the micrometer. The height can be read on the micrometer scale and readjusted to zero each time the hot wire is brought to the plate surface. The precision of lateral positioning is not as important as the vertical one and there is an estimated error in lateral position of at most 0.5 mm.

The traverse mechanism is outside the top of the test section and the hot-wire probe goes through and moves in the slot made in the top wall. This location of the mechanism was chosen because it allows the probe to have a simple shape, has a shorter shaft than a probe from the side wall and does not vibrate at the test speed.

It also creates less disturbance than a probe from the side wall.

The slot was placed above the middle of the plate where the turbulence intensity is smallest.

2.3.4 Spectrum Analyzer

A Unigon Model 4512 spectrum analyzer was used to measure spectra. It has an averaging capability for a chosen time interval. The bandwidth and the amplitude scale could be adjusted. A Polaroid camera attached to the screen enabled pictures of the spectrum to be taken.

CHAPTER III

EXPERIMENTAL PROCEDURE

3.1 Calibration

Calibration of the hot wire was performed with every run because the cold wire resistance was changing due to heat, dust and natural deterioration. To eliminate drifting, it was necessary to allow two hours for the system to warm up before using the hot wire. The contamination problem was solved by changing the wire every few weeks.

Calibration was always performed with the wire at 5 cm above the plate, and 30 cm downstream of the leading edge. The cold wire resistance R_o was measured. The overheat ratio of 1.3 was adjusted by setting the wire resistance R_w to a value of $1.3 R_o$. The wind tunnel speed was increased gradually and each time the wire current and the manometer readings were taken. In such a manner, the calibration curve for the velocity as a function of the wire current was obtained and plotted (Fig. 19). It was almost a straight line as it should be according to King's law [11]:

$$I_w^2 = a + b\sqrt{u} \quad (3.1)$$

After the calibration, the pitot tube was pulled out.

3.2 Smooth Plate

3.2.1 Adjustment of Zero Pressure Gradient

The outer flow velocity was measured along the plate using the

hot wire because it is more accurate than a pitot tube for such small pressure differences as in this case. At each place where the hot wire was positioned, the slot was sealed off with masking tape. The pressure coefficient C_p was calculated from the velocity data.

$$C_p = \frac{p - p_{ref}}{\frac{1}{2} \rho (U_{e, ref})^2} = 1 - \frac{U_e^2}{(U_{e, ref})^2} \quad (3.2)$$

where $(U_{e, ref})$ was chosen at $X = 30$ cm.

Fig. 20 presents the results of an early run. In addition, the mean velocity profiles were taken at each station (Fig. 21). It is clear from both figures that there was a pressure gradient in the critical stability region; that is where, according to stability theory, the disturbances are amplified. Since the concern was to achieve a constant pressure in this region, the rear supports were shortened by 1 cm, and so the plate was tilted by a 1° angle. The angle of attack could be controlled further by elevating the rear of the plate using the screws in the rear supports but this was not necessary.

As can be seen from Fig. 22, this adjustment yielded a constant pressure region between $X = 30$ cm and $X = 60$ cm. The mean velocity profiles in this region show good agreement with the theoretical Blasius curve (Fig. 23). In this region, the Reynolds number based on displacement thickness is 590 to 835 which is in the critical stability range for amplification of Tollmien-Schlichting waves.

Thus, the region between $X = 30$ cm and $X = 60$ cm was chosen as the test region.

3.2.2 Measurement of Mean and Fluctuating Information

The mean and the fluctuating information was taken at the same time. For the smooth plate, the probe was lowered until the support touched the plate. This was repeated several times and the micrometer readings were taken. They were always within ± 0.03 mm of a mean value and thus could be considered accurate enough. At this position, the wire was approximately 0.2 mm from the surface. This was the closest position from the plate and there the first readings were taken. Measurements were repeated at vertical intervals of 0.5 mm until there was no current change, indicating the outer flow regime.

At each point, the current, the series resistance and the average wire voltage $\overline{V(e')^2}$ were measured. This enabled calculation and extraction of the information of interest. The mean velocity was taken from the calibration curve (Fig. 19) for the corresponding current. The fluctuation rms velocity component was calculated as follows [11]:

$$\sqrt{\overline{(u')^2}} = \frac{\sqrt{\overline{(e')^2}}}{S} \quad (3.3)$$

where $S = \frac{R_w I_w \alpha E Z}{2 \bar{u}}$ is a hot-wire sensitivity

$R_w = 1.3 R_o$ - the wire resistance at overheat
 I_w - the wire current

$$\alpha = (R_w - R_o) / R_o = 0.3$$

$E = (1-\epsilon) / (1+2\alpha\epsilon)$ where $\epsilon = R_s / (R_s + R_w)$ and

R_s = the series resistance

$Z = 1 / (1 + \sqrt{\bar{u}_o} / \sqrt{\bar{u}})$ where \bar{u}_o is the corresponding velocity for a zero current and extrapolated from the calibration curve

\bar{u} = the mean velocity

The voltage $\sqrt{(e')^2}$ was measured by taking approximately 50 readings at 5 second intervals.

By calculating $\sqrt{(u')^2} = u_{rms}$, it was easy to get the disturbance energy $\sqrt{(u')^2}$ and the free-stream turbulence intensity $\sqrt{(u')^2} / u_c$ or the local intensity $\sqrt{(u')^2} / \bar{u}$.

3.3 Rough Plate

3.3.1 Additional Adjustments

The finer sandpaper was at first positioned to begin at 3 cm downstream of the leading edge. The Re_k and k/δ^* at this location are 33 and 0.56 respectively. The boundary layer was apparently tripped by the leading edge of the sandpaper and the flow at the first measuring station, $X = 30$ cm, was already turbulent. The paper was then cut back to 6.5 cm downstream of the leading edge of the plate. The corresponding Re_k and k/δ^* were 23 and 0.38 respectively. Here the flow was laminar at the first station and for this location of the leading edge of the sandpaper, the measurements were taken.

The coarser sandpaper began initially at 6.5 cm from the lead-

ing edge of the plate but again the boundary layer was tripped. The corresponding Re_k and k/δ^* were 314 and 1.48 respectively. The flow was turbulent even at $X = 20$ cm. When the paper was cut back to 18.3 cm, the flow at the first station was laminar. At $X = 18.3$ cm, $Re_k = 192$ and $k/\delta^* = 0.88$. This was the location of the leading edge of the coarser sandpaper for the measurements presented herein.

3.3.2 Measurements Taken with Each of the Two Sandpapers

The measurements and the procedure for the finer sandpaper was similar to those for the smooth plate. For measurements with coarser sandpaper, precautions had to be taken to prevent wire damage.

A glass plate of 1.4 mm thickness was placed on the surface under the probe and the probe was lowered until the support touched the glass plate. The micrometer reading was taken. The probe was raised and the glass plate removed. The probe was lowered again by 1.4 mm beneath the reading. At all stations, it was possible to lower the probe an additional 0.5 mm without damaging the wire. The probe location was illuminated, and it was always possible to see a gap between the wire and the grit. This was checked many times. This is possible because of the non-uniform distribution of the grains in the sandpaper matrix and also because of some grains which were positioned above the average. If the plate rested on those higher grains, then the wire could be lowered beneath their height. We could assume that there were enough grains of such size to allow

this to occur. Thus, the first reading for the roughest sandpaper was taken with the wire at 0.3 mm below the highest grains in the near vicinity where the measurements were taken.

In addition to the measurements as taken earlier, special data were taken for the coarser sandpaper. Here the information was taken also at $X = 20$ cm. The hot-wire probe was positioned at the peak energy location. The amplitudes were measured from Polaroid pictures of the analyzer output and the amplification rates were calculated from:

$$\alpha_i = - \frac{1}{A} \frac{dA}{dX} \quad (3.4)$$

The amplitude gradient was measured from the amplitude curves.

Data were also taken using the filters on the hot-wire anemometer panel. At the peak energy location for each station, the energy was measured for different frequency bands. The filters were 1-10, 10-100, 100-5000 Hz.

CHAPTER IV

RESULTS AND DISCUSSION

4.1 Smooth Plate

To provide a reference for the later measurements with surface roughness, a set of mean and fluctuating measurements was taken on the smooth aluminum plate. The mean velocity profiles at $X = 30$, 40 , 50 and 60 cm downstream of the leading edge are shown in Figs. 24 (a-d). Two data sets taken at different times are shown. The Blasius curve taken from Schlichting [12] is plotted for comparison on each of the figures. The points agree with the Blasius curve within the experimental error. The profiles corroborate the earlier indication from surface pressure measurements that the region $30 < x < 60$ cm is a constant pressure region.

One set of test results for the fluctuation energy nondimensionalized with respect to U_e^2 versus dimensional boundary layer coordinate y and nondimensional η is presented in Figs. 25a and 25b respectively.

The free-stream turbulence and the wind tunnel fan rotation affect the magnitude of the disturbance energy, but the shape and order of magnitude of the curves remains consistent. Even though the data points are not always on the curve lines, the deviation is within the experimental error and the curve lines are definitely

characteristic of the phenomena taking place according to other test results taken in the present investigation. The shape is similar to that obtained in other experimental studies for a smooth plate, for example that of Strazisar et al. [8,9].

The integrals under the curves and the peak values are increasing consistently and gradually in the downstream direction. The energy content is distributed over the whole boundary layer but is concentrated mainly in the middle. It is almost symmetrically distributed. The peak moves away from the wall but remains at $\eta = 2.3$ or $y_{max}/\delta \approx 0.43$ and $y_{max}/\delta^* \approx 1.37$. The peak energy is increasing approximately linearly with distance downstream.

The local disturbance intensity which is with respect to the local velocity is plotted in Fig. 26. It is seen to decrease near the wall with downstream distance. The energy integrals and peak values are increasing but very little. Both the energy and the local intensity are increasing in the vicinity of the edge of the boundary layer, thus indicating that the response to free-stream disturbances is not confined to the interior of the boundary layer. The turbulence intensity at the outer edge is seen to increase about 0.02% with every 10 cm downstream from the leading edge.

The reasons for showing both energy and local turbulence intensity will become apparent later in the cases with roughness.

4.2 Distributed Roughness of Re_k ($X = 30$ cm) = 10.6

Similar measurements were taken for this roughness as for the

smooth surface. The mean velocity profiles at $X = 30, 40, 50$ and 60 cm downstream of the leading edge are shown in Figs. 27 (a-d). Just as for the smooth case, a number of data sets were taken and the Blasius curve is plotted for comparison on each of the figures. The zero reference height, as for the smooth wall case, was assumed to be 0.2 mm beneath the hot-wire when the probe support touched the surface. With this choice of $\eta = 0$ ($y = 0$), the Blasius curve fits the data points within the experimental error.

One set of test results for the energy is presented in Figs. 28 a,b. The shape and order of magnitude of the curves for this run remains consistent for the results of other tests taken in this investigation but not shown. The energy has the same shape and the same gradual increase as for the smooth case. It is again mostly concentrated at the center of the boundary layer and the peak remains at $\eta \approx 2.3$ as for the smooth surface.

We can see already slightly more curvature near the wall than in the smooth wall case (Fig. 25b) as the flow proceeds in the downstream direction. The energy at the outer edge of the boundary layer is also slightly larger than for the smooth plate. Within the boundary layer the energy levels are slightly smaller than for the smooth surface perhaps because the speed was lower by 0.2 m/sec and possibly because the flow was less turbulent initially, thus affecting the initial energy levels. Although the energy peak at $X = 30$ cm is smaller than for the smooth wall case, the energy growth - the ratio of energy at the last station to that at the first station -

is 10% larger than before and that, perhaps, is an indication of a slight roughness effect.

A more pronounced indication of the roughness effect is shown by the local turbulence intensity distribution presented in Fig. 29. Even though the energy was smaller, the intensities were larger than those for the smooth wall (Fig. 26) in the vicinity of the wall. The intensities of the peaks close to the wall are increasing with downstream distance in contrast to the results for the smooth surface.

In summary, this small roughness (beginning from $Re_k = 22.8$ and $k/\delta^* = 0.38$ at $X = 6.5$ cm) has only a very small effect. It doesn't perturb the flow to the nonlinear regime and both the mean velocity and the disturbance energy profiles resemble those of laminar flow on a smooth plate. Although the overall effects are small, we could detect changes in the local turbulence intensity distributions, particularly in the vicinity of the wall.

4.3 Distributed Roughness of Re_k ($X = 30$ cm) = 155

4.3.1 Mean and Fluctuation Measurements

A set of mean velocity profiles is shown in Figs. 30 (a - d). In this case the roughness is large enough so that the effective zero velocity location for the boundary layer could not be determined a priori. The data point closest to the wall was 0.3 mm below the top of the largest grains. This point was chosen as the reference location for the rest of the data taken. The nominal

grit size is known and thus the distance of the reference location point from the nominal bottom of the grains is also known. By fitting a curve through the data points, the extrapolated zero velocity point can be located. For the first two stations ($X = 30$ cm, $X = 40$ cm), a Blasius curve could reasonably be put through the data points and the extrapolated zero velocity locations were at approximately the same distance from the nominal bottom of the grit (0.2 mm). An attempt to fit the data points with a similarity profile for $\beta = -0.1$ was unsuccessful. These two measured profiles are much closer to the Blasius curve and compare very well with the measured data on the smooth plate once an adjustment is made for the extrapolated zero.

Curves through the mean velocity data points for the two downstream stations ($X = 50$ cm, $X = 60$ cm) are shown in Figs. 30c and 30d. The extrapolated zero velocity location is chosen to be the same as in Figs. 30a and 30b. Blasius curves are drawn for comparison. At $X = 50$ cm the mean velocity profile has changed significantly from that at $X = 40$ cm. At $X = 60$ cm there is the beginning of the emergence of a turbulent profile shape.

If there are inflection points near the wall in Figs. 30a and 30b, it is practically impossible to detect them considering the experimental error. It is also very difficult to do a detailed search in the vicinity of the grit because of prospective wire damage and probe interference effects.

Fluctuation data for two separate tests taken a week apart are shown in Figs. 31a, b. The first test results are indicated by I and the second by II. The first test corresponds to the mean velocity results shown earlier (Fig. 30).* The $\eta = 0$ locations used in these figures for each station were taken from the extrapolated zero velocity points of the mean velocity profiles. The shape of the energy distributions is not smooth but somewhat oscillatory. Both tests show more than one local peak and the number increases with the distance downstream. The first two stations display more or less their previous shape. Their peaks are in the vicinity of $\eta \approx 2.3$ and only the second test deviates from this slightly at the second station. The downstream profiles here are much fuller than for the smooth plate or the finer roughness and there is significant increase in energy content near the wall.

For the finer roughness the only clear indication of a roughness effect was through the changes in the turbulence intensity distributions. Here we see a large effect on the energy distributions as well. The peaks are moving closer to the wall and most of the energy content is concentrated in the $\eta < 4$ region for the first three stations. Farther downstream there is also significant increase in energy content at the outer edge of the boundary layer.

* Mean velocity profiles for test II (4/21/80) were measured at $X = 30$ cm and $X = 40$ cm, they are very close to the profiles of Figures 30a and 30b. The profiles at $X = 50$ cm and $X = 60$ cm differ slightly from those of Figures 30c and 30d in a manner consistent with the different progressions to transition on those two days.

In between $X = 40$ cm and $X = 50$ cm where a velocity profile change takes place, the energy increases by an order of magnitude. Figs. 32a,b present the local turbulence intensity for these two tests respectively, again using the extrapolated zero from Test I. The local intensity rises to more than 15% between $X = 40$ cm and $X = 50$ cm emphasizing that the disturbances are in the non-linear regime.

In Test I, there is not much overall energy change between the last two stations but there is a noticeable buildup in the outer portion of the boundary layer. Accompanying this is a definite change in the mean velocity profile (Figs. 30c,d) and an increase in the boundary layer thickness even though it is not yet a fully turbulent flow.

Test II shows a flow that seems less disturbed initially. Less of an increase in energy occurs between $X = 40$ cm and $X = 50$ cm. As a consequence, there is still an increase in energy between the last two stations. Only the last station indicates a significant energy increase in the outer portion of the boundary layer. The mean velocity profiles which are not presented here, again indicate a Blasius profile for the first two stations and a very slight change relative to Test I at the third station. The intensity peak at the last station reaches the same magnitude as at the last two stations of Test I.

The intensity shape is bumpy. However, the main peaks are approaching the wall, consistent with the observation for the $Re_k = 10.6$ case. The peaks are within the region $n < 0.5$. At the measurement point closest to the wall, the total amplitude ratio relative to free-

stream turbulence level (assumed to be 0.02%) for both experiments is already about 1500 which is $e^{7.3}$. The boundary layer at this point is however not yet fully turbulent. Maybe the ratio is larger closer to the wall but it was impossible to measure any closer.

The consistency of the peak intensity development shown by Figs. 32a, b with that of the finer roughness indicates that the extrapolated zero point is reasonably chosen. The development of the energy and the intensity indicate that the fully turbulent regime is not yet reached.

An attempt to isolate a roughness effect for Test II by subtracting Fig. 26 (the smooth plate intensity) from Fig. 32b (the rough plate intensity) is presented in Fig. 33. The curves are essentially the same as in Fig. 32b indicating that the overwhelming contributions to the data in Fig. 32b are due to the roughness.

Fig. 34 shows the variations of the peak local intensity and the square root of the peak nondimensional energy with Re_x . These results are consistent with what was said earlier: (a) the intensity is more sensitive than the energy and thus a better indication of the degree to which the flow is disturbed; (b) the flow in Test I is more disturbed.

In summary, the intensity magnitudes for both experiments are above 15% at the third station ($X = 50$ cm) and thus are clearly non-linear. The intensity for the second station is 4.5 - 8% and thus significant too and probably non-linear. The main conclusion is that the disturbances grow to non-linear amplitudes before detectable velocity profiles are observed.

4.3.2 The Spectrum

In addition to mean and fluctuation measurements, one set of tests was made using the Unigon spectrum analyzer. Figs. 35 - 39 show the spectra taken at $X = 20, 30, 40, 50$ and 60 cm with the coarsest paper and $U_e = 6$ m/sec. For $X = 20$ cm to $X = 40$ cm (Figs. 35, 36, 37) gain settings were inadequate to get data above 20 Hz from those pictures. It was possible to read the amplitude above 20 Hz for the last two stations but the accuracy is doubtful, and since the amplitude slope is very sensitive to any small amplitude change, the calculated α_i values are doubtful too. Nevertheless it is possible to extract some important information from this test.

Amplitude distributions for frequencies up to 17.2 Hz are shown in Fig. 40. They have a shape resembling what is obtained in linear stability studies. Fig. 41 presents the calculated amplification rates $-\alpha_i$. For 17.2 Hz amplification occurs at $Re_{\delta^*} \approx 550$. As the Re_{δ^*} increases, successively lower frequencies become amplified but their maximum amplification rate is diminishing. The highest amplification rate for 17.2 Hz is located at $Re_{\delta^*} = 650$. Lower frequencies show peak α_i at successively larger values of Re_{δ^*} . These peaks occur in the non-linear region of the flow as identified from energy and intensity distributions. Fig. 42 shows again that as Re_{δ^*} increases, the lower frequencies become important. A plot of $\alpha_{i_{max}}$ versus Re_{δ^*} (Fig. 43) indicates that higher frequencies (above

17.2 Hz) may be important below $Re_{\delta^*} = 650$. Note that the Tollmien-Schlichting band at $Re_{\delta^*} = 650$ is between 45 - 85 Hz. In fact if we extrapolate the trends of Fig. 41 to higher frequencies, it would suggest the higher frequencies become more important close to the leading edge.

Amplification rates $-\alpha_i$ for the frequencies up to 130 Hz at $X = 50$ cm are shown in Fig. 44. Similar behavior of α_i is found at $X = 60$ cm. Amplification is shown at all frequencies. There does not seem to be anything special about the Tollmien-Schlichting band. Again, at $X = 50$ cm, the disturbances are non-linear.

The experimental "neutral curve" for frequencies up to 17.2 Hz is below the neutral curve for the linear stability of non-parallel flat plate flow as calculated by Saric [13] (Fig. 45). It is also below the neutral curve for the linear stability of non-parallel Falkner-Skan flow corresponding to $\beta = -0.1$. This corroborates the earlier indication that disturbance growth was governed by non-linear growth effects rather than by linear instability of an inflectional mean velocity profile which hasn't been detected in any case.

From the trend of the curve we can definitely say that there is earlier amplification and very likely earlier transition than for the smooth surface. While the linear theory for a smooth plate predicts $\alpha_{i_{max}}$ for Re_{δ^*} above 684, here it is larger much below this number. The order of magnitude of $(\alpha_i \delta_{cr}^*)_{max}$ is also totally different.

The maximum value of $(\frac{i}{Re_{\delta}^*})^{-\alpha/\delta^*}$ for non-parallel smooth flat plate flow is approximately 9.55×10^{-6} and occurs at $Re_{\delta^*} = 795$ [9]. For the same Re_{δ^*} the present data for the rough case shows it equal 2.67×10^{-5} and the value of α_i is even higher for lower Re_{δ^*} . This means faster transition. Considering the state of the boundary layer at $X = 60$ cm ($Re_{\delta^*} = 835$), transition might be completed at $Re_X \approx 350,000$ which is very low compared to the value of 3×10^6 that might be expected on a smooth plate for the low free-stream turbulence intensity of the tunnel.

Frequencies corresponding to roughness wavelengths are of order $\frac{U_k}{k} = (\frac{\partial u}{\partial y})_w$. In the present experiment such frequencies would be in the range of 1.5 to 3 KHz. No growth was observed in these frequency bands.

4.3.3 Filtering

Another experiment was performed using the built in filters on the hot-wire anemometer set, at the peak energy location at $X = 30$, 40, 50 and 60 cm downstream from the leading edge. The filters were 1-10, 10-100, 100-5000 Hz. Fig. 46 shows the energy results for these frequency levels.

There is a shift in energy to higher frequencies. Most of the energy in the non-linear regime is concentrated in the 100-5000 Hz band. This didn't show up from the spectrum because even though the amplitude in the high frequency range is small, its integral is significant and very sensitive to a small amplitude increase, since

the band width of the 100-5000 Hz band is so large. Major high frequency content is probably in the 100-200 Hz band. The mechanism is driven by frequencies up to about 140 Hz as indicated by the spectra (Figs. 38, 39), but the energy is dissipated into higher frequencies.

4.4 Leading Edge of the Distributed Roughness

As described in the preceding chapter for both roughness sizes, the leading edge of the sandpaper had to be cut back in order that the boundary layer not be tripped by the leading edge of the sandpaper. Such tripping did occur before cutting back the sandpaper, despite the use of a filler to avoid a step at the leading edge of the sandpaper.

The finer roughness sandpaper was cut from $X = 3$ cm with the corresponding $Re_k = 33$ and $k/\delta^* = 0.56$, to $X = 6.5$ cm downstream from the leading edge and the corresponding $Re_k = 22.8$ and $k/\delta^* = 0.38$. Before the cutting back the sandpaper, the flow was turbulent over the whole test region and after cutting it back it was laminar.

The coarser roughness paper was cut back from $X = 6$ cm with the corresponding $Re_k = 314$ and $k/\delta^* = 1.48$, to $X = 18.3$ cm with corresponding $Re_k = 198$ and $k/\delta^* \approx 0.88$. Before cutting the sandpaper back, transition was detected already at $X = 20$ cm and turbulent flow occurred in the whole test region. After cutting back the sandpaper, laminar mean profiles were obtained at least to $X = 40$ cm (Fig. 30).

Even though Re_k was equal to 198 at the leading edge of the coarser sandpaper and only 33 at the leading edge of the finer sandpaper and the filler ramp angle was approximately the same in both cases, the latter tripped the boundary layer while the former did not. Thus Re_k is not the only parameter affecting the flow. The same can probably be said about k/a^* . Thus, the response of the flow to the leading edge of a roughness region cannot be simply described in terms of these two parameters. The filler strip geometry and the smoothness achieved are important factors in influencing the flow.

CHAPTER V

SUMMARY AND CONCLUSIONS

A preliminary experimental study has been completed of the disturbances in a laminar boundary layer due to distributed surface roughness. Tests were conducted on a smooth plate and with two different grades of sandpaper covering.

Over the portion of the smooth plate displaying zero pressure gradient ($30 \text{ cm} < x < 60 \text{ cm}$), the mean flow velocity profiles agree with the Blasius profile within the experimental error. The u'_{rms} distributions display a peak at $\eta \approx 2.3$ that increases slightly with distance downstream reaching a level of $0.007 U_e$ at $X = 60 \text{ cm}$.

For distributed roughness having $Re_k \approx 10$, the results are quite comparable to those for the smooth plate. The mean flow velocity profiles agree with the Blasius curve within the experimental error and the u'_{rms} distributions are closely comparable in level and distribution to those for the smooth plate. There is however indication of a slight increase in local intensity in the very near vicinity of the wall. It is well to point out that although the dimensionless turbulent energy $(u'_{\text{rms}}/U_e)^2$ and the local turbulent intensity $(u'_{\text{rms}}/\bar{u})$ involve the same fluctuation amplitudes, the local turbulent intensity is a much more sensitive indicator of effects of roughness.

For distributed roughness with $Re_k \approx 150$, the picture is different. At $X = 30$ cm and at $X = 40$ cm, the mean velocity profile is best fit by a Blasius profile whose effective origin is somewhere within the roughness height. Beyond $X = 40$ cm the mean profile seems to progress toward a turbulent profile. Up to $X = 40$ cm, the u'_{rms} still peaks at $\eta \approx 2.3$ but the local intensity is now of the order of 5%. Beyond $X = 40$ cm there is a large increase in the u'_{rms} levels and an increase in the number of peaks. Very large local intensities are obtained in the near vicinity of the wall ($\eta < 0.5$) but there is also noticeable buildup over the entire boundary layer to the outer edge. A study of disturbance spectra for this case shows largest amplitudes and amplifications at frequencies well below the Blasius neutral curve. The maximum amplification rates are about three times as large as those for Tollmien-Schlichting instability over a smooth plate. Transition occurs at $Re_X \approx 350,000$ which is much below the value of 3×10^6 or so that might be expected for a smooth surface at the turbulence level of the tunnel.

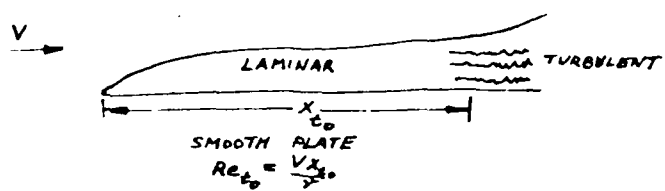
To conclude, one observes that disturbances can grow to non-linear magnitudes before velocity profile changes are observed. The indicated importance of frequencies below those of the Blasius neutral curve was not expected and requires more careful examination.

REFERENCES

1. Dryden, H.L.: Review of Published Data on the Effects of Roughness on Transition from Laminar to Turbulent Flow, *J. Aeronautical Sci.*, Vol. 20, No. 7, pp. 471-482, July 1953.
2. Smith, A.M.O. and Clutter, D.W.: The Smallest Height of Roughness Capable of Affecting Boundary-Layer Transition. *J. Aerospace Sci.*, Vol. 26, No. 4, pp. 229-245, April 1959.
3. Klebanoff, P.S. and Tidstrom, K.D.: Mechanism by Which a Two-Dimensional Roughness Element Induces Boundary Layer Transition. *Physics of Fluids*, Vol. 15, No. 7, pp. 1173-1188, July 1972.
4. Singh, K. and Lumley, J.L.: Effect of Roughness on the Velocity Profile of a Laminar Boundary-Layer, *Appl. Sci. Res.*, Vol. 24, pp. 168-186, 1971.
5. Lessen, M. and Gangwani, S.T.: Effect of Small Amplitude Wall Waviness Upon the Stability of the Laminar Boundary Layer. *Physics of Fluids*, Vol. 19, No. 4, pp. 510-513, 1976.
6. Merkle, C.L., Tzou, K.T-S., and Kubota, T.: An Analytical Study of the Effect of Surface Roughness on Boundary-Layer Stability, Dynamics Technology, Inc., Report DT-7606-4, October 1977.
7. Achenbach, E.: Influence of Surface Roughness on the Cross-Flow around a Circular Cylinder, *J. Fluid Mech.*, Vol. 46, part 2, pp. 321-335, 1971.
8. Strazisar, A.J., Prahl, J.M. and Reshotko, E.: Experimental Study of the Stability of Heated Laminar Boundary Layers in Water, Case Western Reserve University, Dept. of Fluid, Thermal and Aerospace Sciences, Report FTAS/TR-75-113, 1975.
9. Strazisar, A.J., Reshotko, E. and Prahl, J.M.: Experimental Study of the Stability of Heated Laminar Boundary-Layers in Water. *J. Fluid Mech.*, Vol. 83, part 2, pp. 225-247, 1977.

10. Fabula, A.G.: Operating Characteristics of Some Hot Film Velocity Sensors in Water, in Melnik, W.L. and Weske, J.R. eds.: Advances in Hot-Wire Anemometry. AFOSR Report 68-1492, Department of Aerospace Engineering, University of Maryland, pp. 167-193, July 1968.
11. Hinze, J.O.: Turbulence, McGraw-Hill, 1975.
12. Schlichting, H.: Boundary Layer Theory, 6th edition, McGraw-Hill, 1968.
13. Saric, W.S. and Nayfeh, A.H.: Non-Parallel Stability of Boundary Layer Flows. Physics of Fluids, Vol. 18, pp. 945-950, 1975.

a)



b)

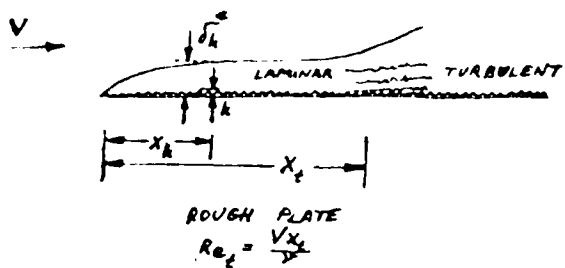


Fig. 1. Schematic diagram of effect of distributed roughness on transition on a flat plate.

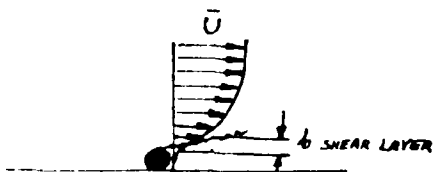
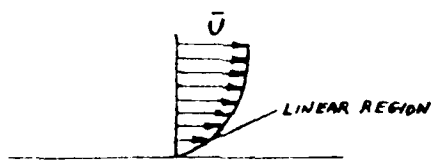


Fig. 2. The mean velocity distortion due to 2-D roughness element.



Fig. 3. View of wind tunnel looking upstream toward entrance, shown is the test section with the plate installed.



Fig. 4. Side view of test section with plate installed. The hot-wire and pitot-static probes are shown in the calibration position.

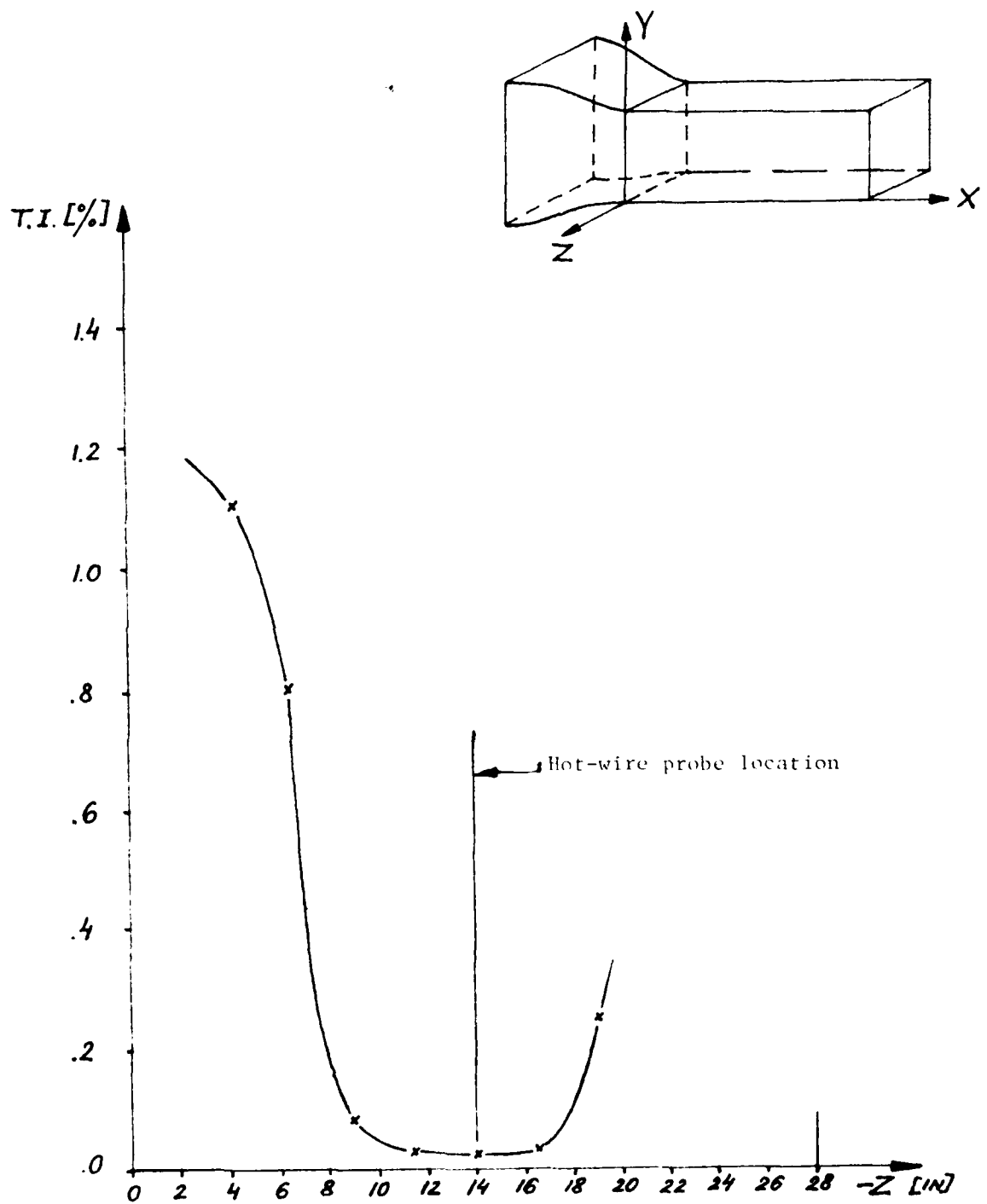


Fig. 5. Turbulence intensity profile in Z direction.

$X = 49.25''$, $Y = 17.5''$, $U_e = 6$ m/sec.

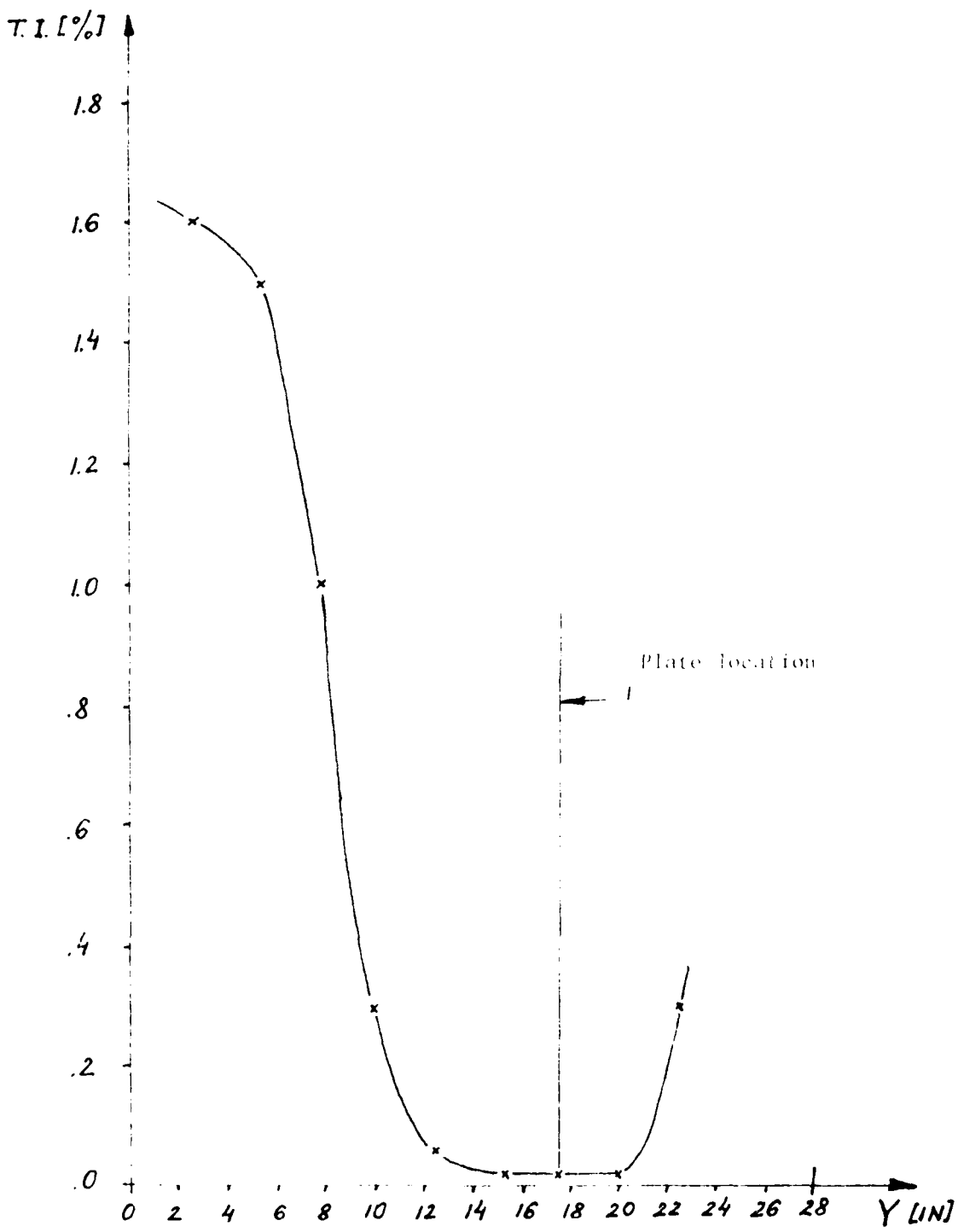


Fig. 6a. Turbulence Intensity profile in Y direction.
 $X = 49.7^{\prime\prime}$, $Z = -15.0^{\prime\prime}$, $V_e = 6$ m/sec.

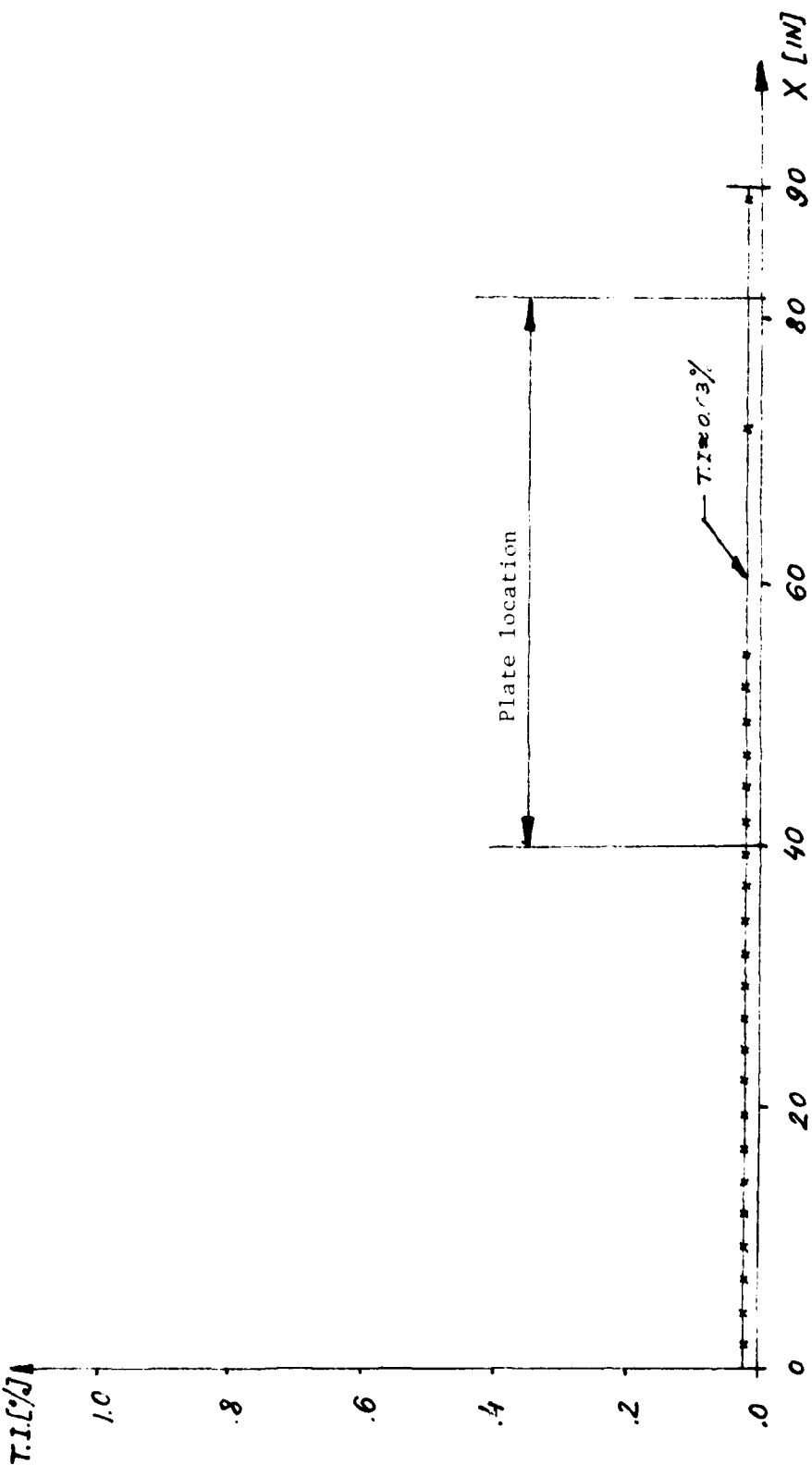


Fig. 7. Turbulence intensity profile in X -direction. $Z = -14.0"$, $Y = 17.5"$, $U_e = 6$ m/sec.



Fig. 8. The front view of the model.

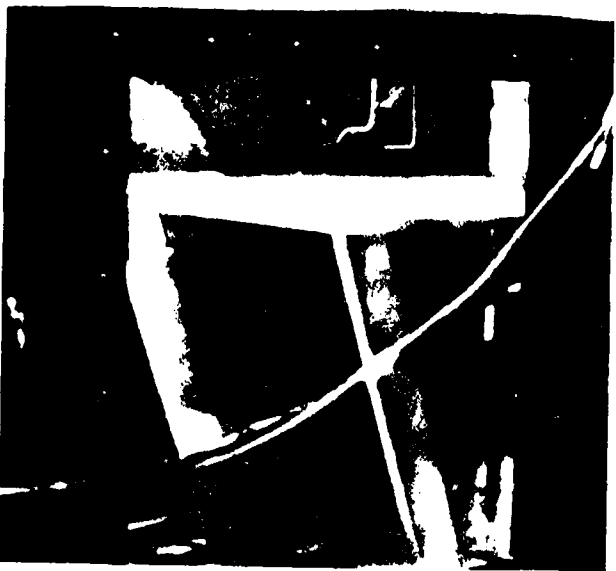


Fig. 9. General view of the model with sandpaper.

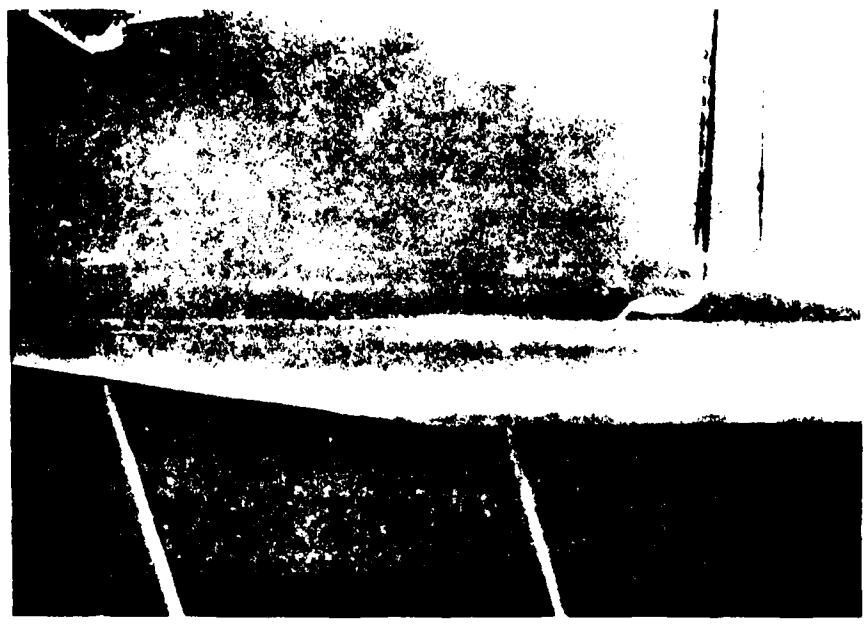


Fig. 10. Hot-wire probe and pitot tube over smooth plate.

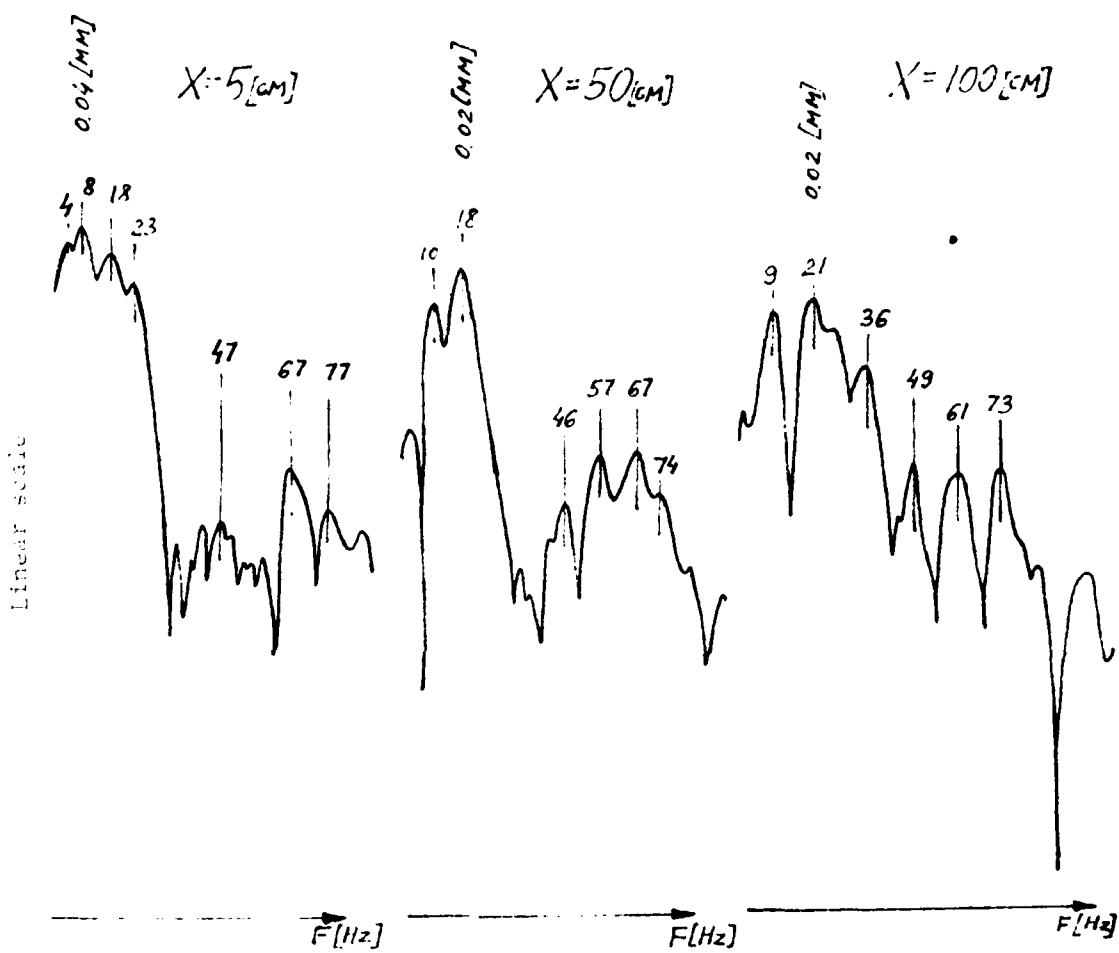


Fig. 11. Plate vibrations at $U_e = 6 \text{ m/sec.}$

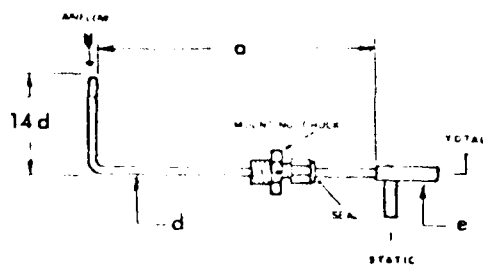


Fig. 12. The Prandtl type pitot-static tube, Sensor United model PAC-12KL.

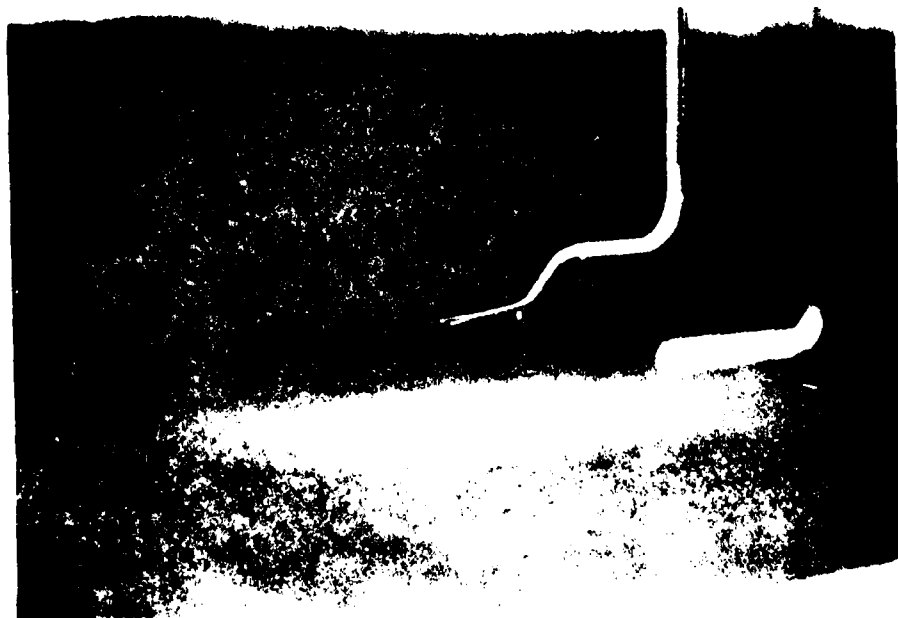


Fig. 13. Hot-wire probe and pitot tube above a rough surface.

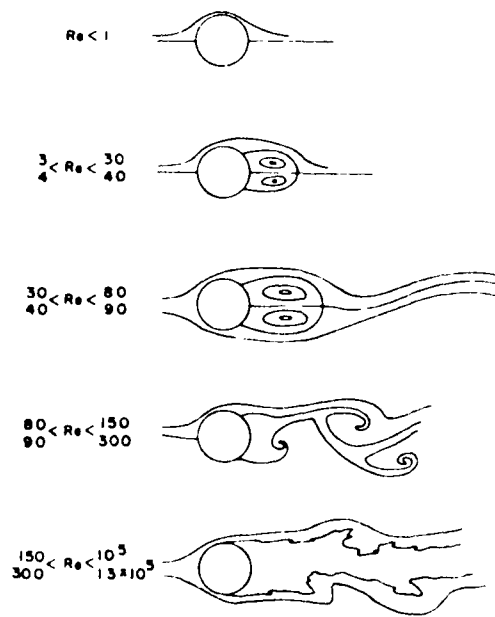


Figure 14. Flow Regimes About Unheated Circular Cylinders of High Length-to-Diameter Ratio Versus Reynolds Number (Morkovin, 1964).

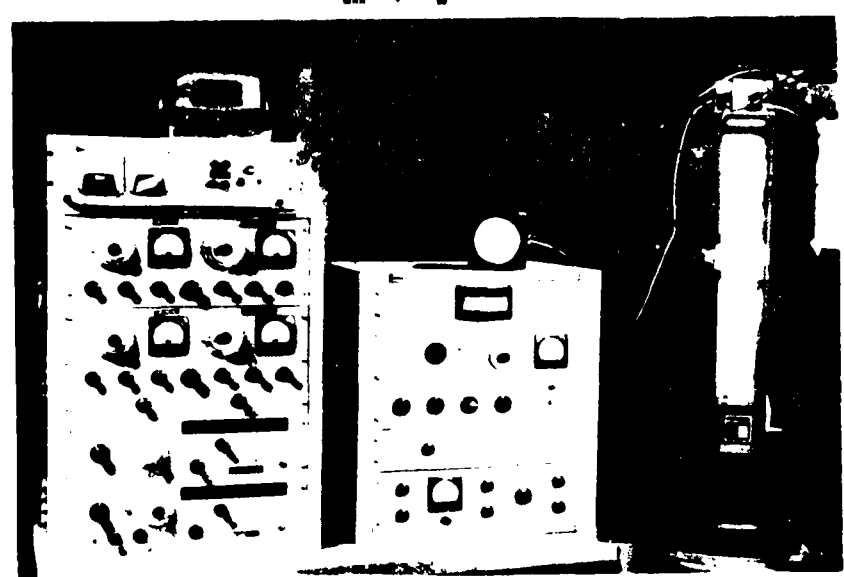


Fig. 15. The hot-wire anemometer (Shapiro & Edwards, model 50), and Merriam manometer.

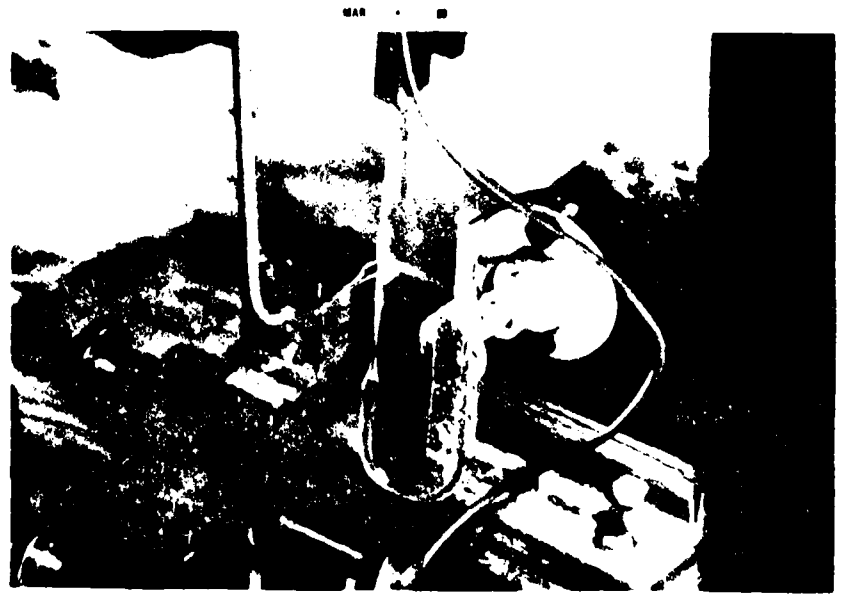


Fig. 16. A close-up of the hot-wire probe during the etching process.

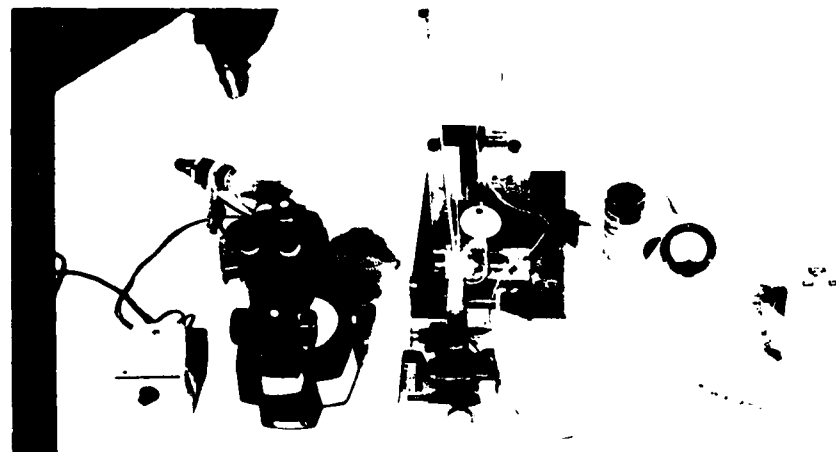


Fig. 17. The hot-wire probe in the process of the hot-wire etching.

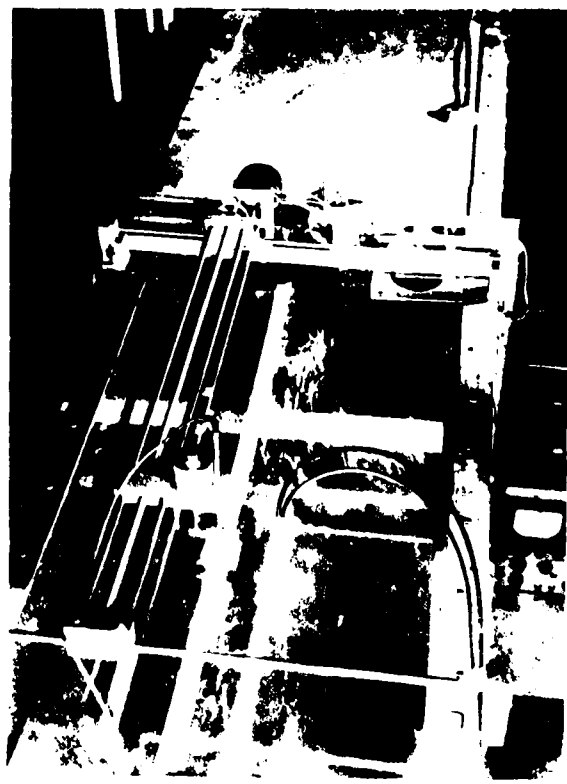


Fig. 18. The top view of the test section with the traversing mechanism.

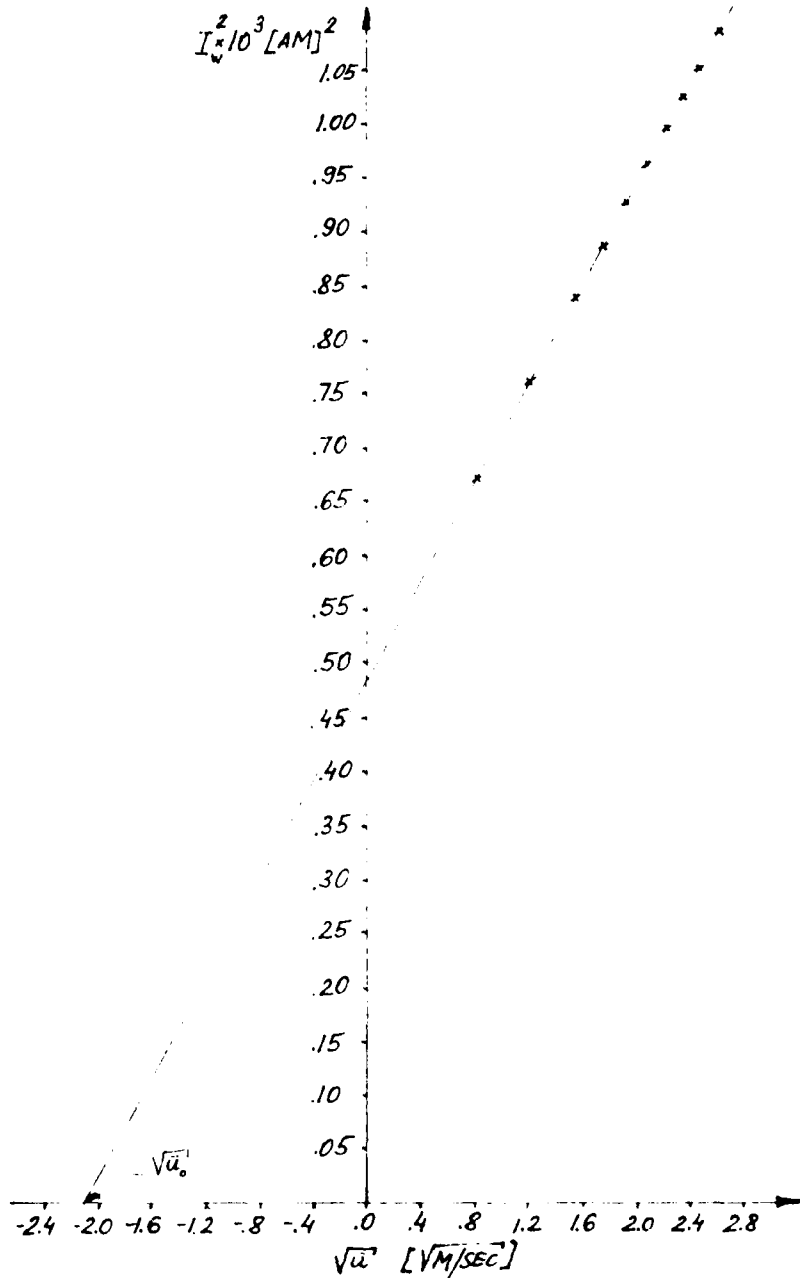


Fig. 19. Hot-wire calibration curve.

$$C_p = 1 - \frac{U_e^2}{U_e} \left(\frac{x}{x+30} \right)^2$$

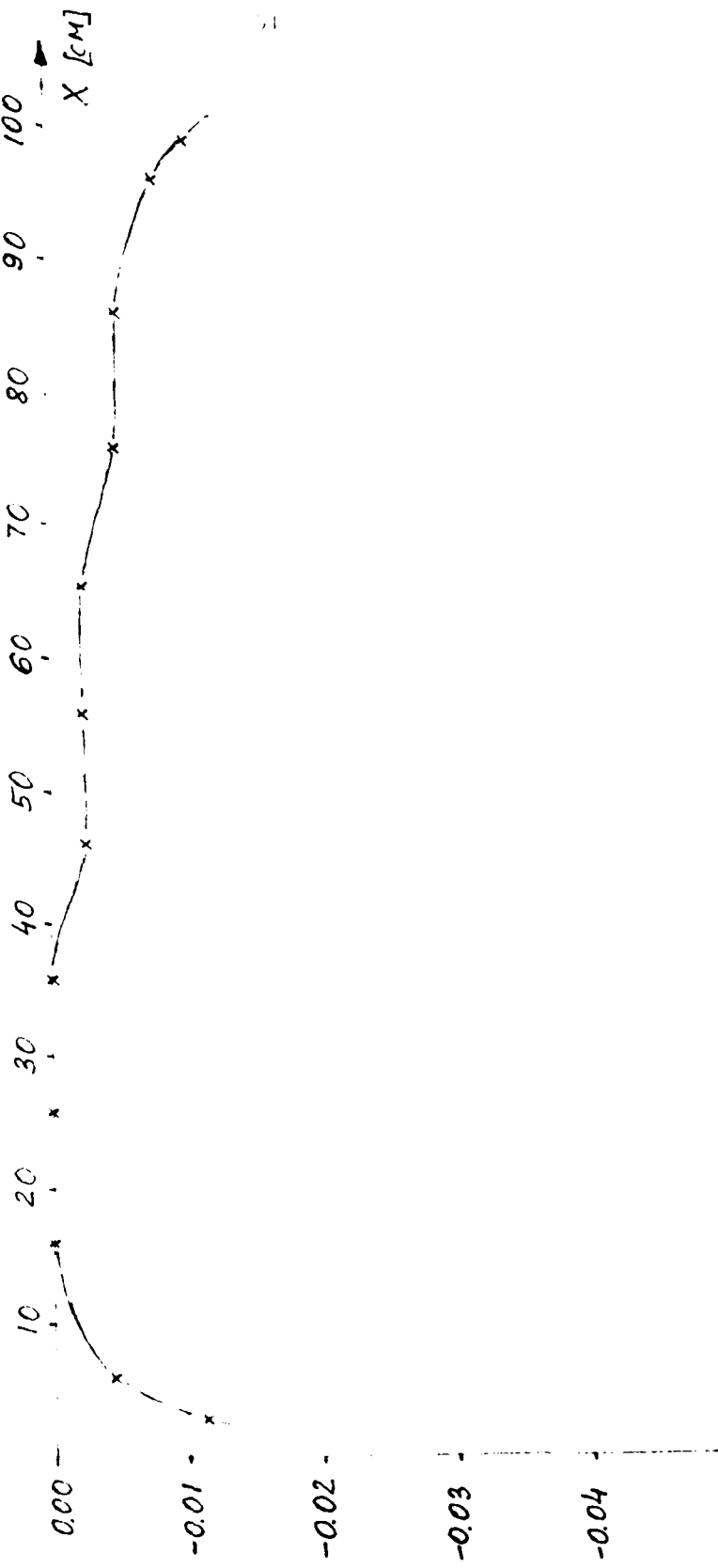


Fig. 20. Pressure coefficient for the plate at 0° angle of attack.

$\Delta \bar{u}/U_e$

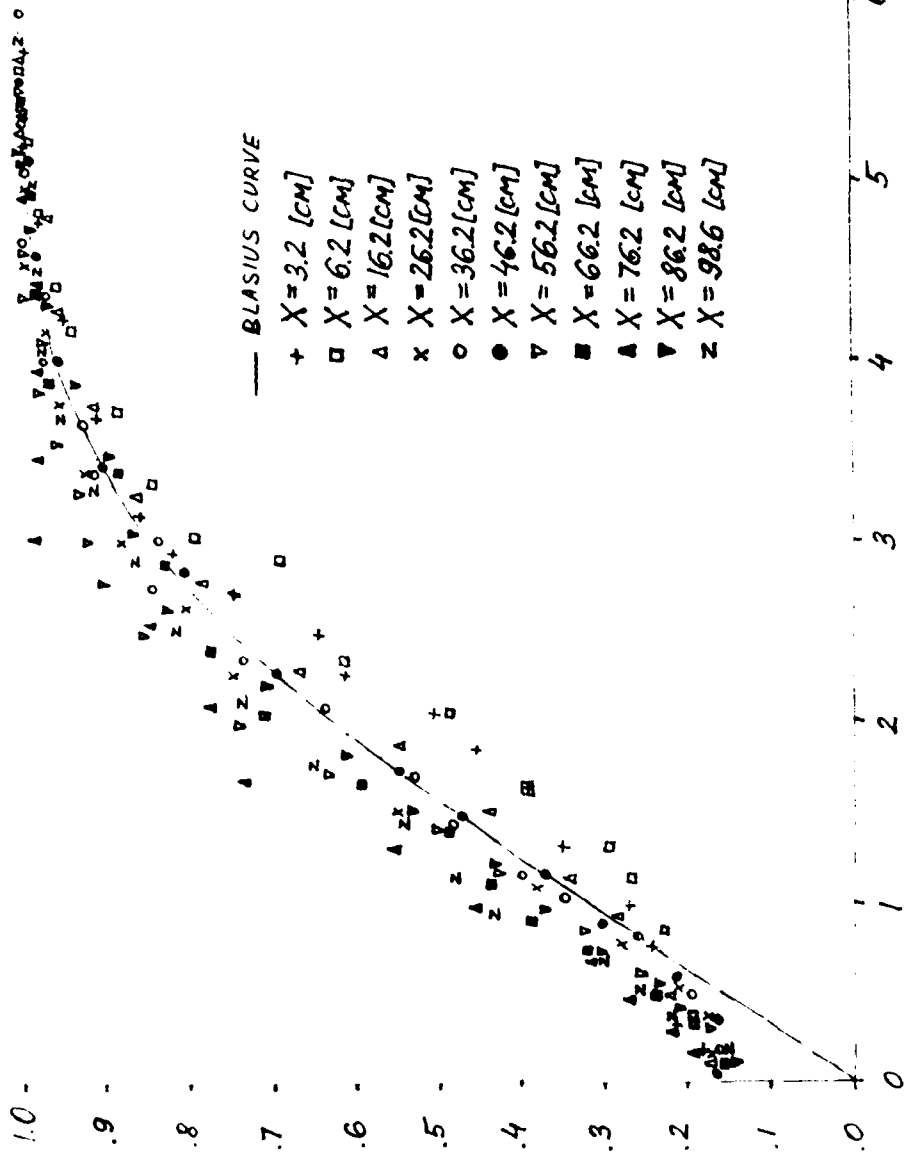


Fig. 2j. Mean velocity profiles for the plate at 0% of attack.

$$C_p = 1 - \frac{U_e^2}{(U_e)^2} \quad (x=30 \text{ cm})$$

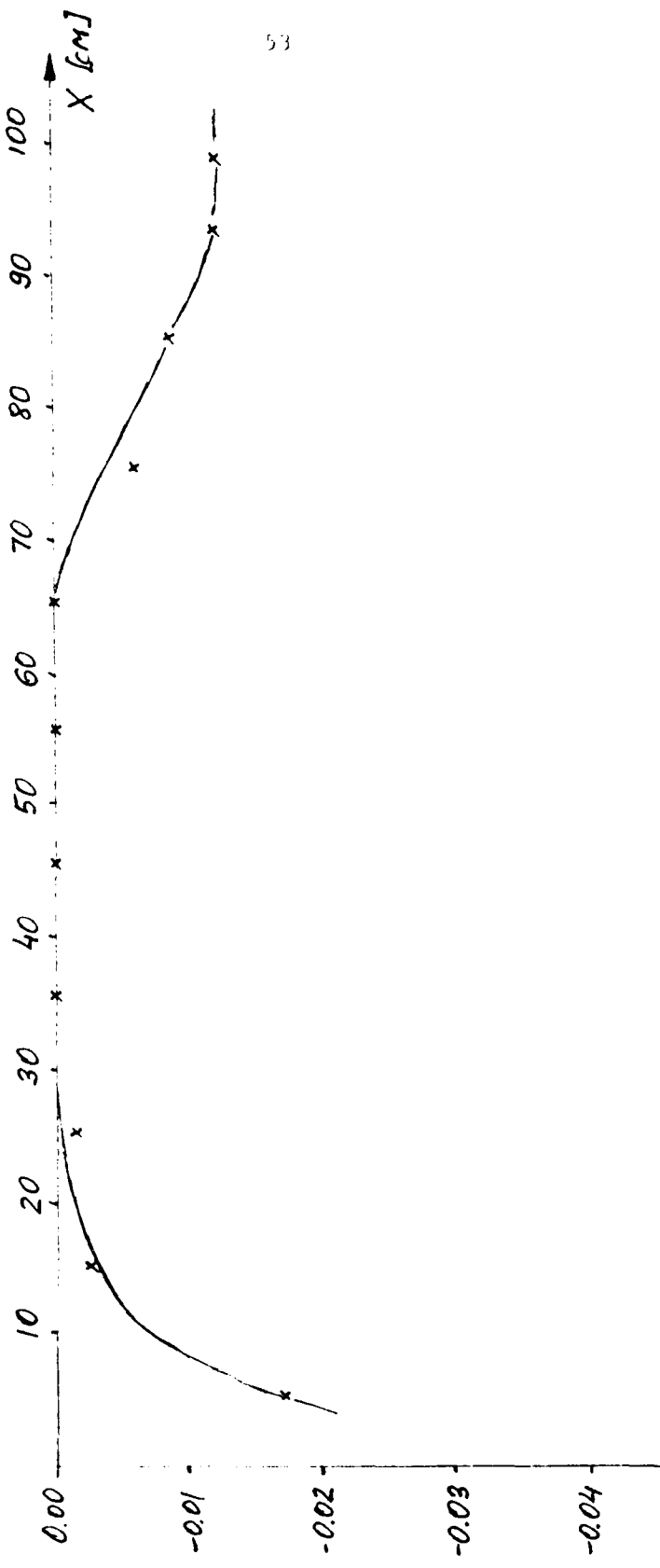


Fig. 22. Pressure coefficient for the plate tilted at 1° angle of attack.

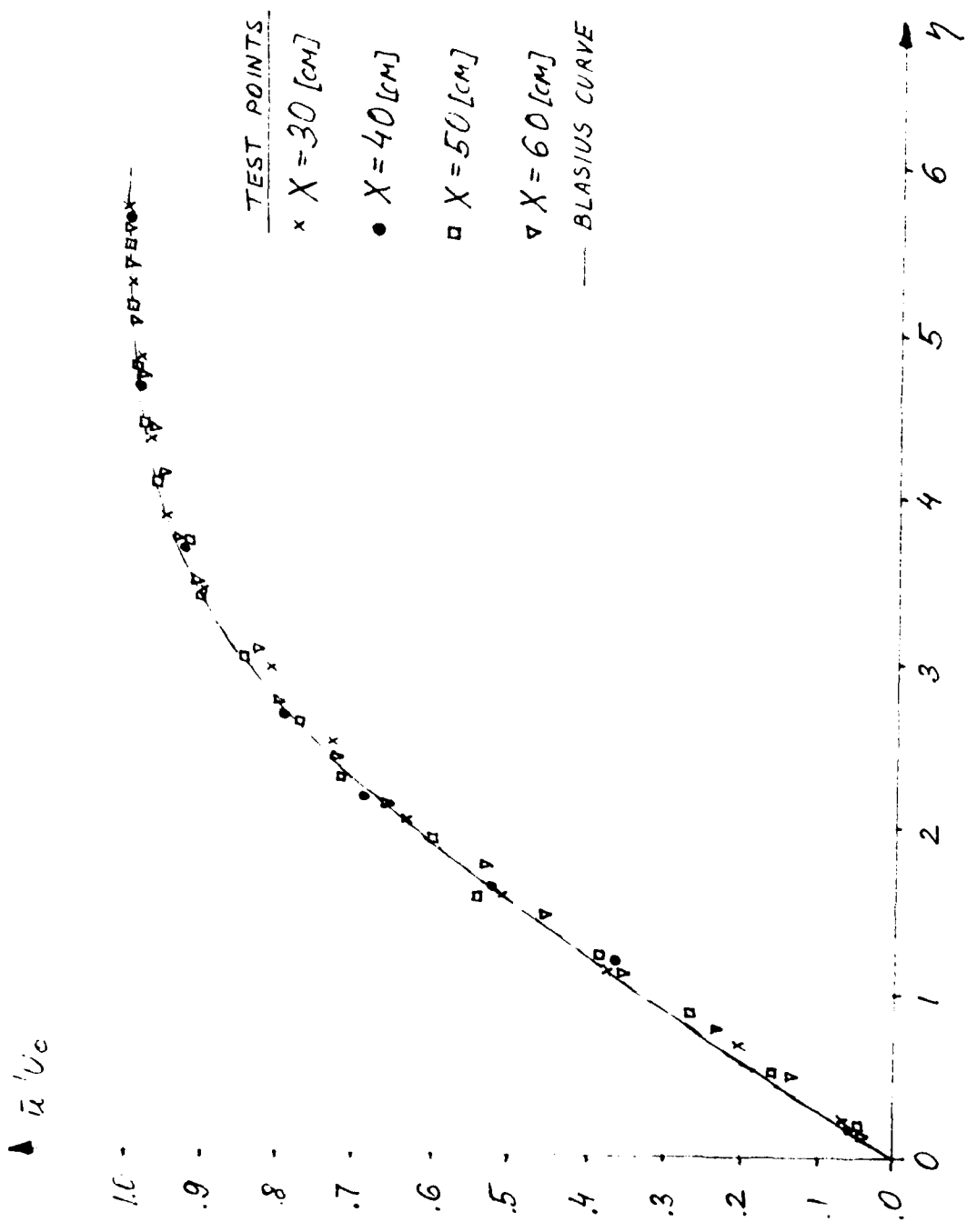


Fig. 23. Mean velocity profiles for the plate tilted at 1° angle of attack.

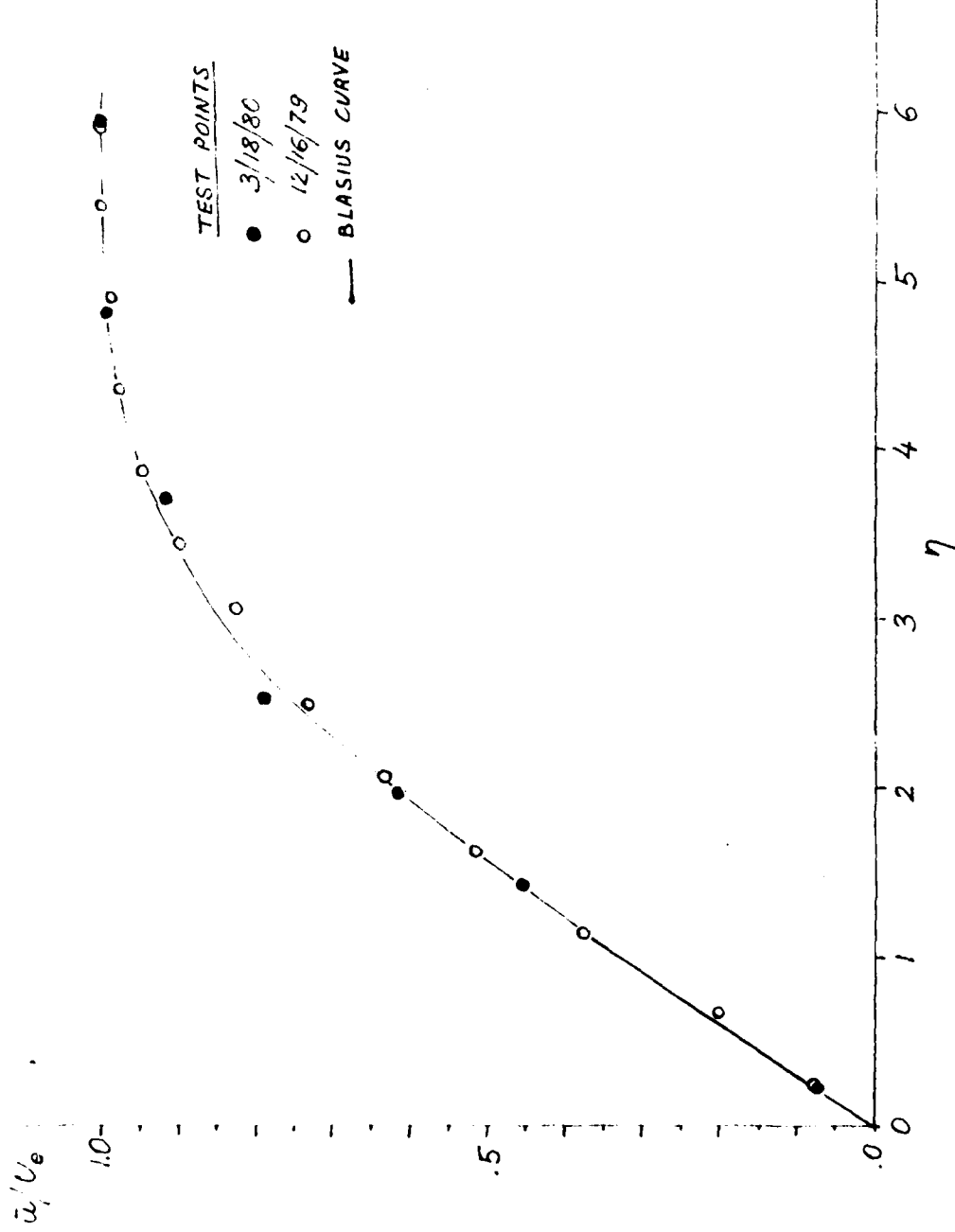


Fig. 24a. Mean velocity profile for a smooth plate, $x = 3$ cm.

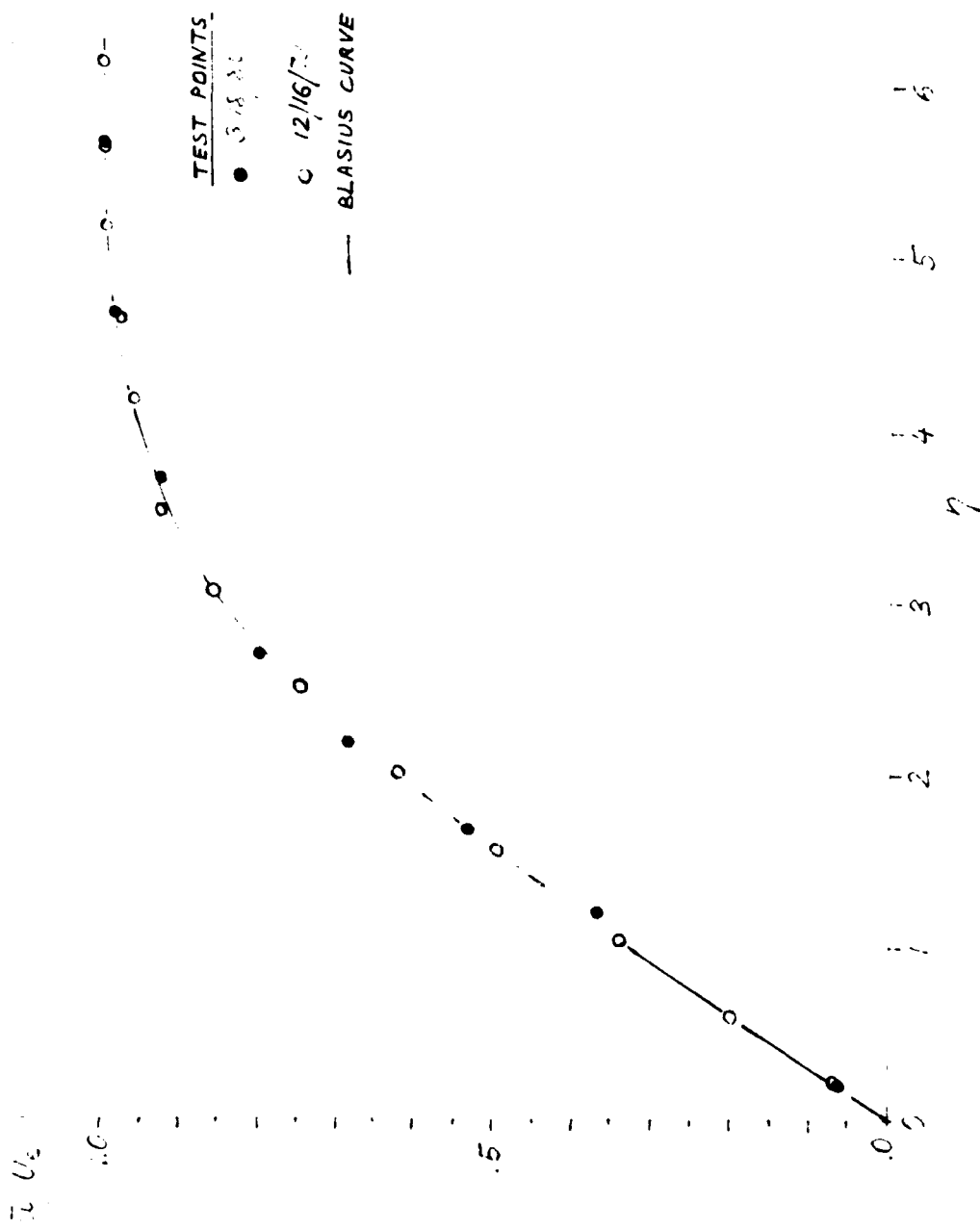


Fig. 22b. Mean velocity profile for a smooth plate, $X = 20$ cm.

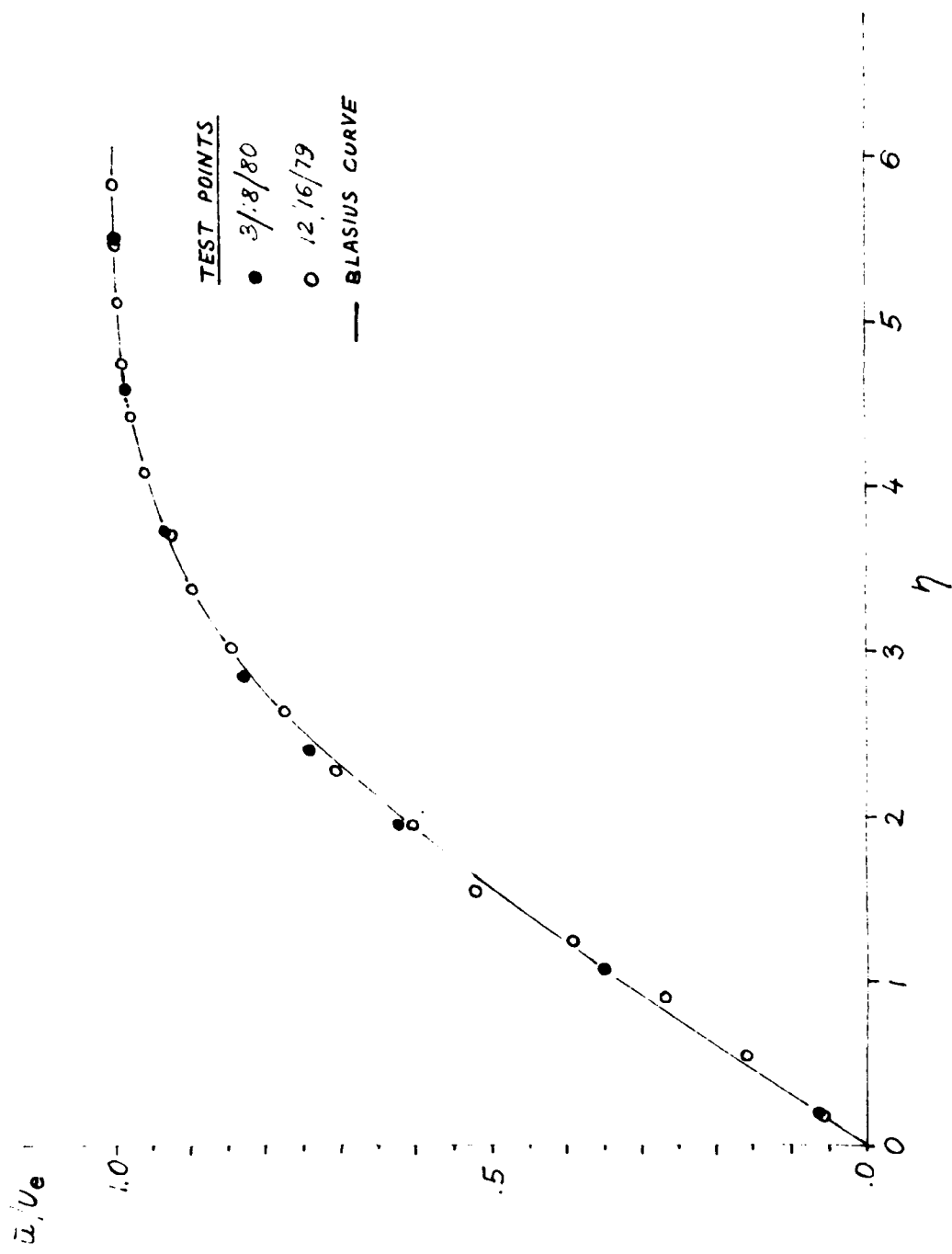


Fig. 24c. Mean velocity profile for a smooth plate, $X = 50$ cm.

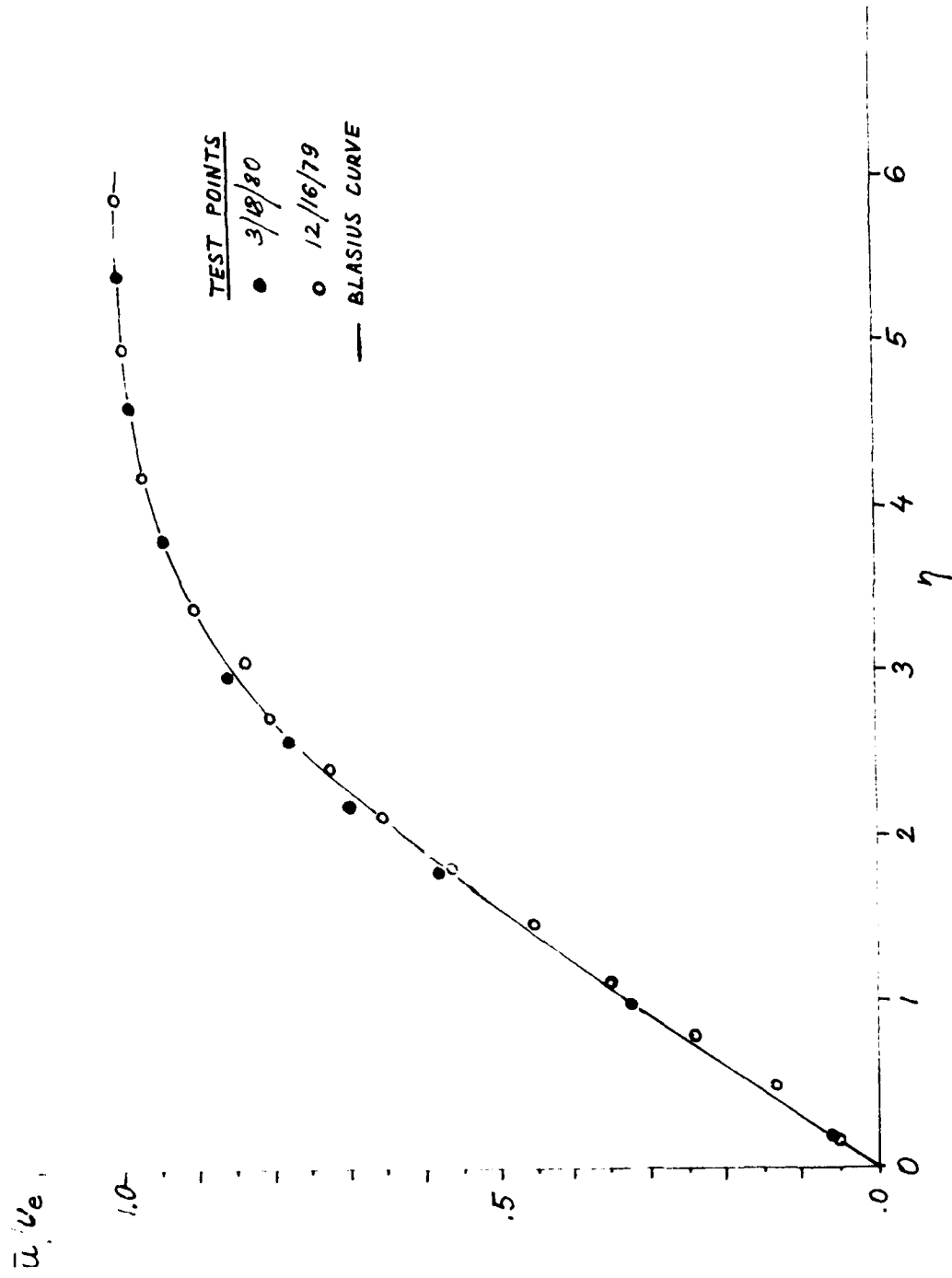


Fig. 24d. Mean velocity profile for a smooth plate, $X = 60$ cm.

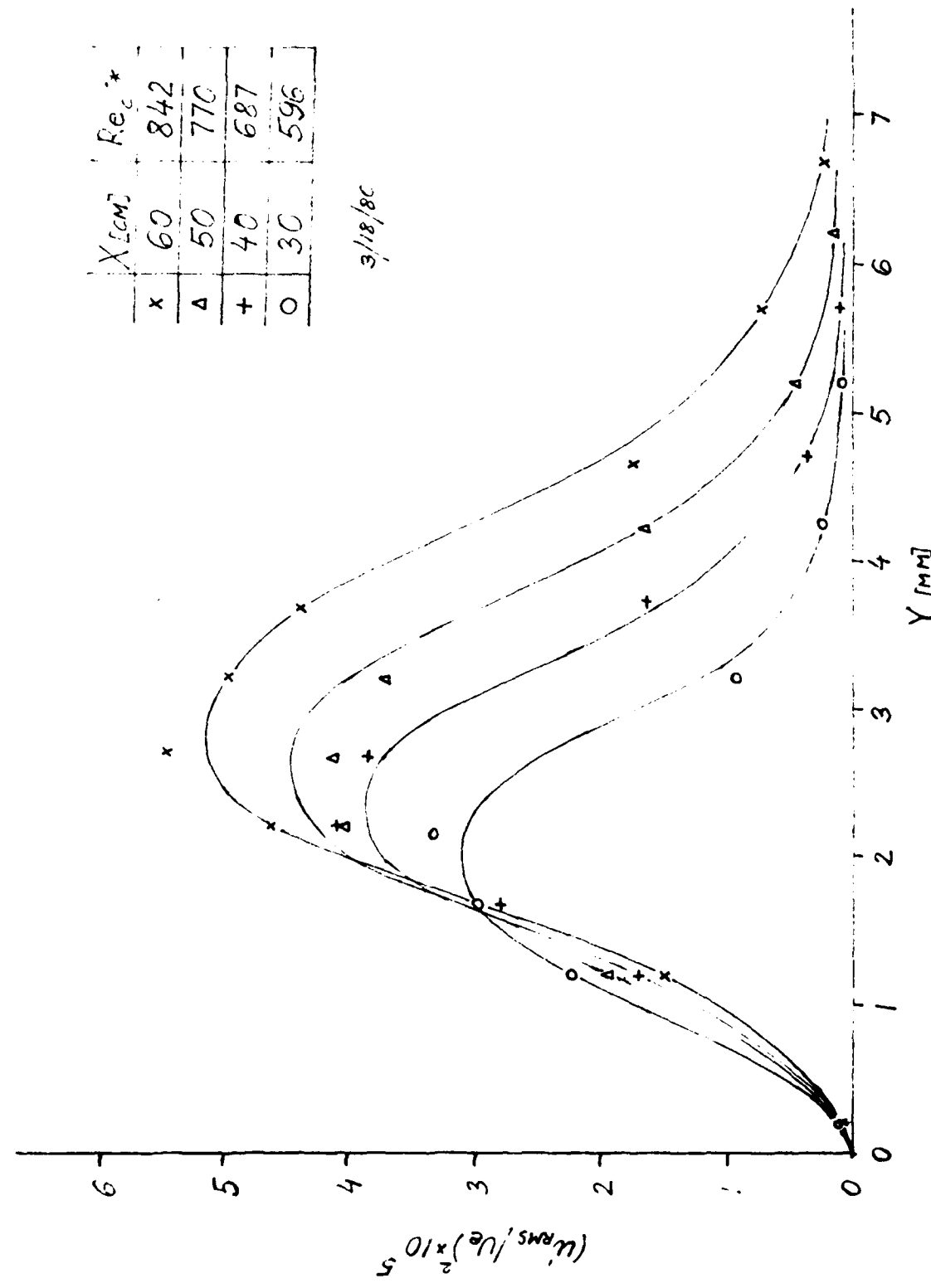


Fig. 25a. Energy profiles for a smooth plate, $U_e = 6.1 \text{ m/sec.}$

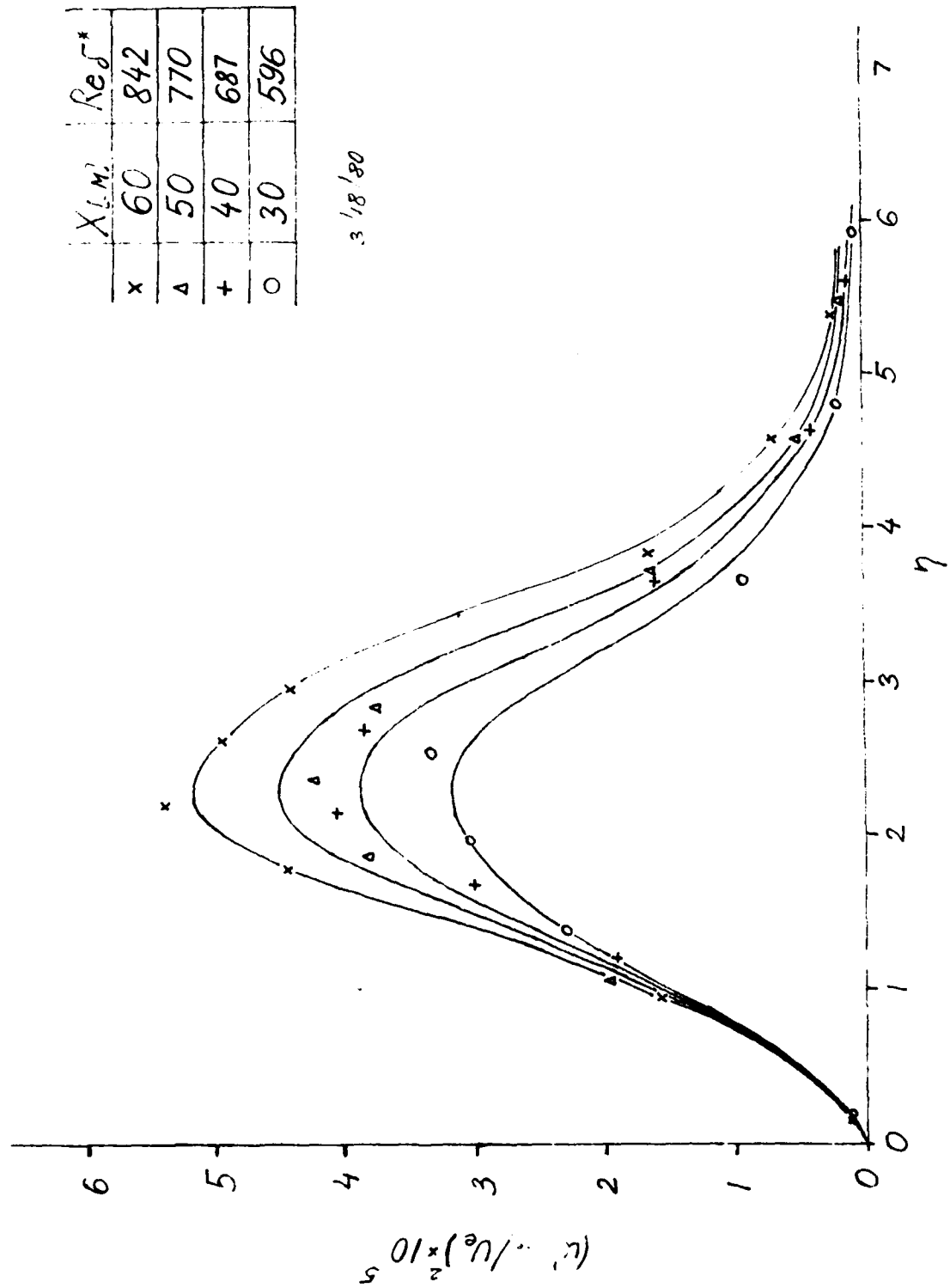


Fig. 25b. Energy profiles for a smooth plate, $U_e = 6.1$ m/sec.

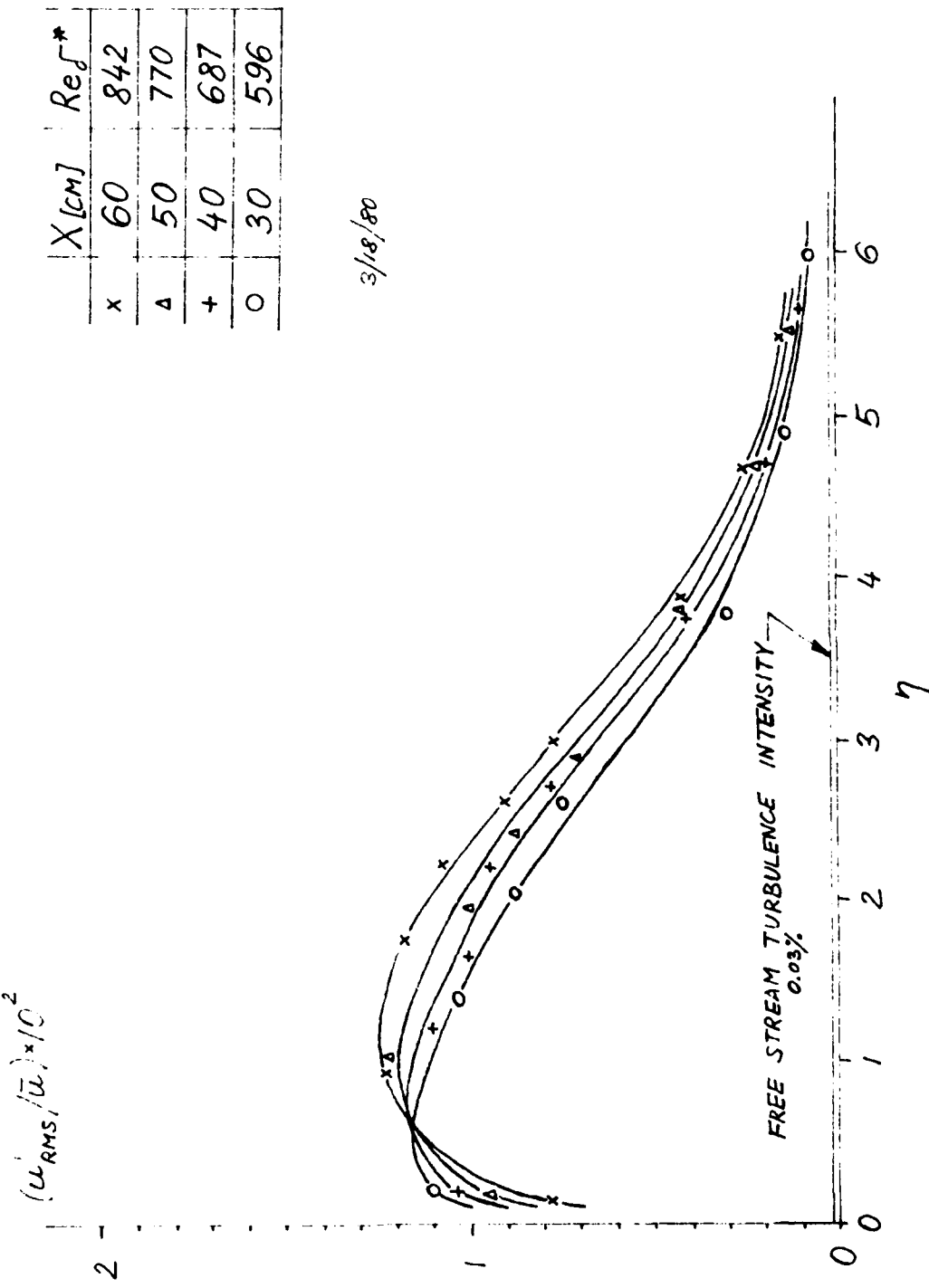


Fig. 26. Local intensity profiles along a smooth plate, $U_e = 6.1 \text{ m/sec.}$

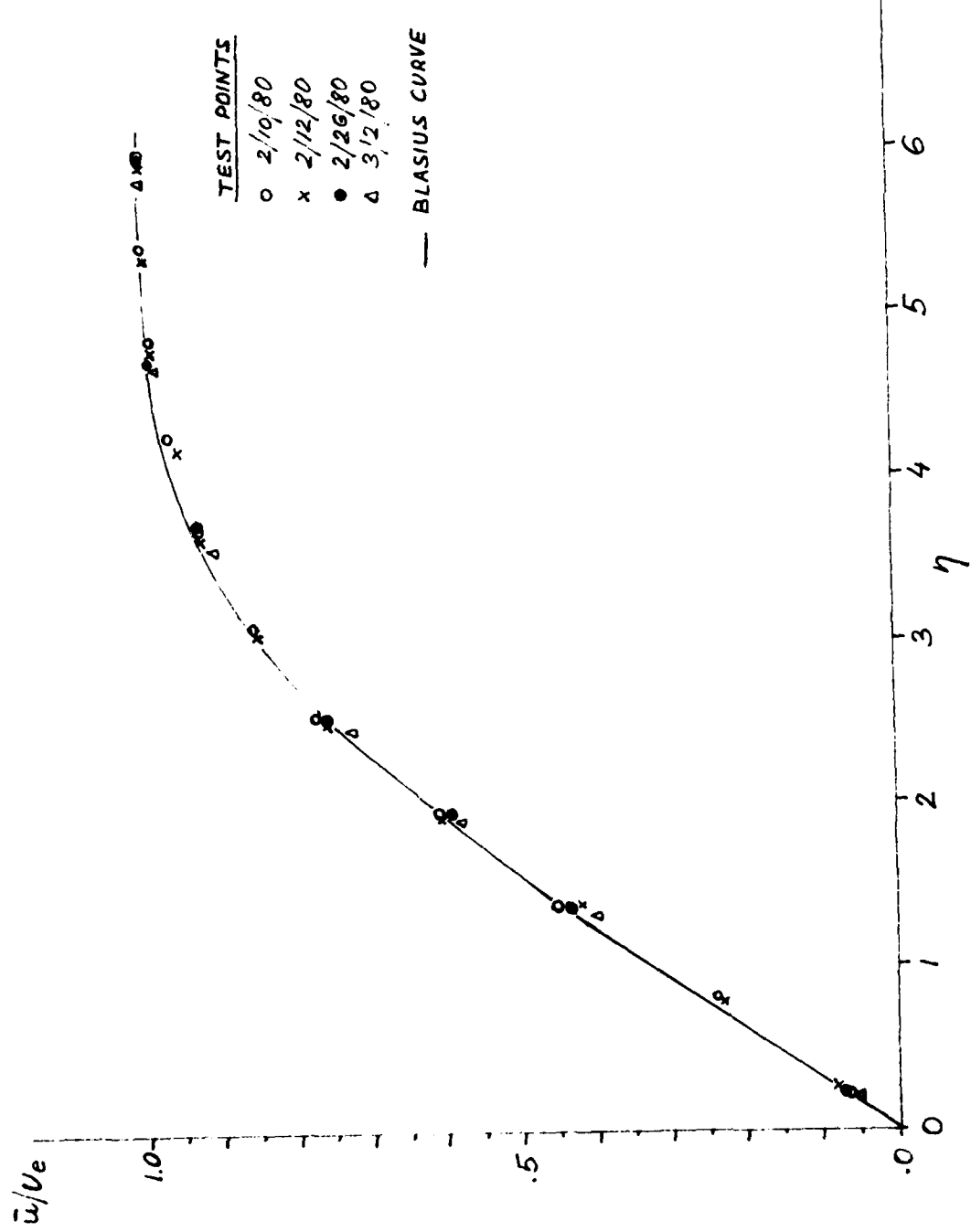


Fig. 27a. Mean velocity profile for a rough plate, Re_k ($X = 30$ cm) = 10,6; $X = 30$ cm.

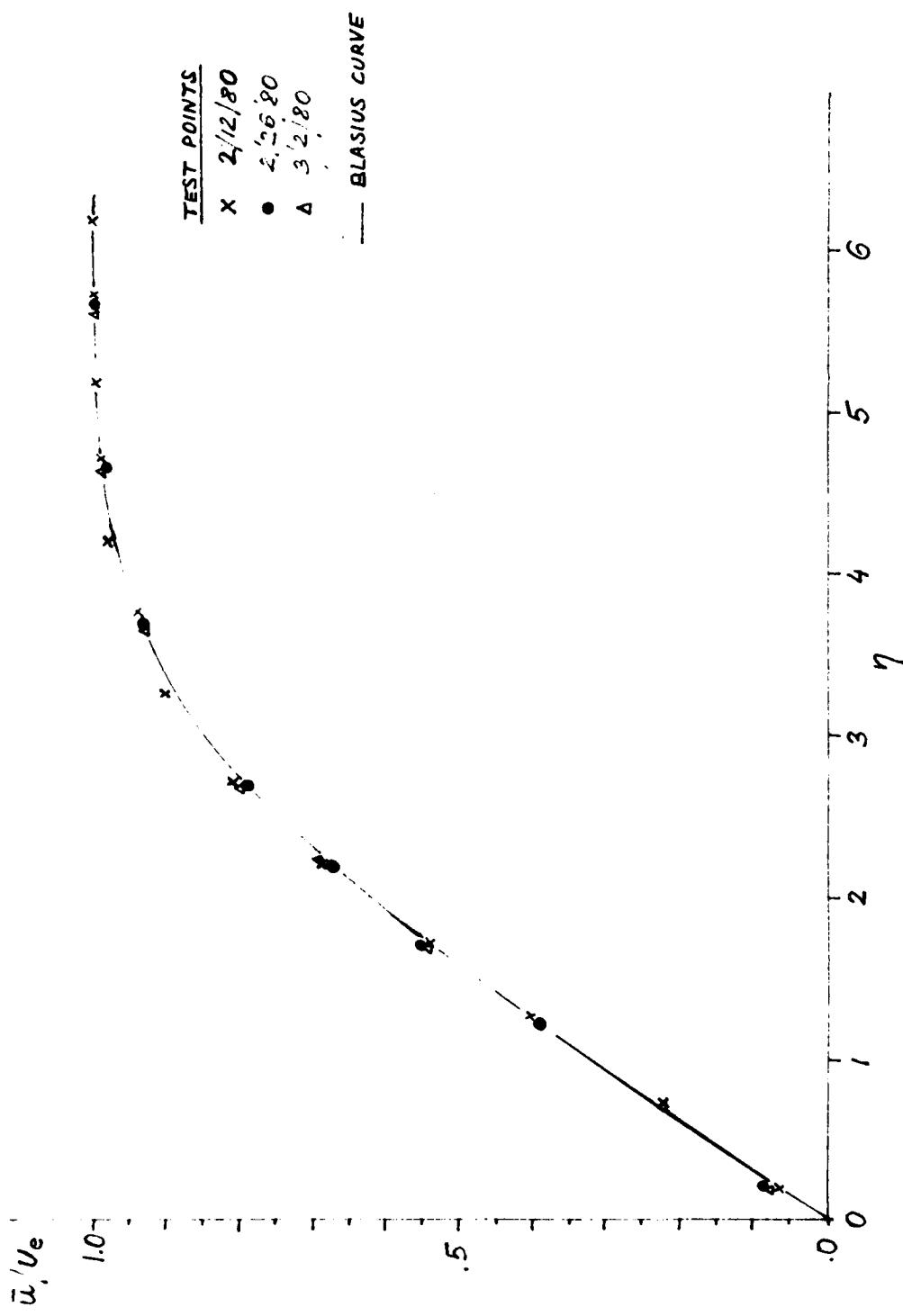


Fig. 27b. Mean velocity profile for a rough plate, Re_k ($X = 30$ cm) = 10.6; $X = 40$ cm.

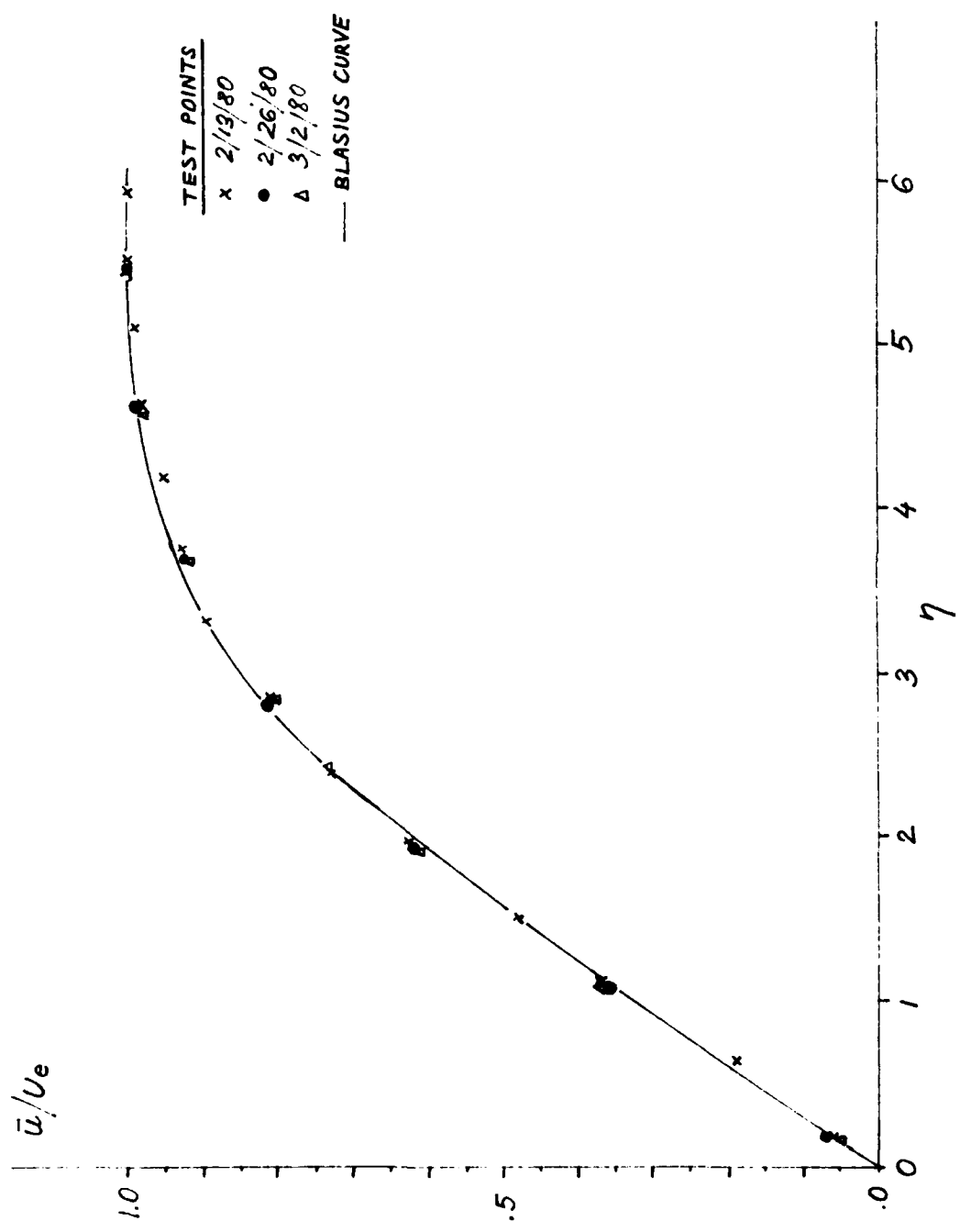


Fig. 27c. Mean velocity profile for a rough plate, Re_k ($X = 30$ cm) = 10.6; $X = 50$ cm.

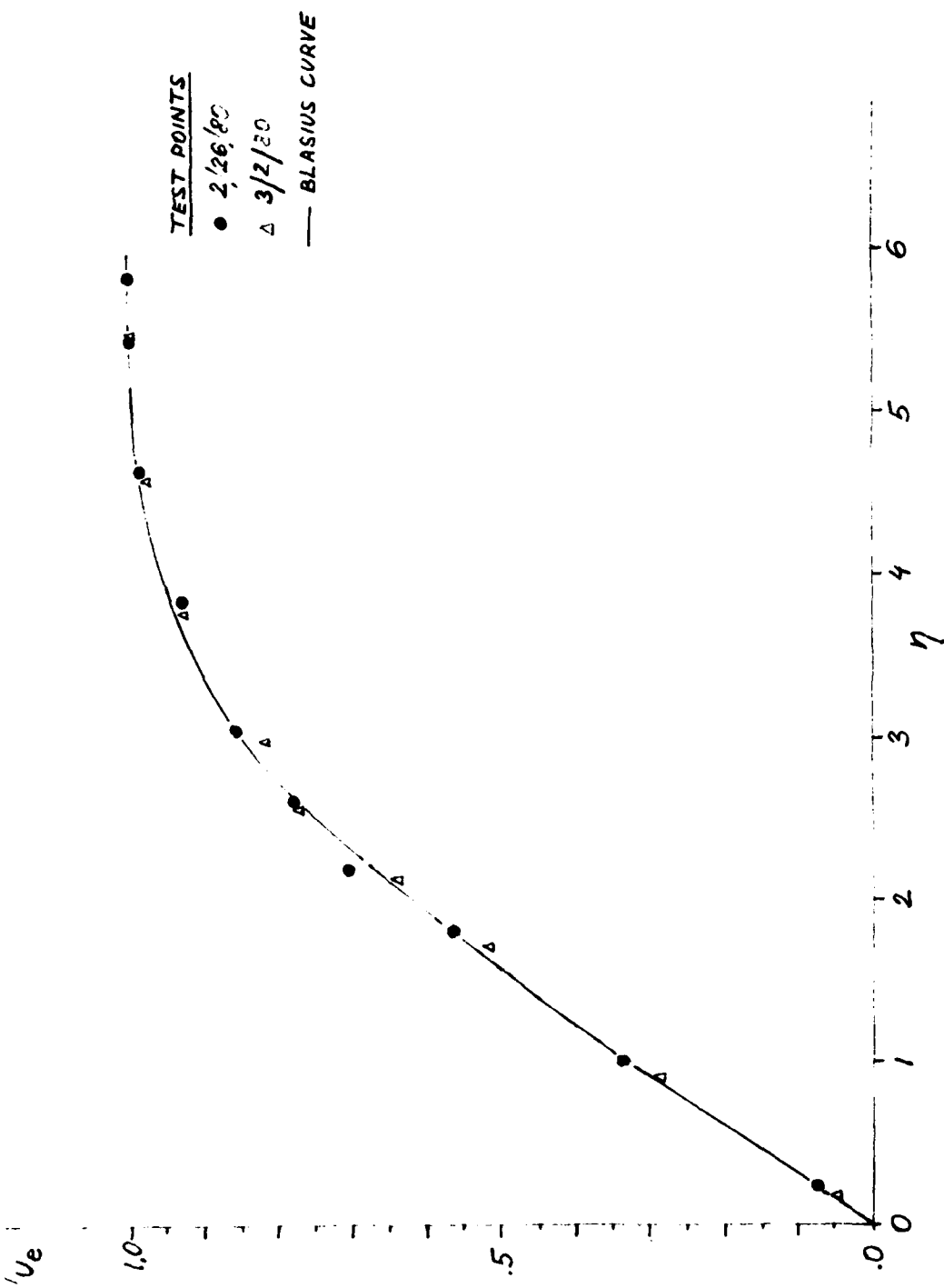


Fig. 27d. Mean velocity profile for a rough plate, Re_k ($X = 30$ cm) = 10.6; $X = 60$ cm.

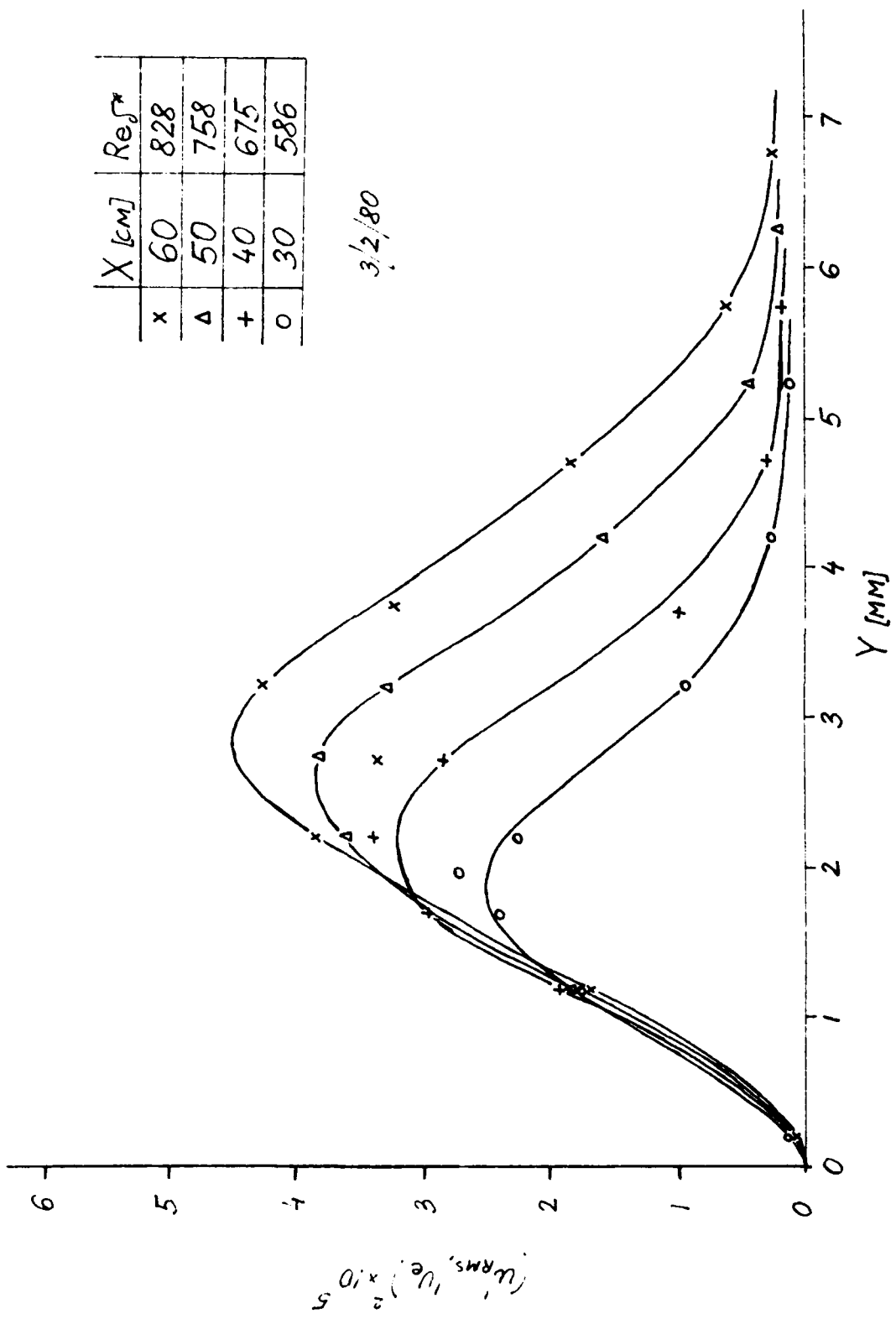


Fig. 28a. Energy profiles for a rough plate, Re_k ($X = 30$ cm) = 10.6; $U_e = 5.9$ m/sec.

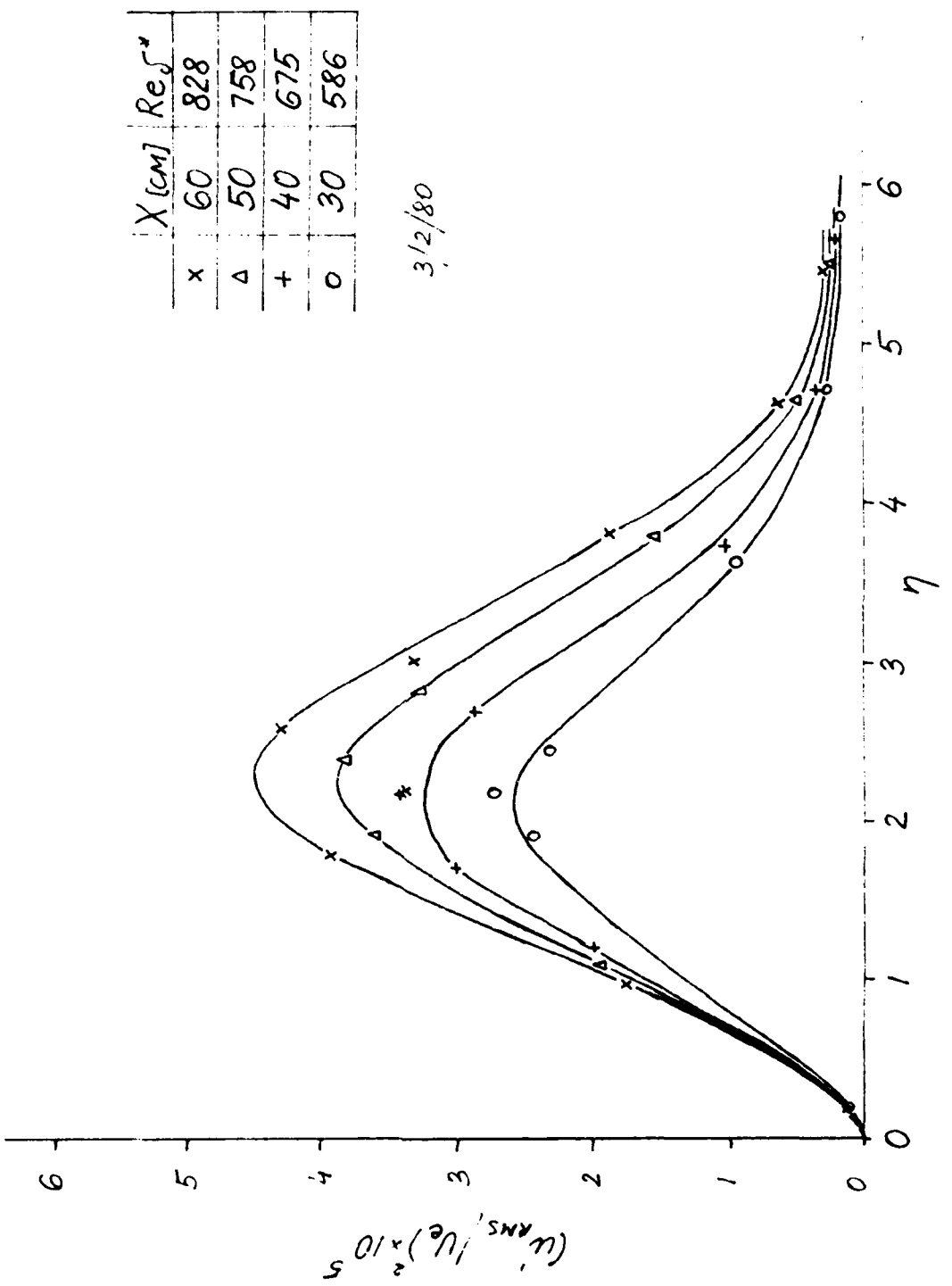


Fig. 28b. Energy profiles for a rough plate, Re_k ($X = 30$ cm) = 10.6; U_e = 5.9 m/sec.

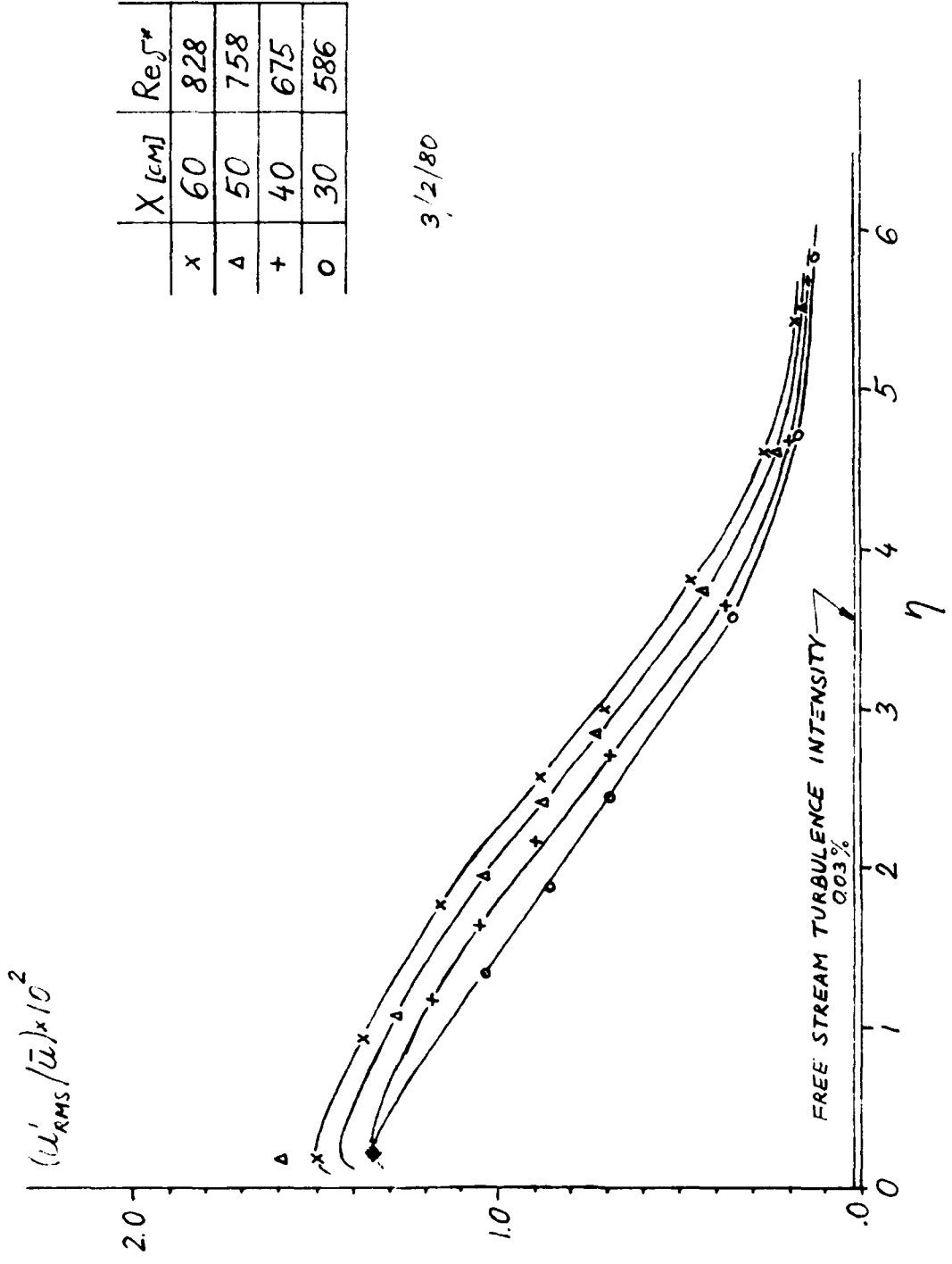


Fig. 29. Local turbulence intensity profile along a rough plate, Re_k ($X = 30$ cm) = 10.6; $U_e = 5.9$ cm/sec.

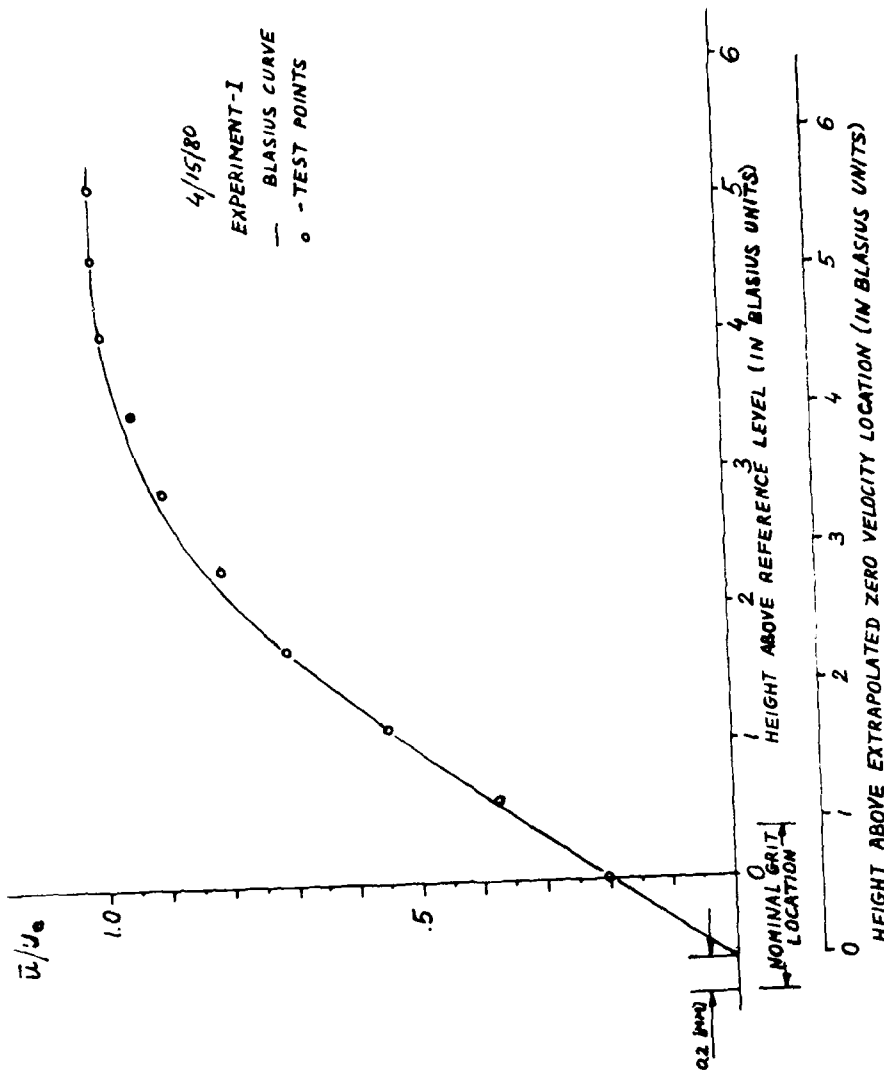


Fig. 30a. Mean velocity profile for a rough plate, Re_k ($X = 30$ cm) = 155; $X = 30$ cm.

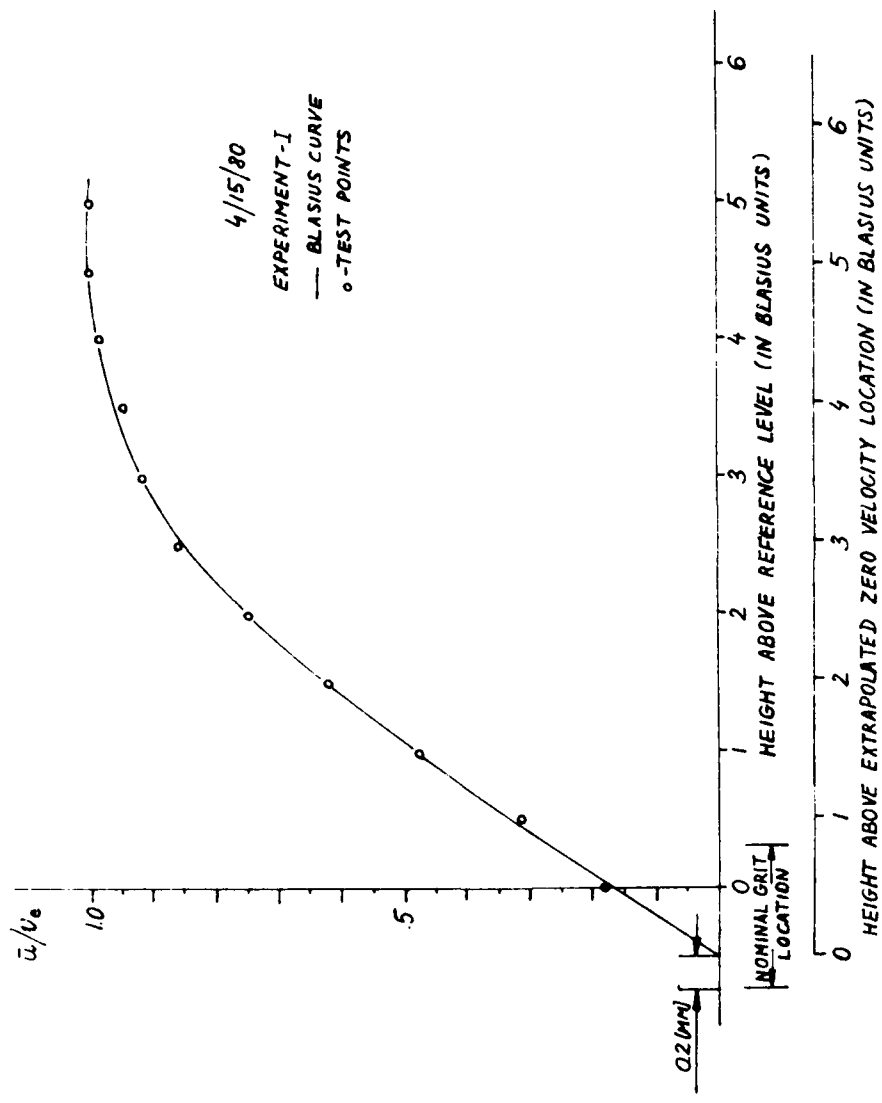


Fig. 30b. Mean velocity profile for a rough plate, Re_K ($X = 30$ cm) = 153; $X = 40$ cm.

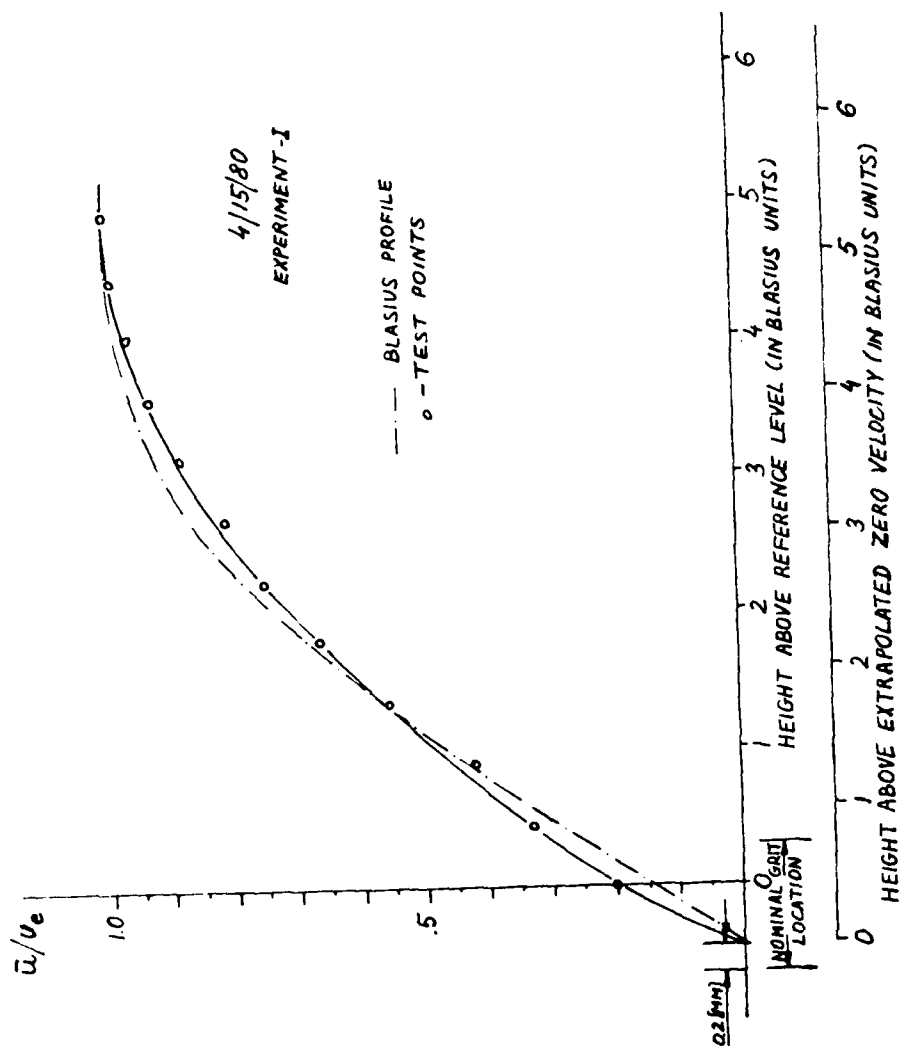


Fig. 30c. Mean velocity profile for a rough plate, Re_k ($X = 30$ cm) = 155; $X = 50$ cm.

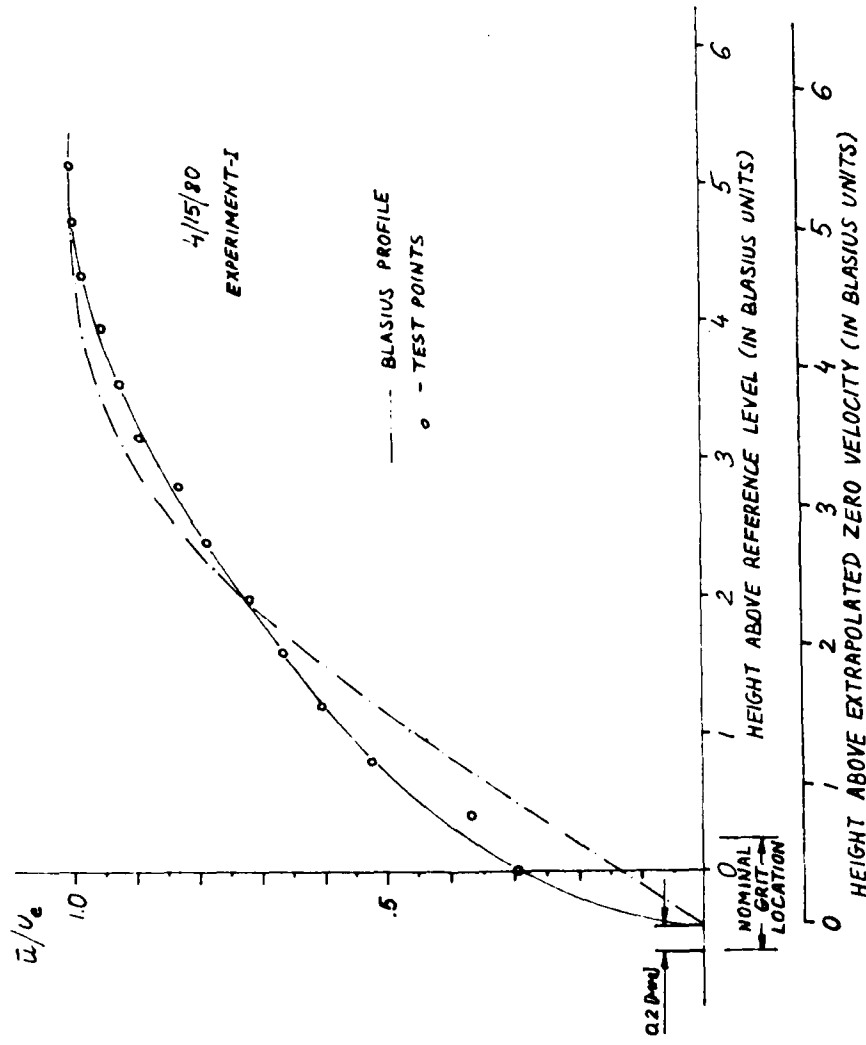
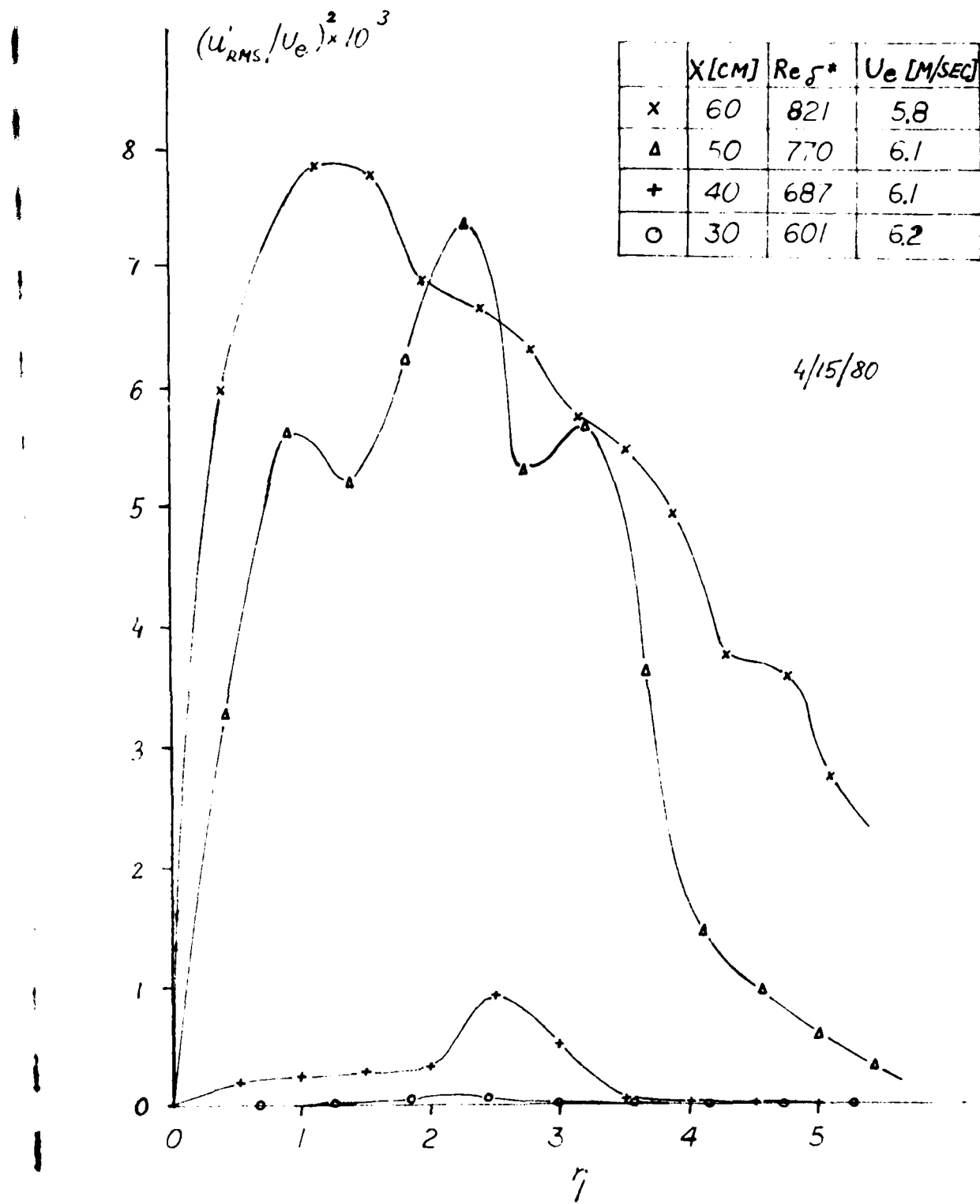


Fig. 30d. Mean velocity profile for a rough plate, Re_k ($X = 30$ cm) = 155; $X = 60$ cm.



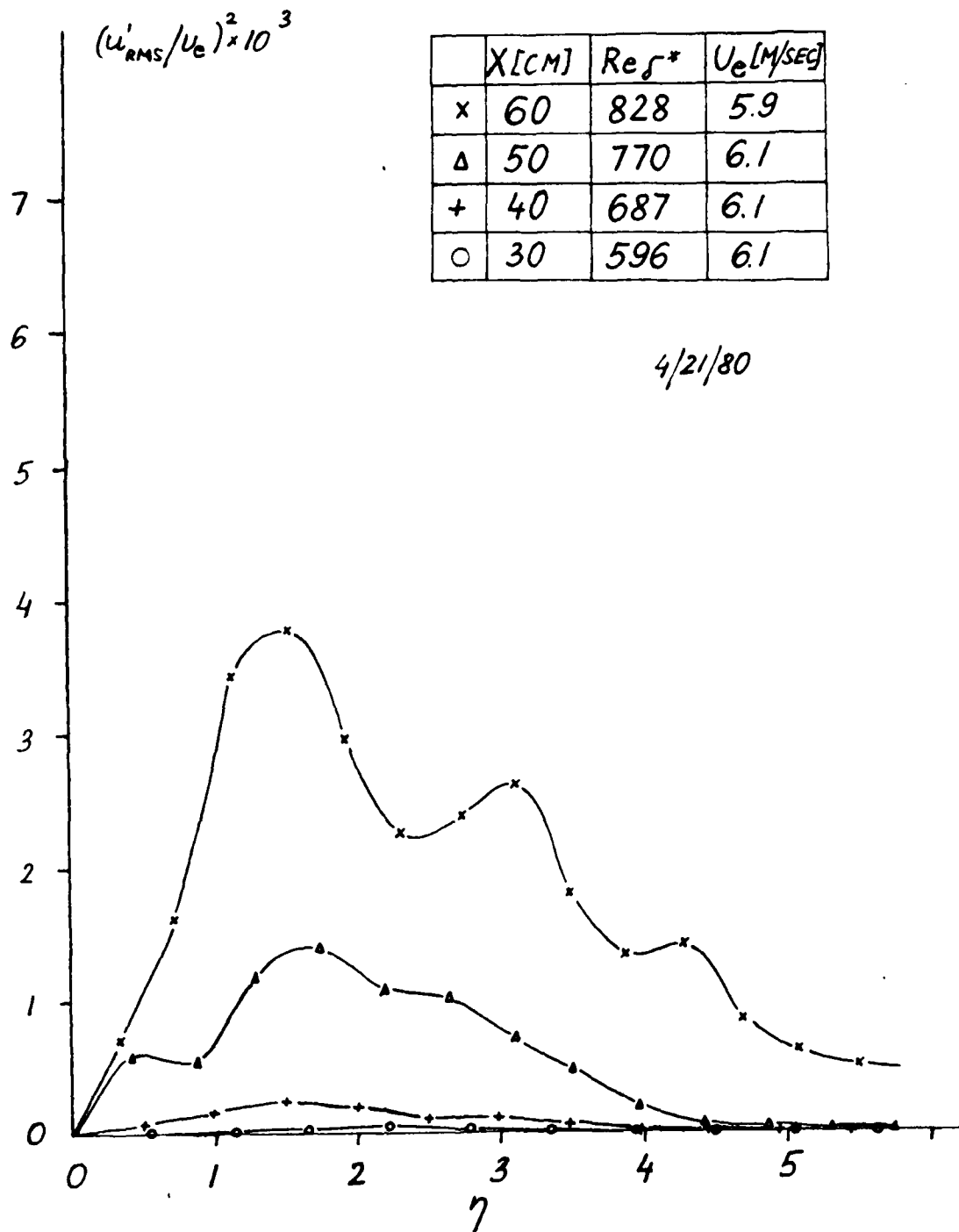


Fig. 31b. Test II - Energy profiles for a rough plate, Re_k ($X = 30$ cm) = 155.

u'_{RMS}/\bar{u}

	$X [CM]$	$Re \delta^*$	$U_e [M/SEC]$	A_{MAX}/A_0	A_e/A_0
x	60	821	5.8	75	7.4
Δ	50	770	6.1	5.1	2.7
+	40	687	6.1	3.9	4.7
○	30	601	6.2	0.98	3.2

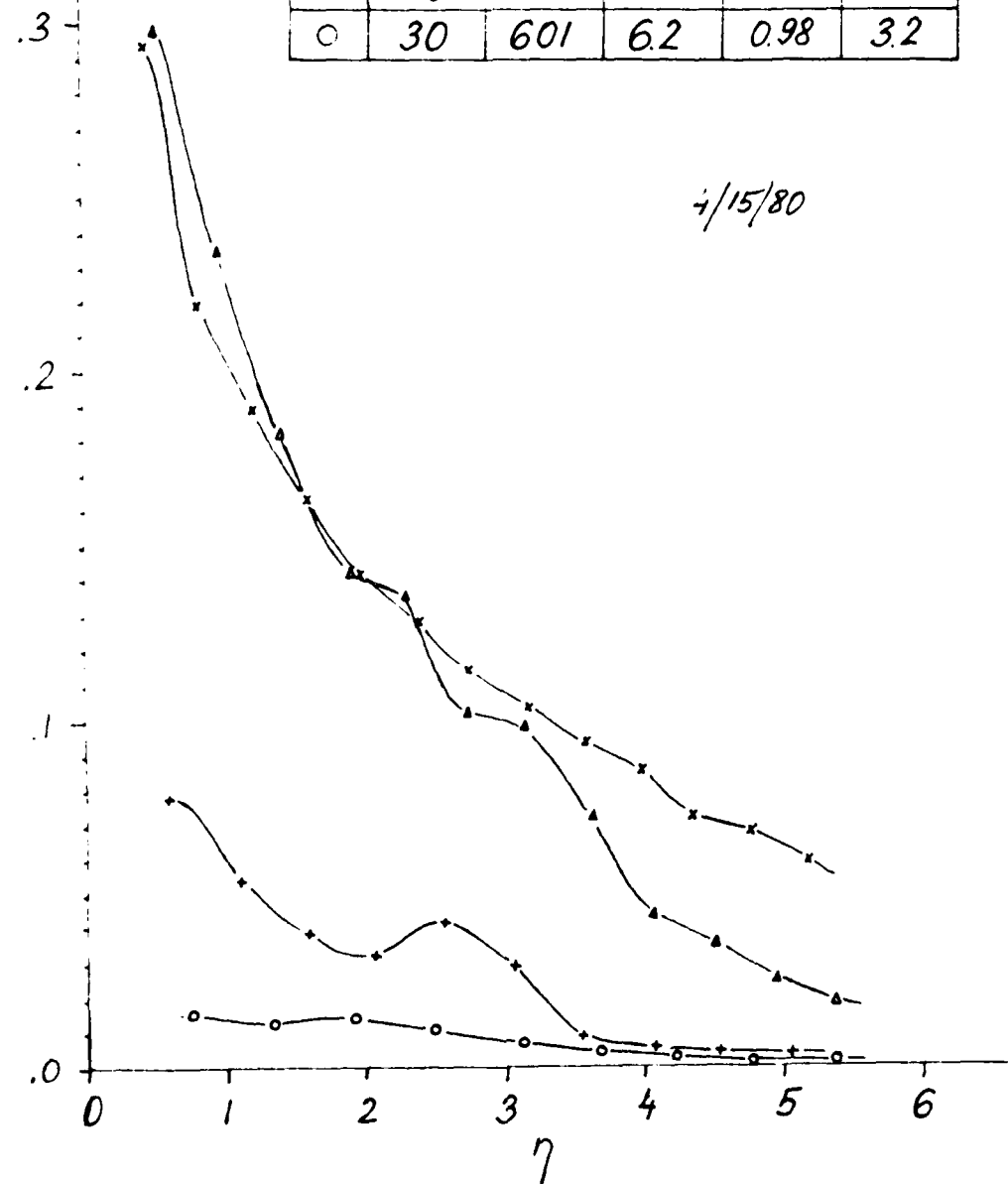


Fig. 32a. Test I - Local turbulence intensity profiles for a rough plate,
 Re_k ($X = 30$ cm) = 155.

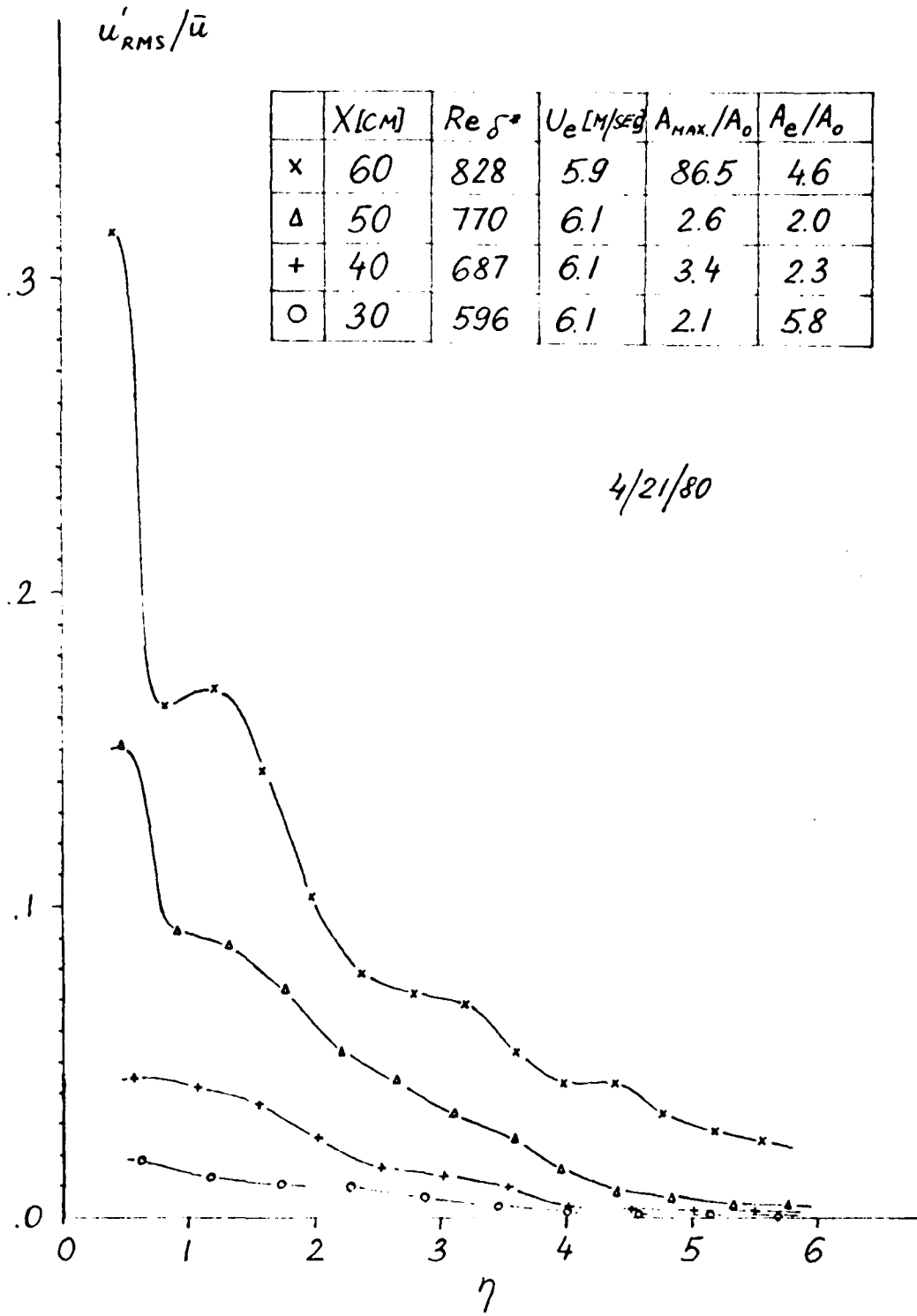


Fig. 32b. Test 11 - Turbulence intensity profiles for a rough plate,
 Re_k ($X = 30$ cm) = 155.

$$(u'_{RMS}/\bar{u})_{ROUGH} - (u'_{RMS}/\bar{u})_{SMOOTH}$$

(FIG. 326) - (FIG. 26)

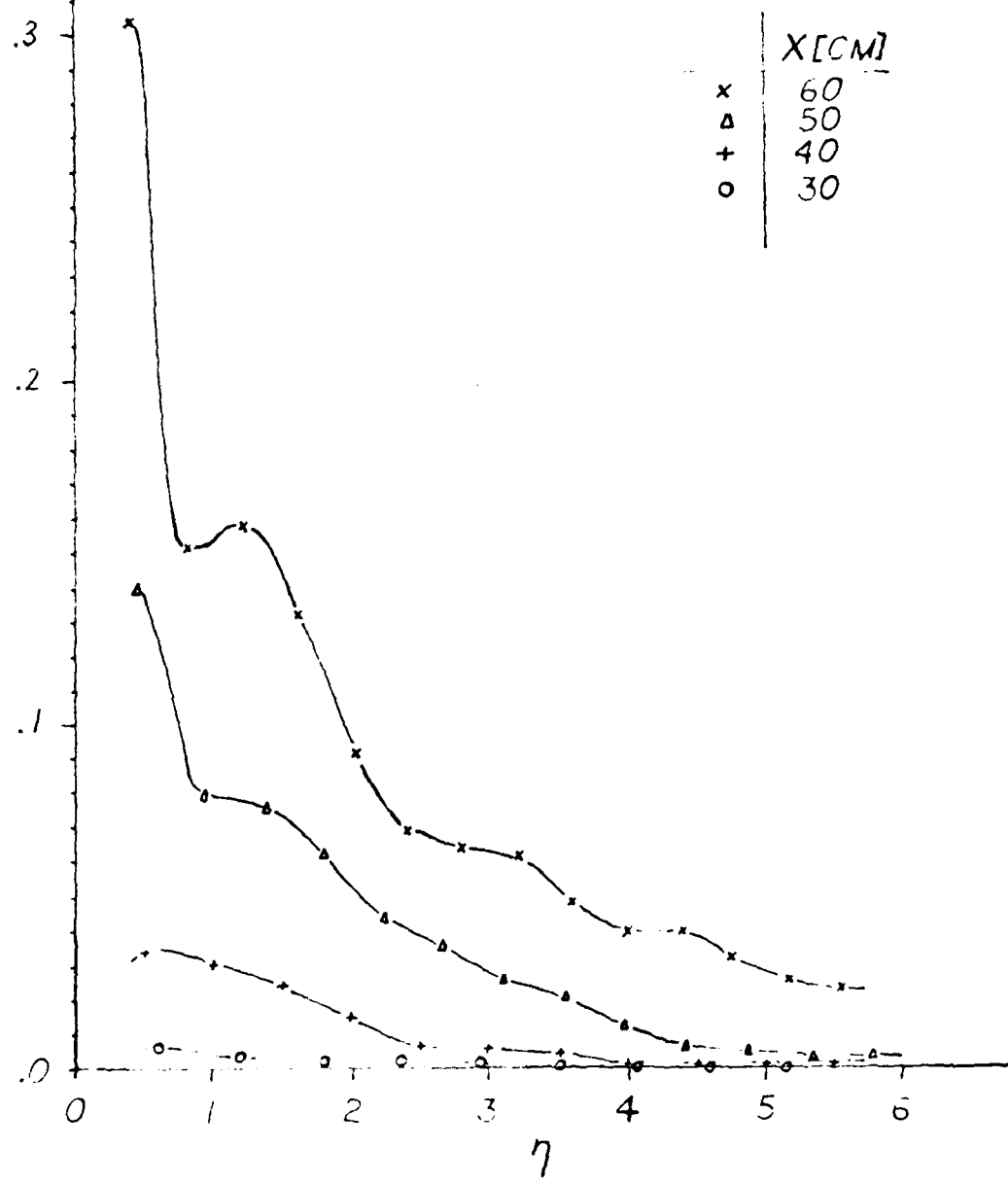


Fig. 33. Test II ~ Local turbulence intensity due to roughness only,
 Re_k ($X = 30$ cm) = 155.

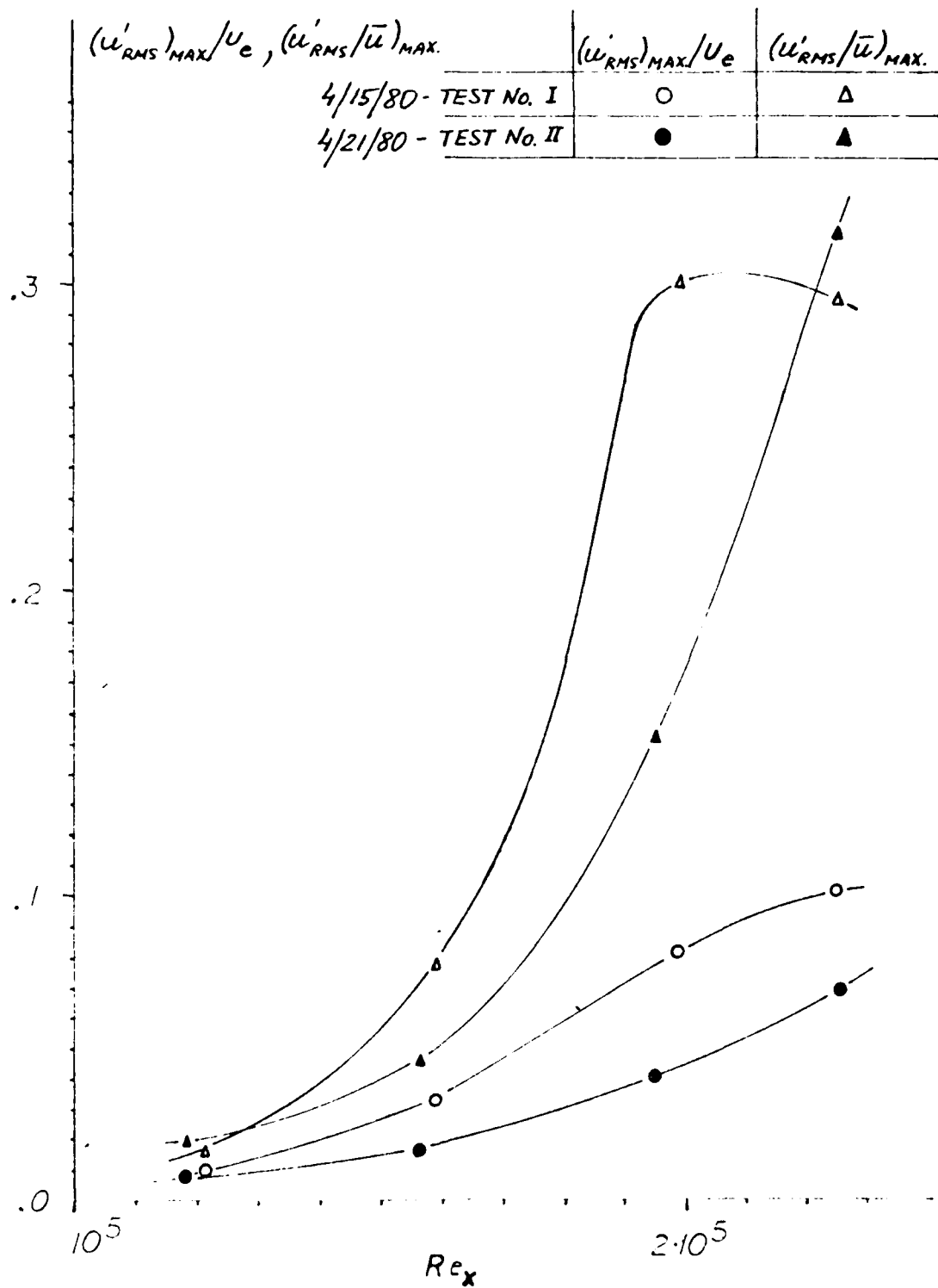


Fig. 34. $(u'_{\text{rms}})_{\text{MAX}}/U_e$ and $(u'_{\text{rms}}/\bar{u})_{\text{MAX.}}$ versus Re_x for Test I and II,
 Re_k ($X = 30$ cm) = 155.

5/2/80

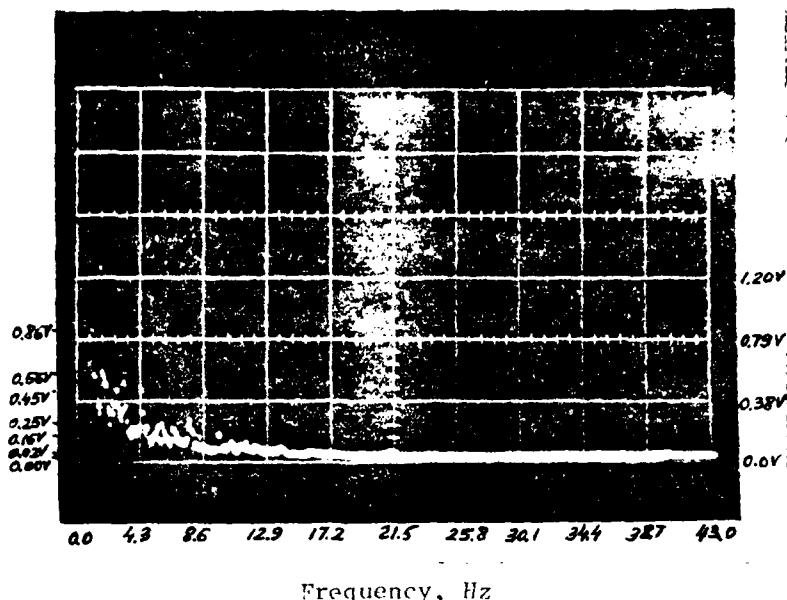


Fig. 35. Spectrum at $X = 20$ cm, $Y = 1.0$ mm.
 Re_k ($X = 30$ cm) = 155

5/2/80

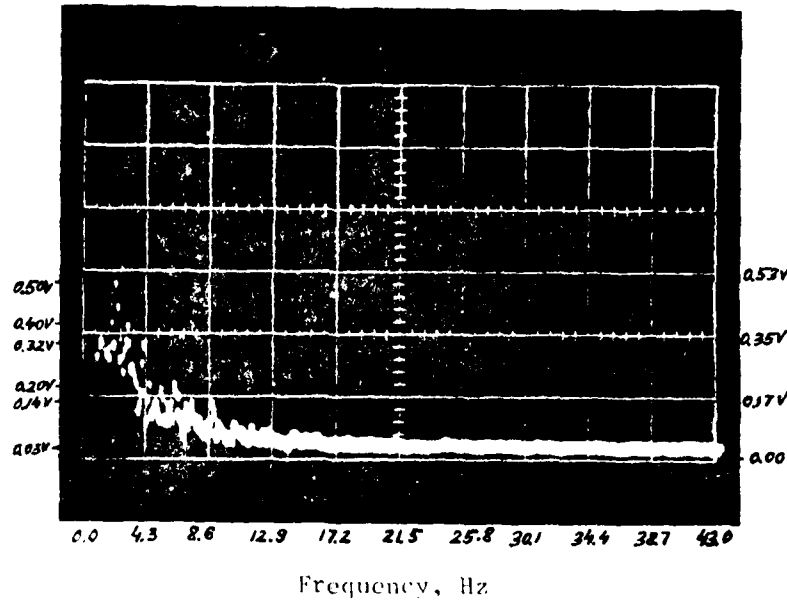


Fig. 36. Spectrum at $X = 30$ cm, $Y = 1.5$ mm.
 Re_k ($X = 30$ cm) = 155

5/2/80

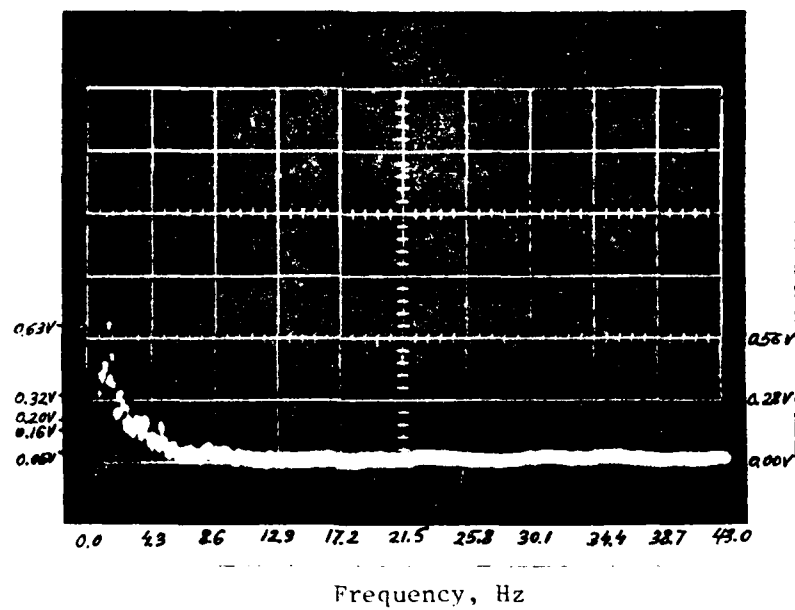


Fig. 37. Spectrum at $X = 40$ cm, $Y = 1.7$ mm.
 Re_k ($X = 30$ cm) = 155

5/2/80

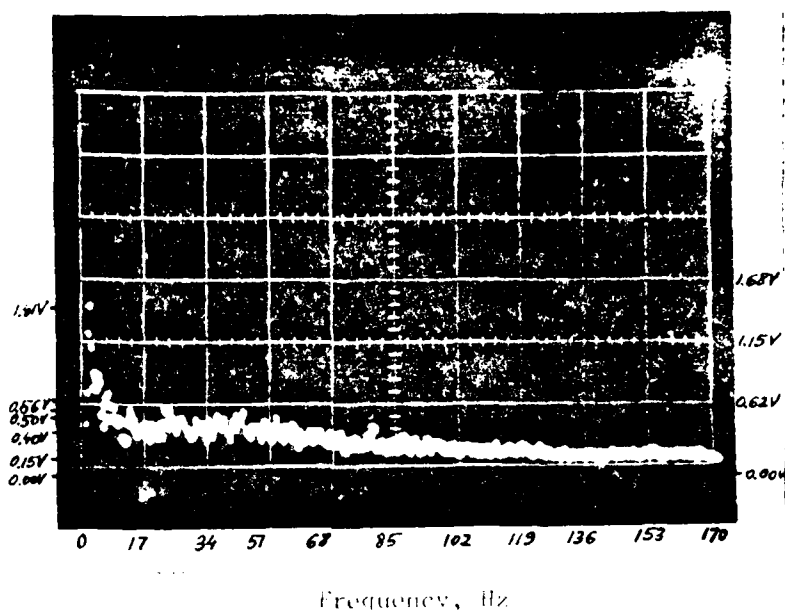


Fig. 38. Spectrum at $X = 50$ cm, $Y = 1.75$ mm.
 Re_K ($X = 30$ cm) = 155

5/2/80

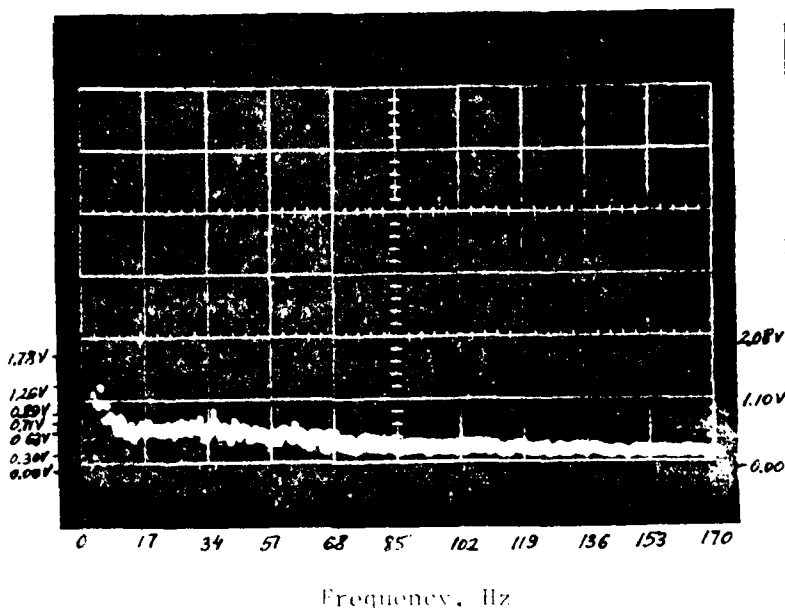


Fig. 39. Spectrum at $X = 60$ cm, $Y = 1.25$ mm.
 Re_K ($X = 30$ cm) = 155

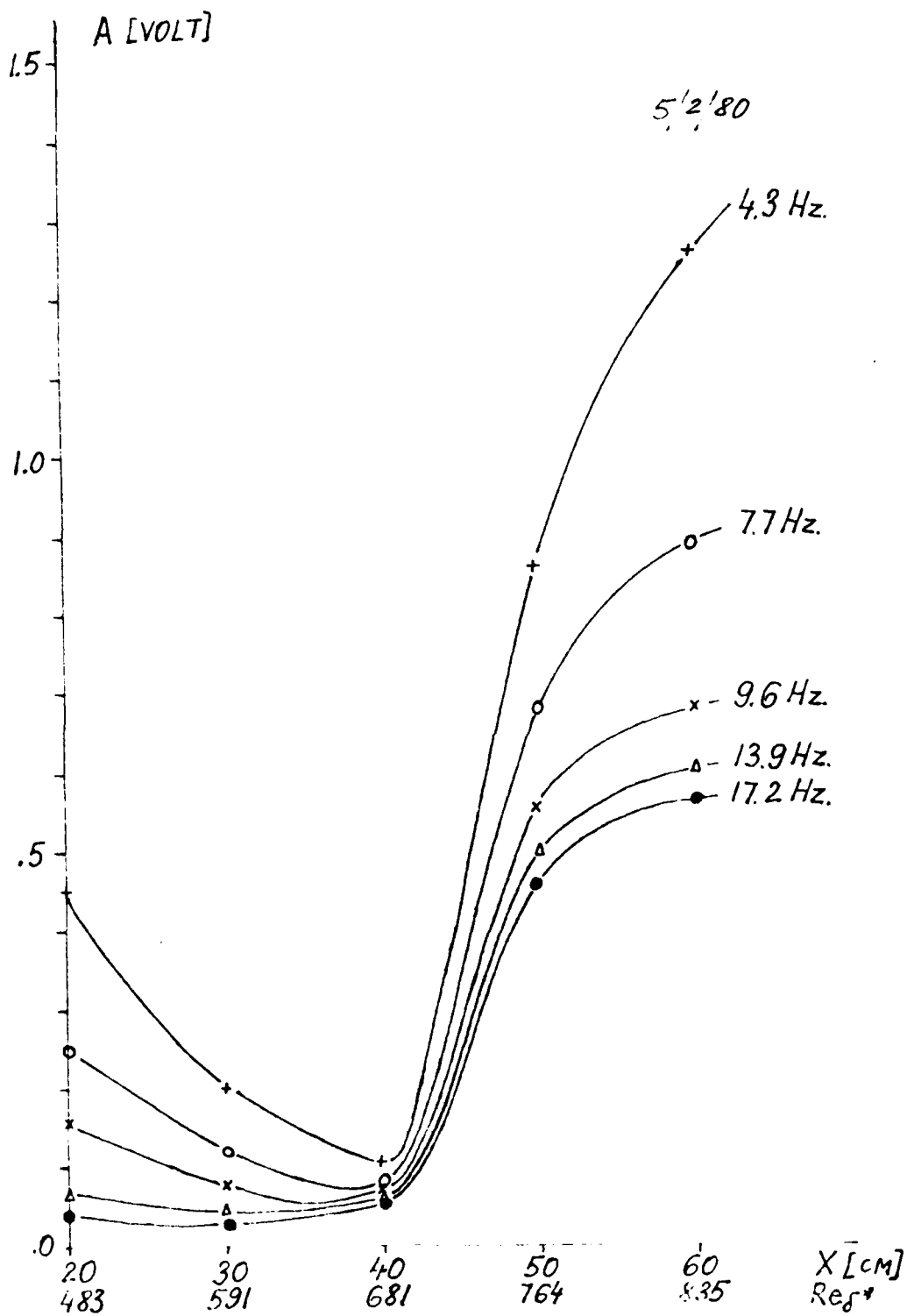


Fig. 40. Amplitudes of disturbances with frequencies from 4.3 Hz to 17.2 Hz versus X ; Re_k ($X = 30$ cm) = 155.

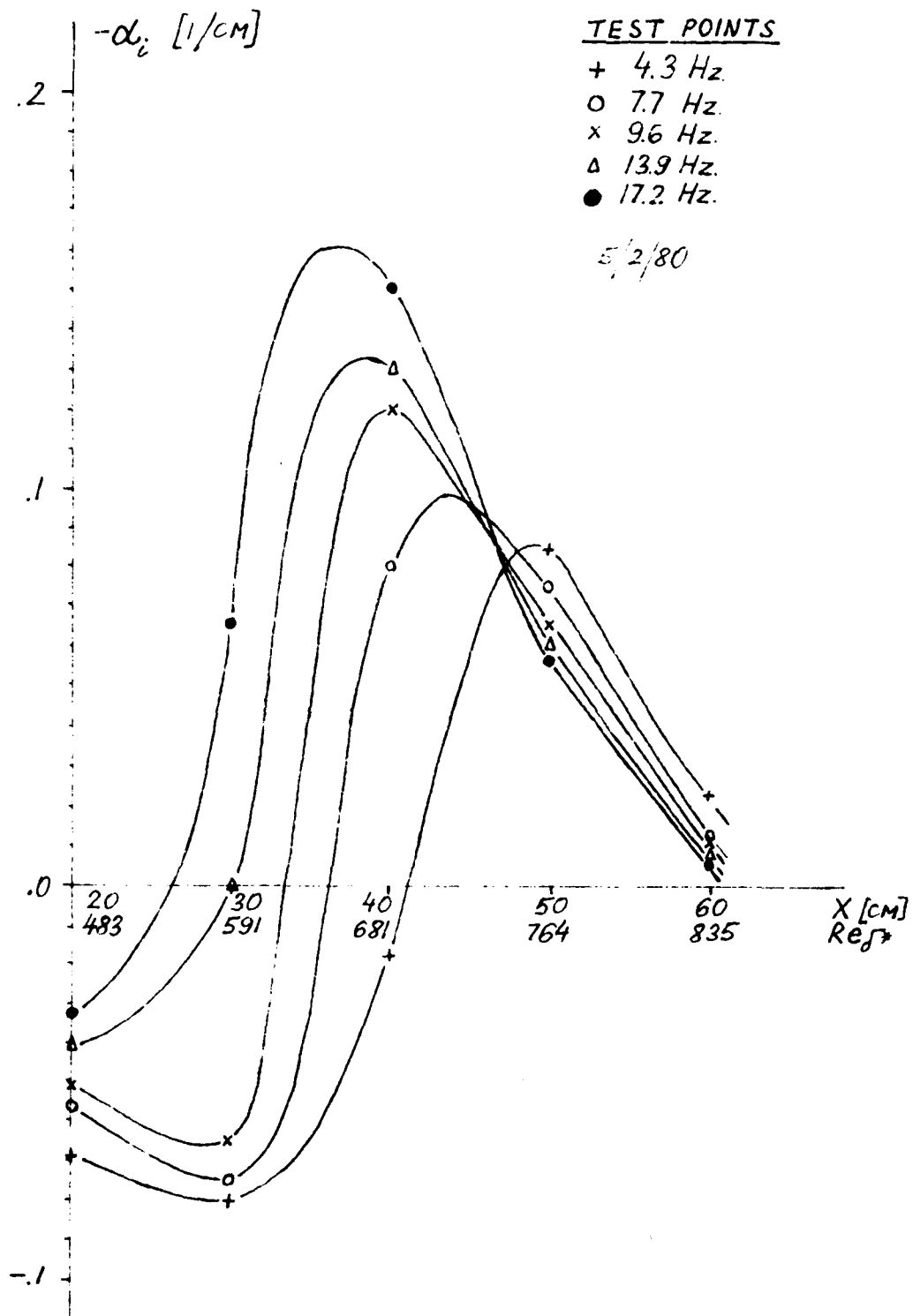


Fig. 41. Amplification rates versus X , for disturbances with frequencies from 4.3 Hz to 17.2 Hz; Re_k ($X = 30$ cm) = 155.

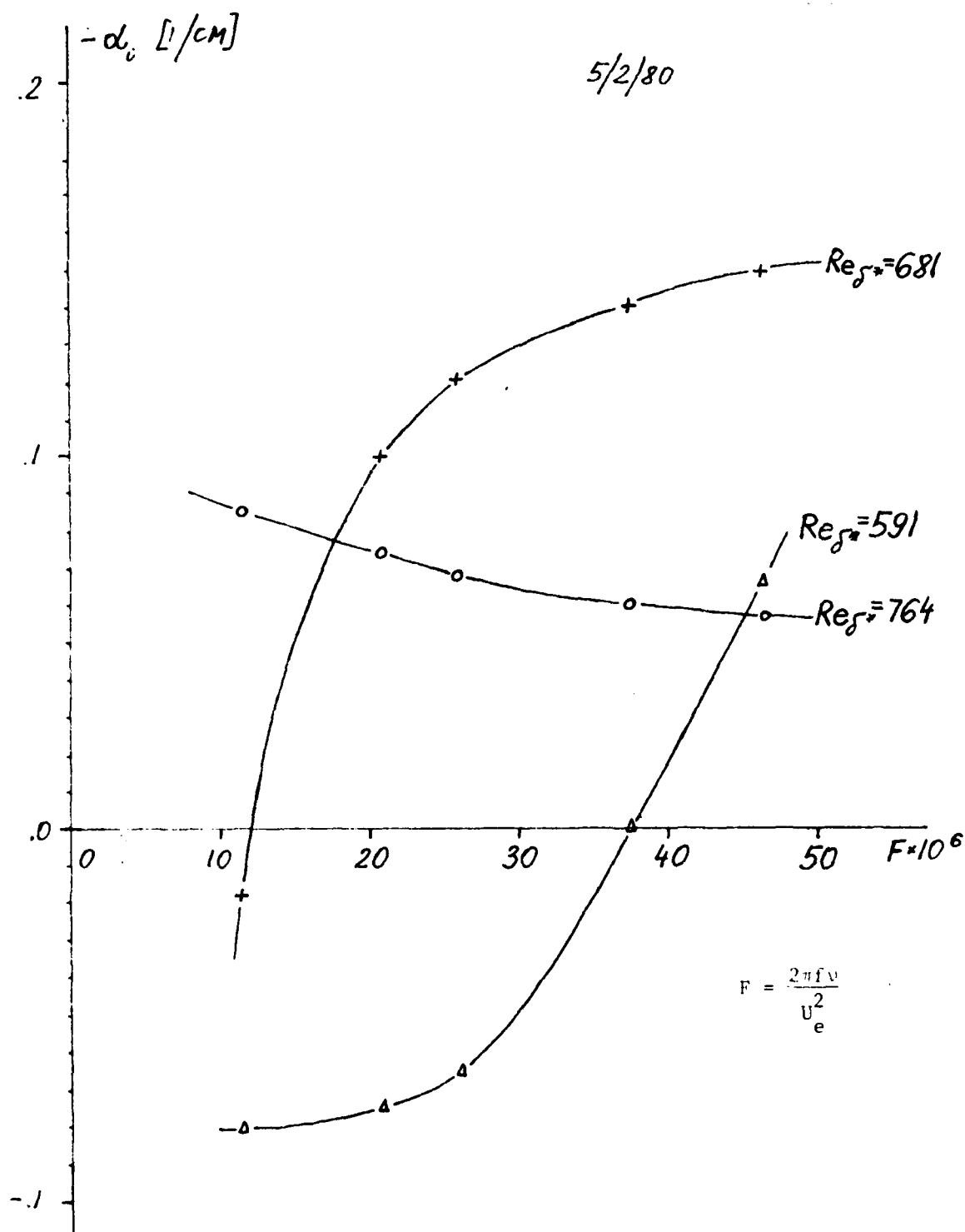


Fig. 42. Amplification rate versus frequency for a constant Re_{s^*} in the 4.3 Hz to 17.2 Hz band; Re_k ($X = 30$ cm) = 155.

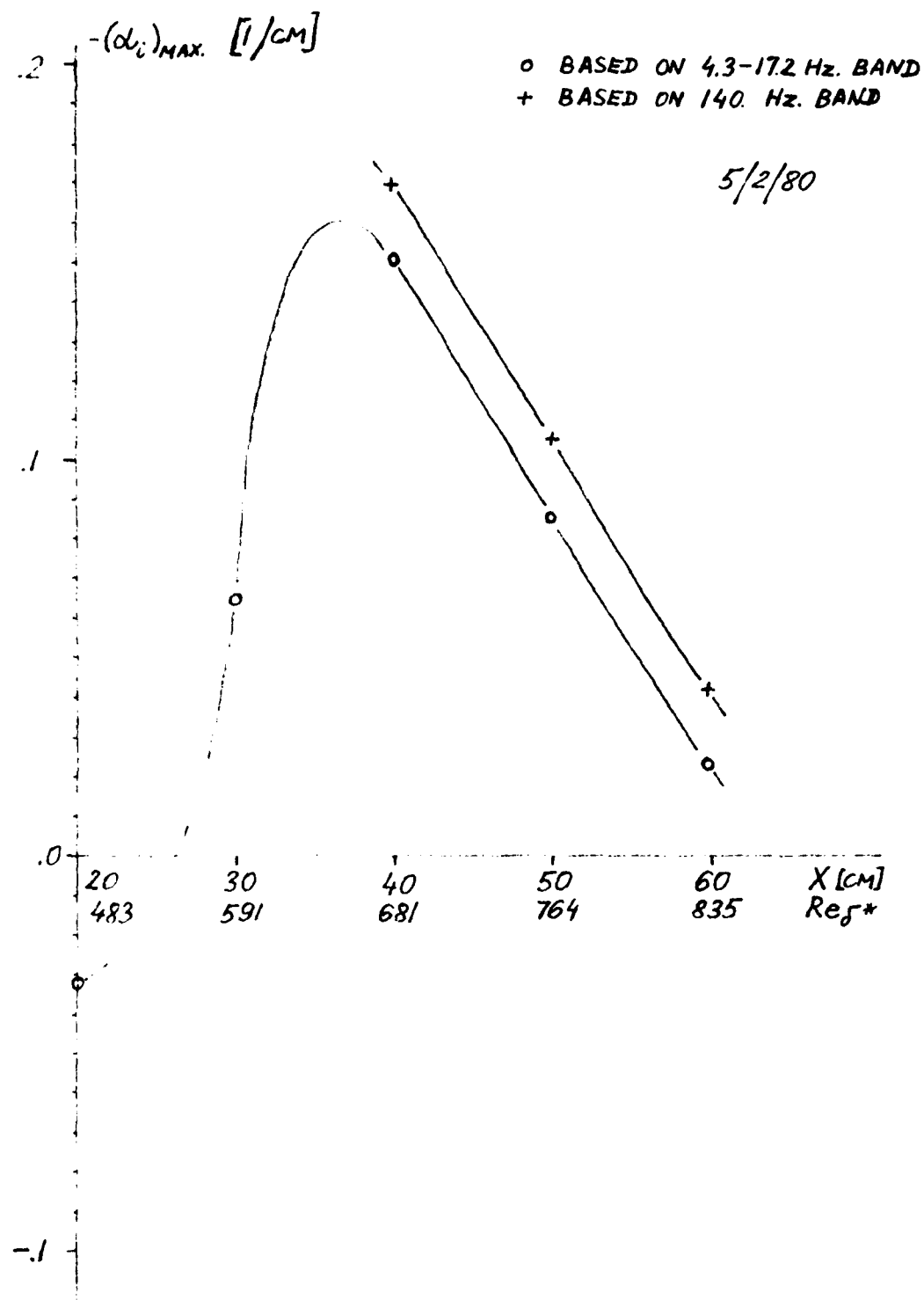


Fig. 43. The highest amplification rate versus X .
 Re_k ($X = 30$ cm) = 155.

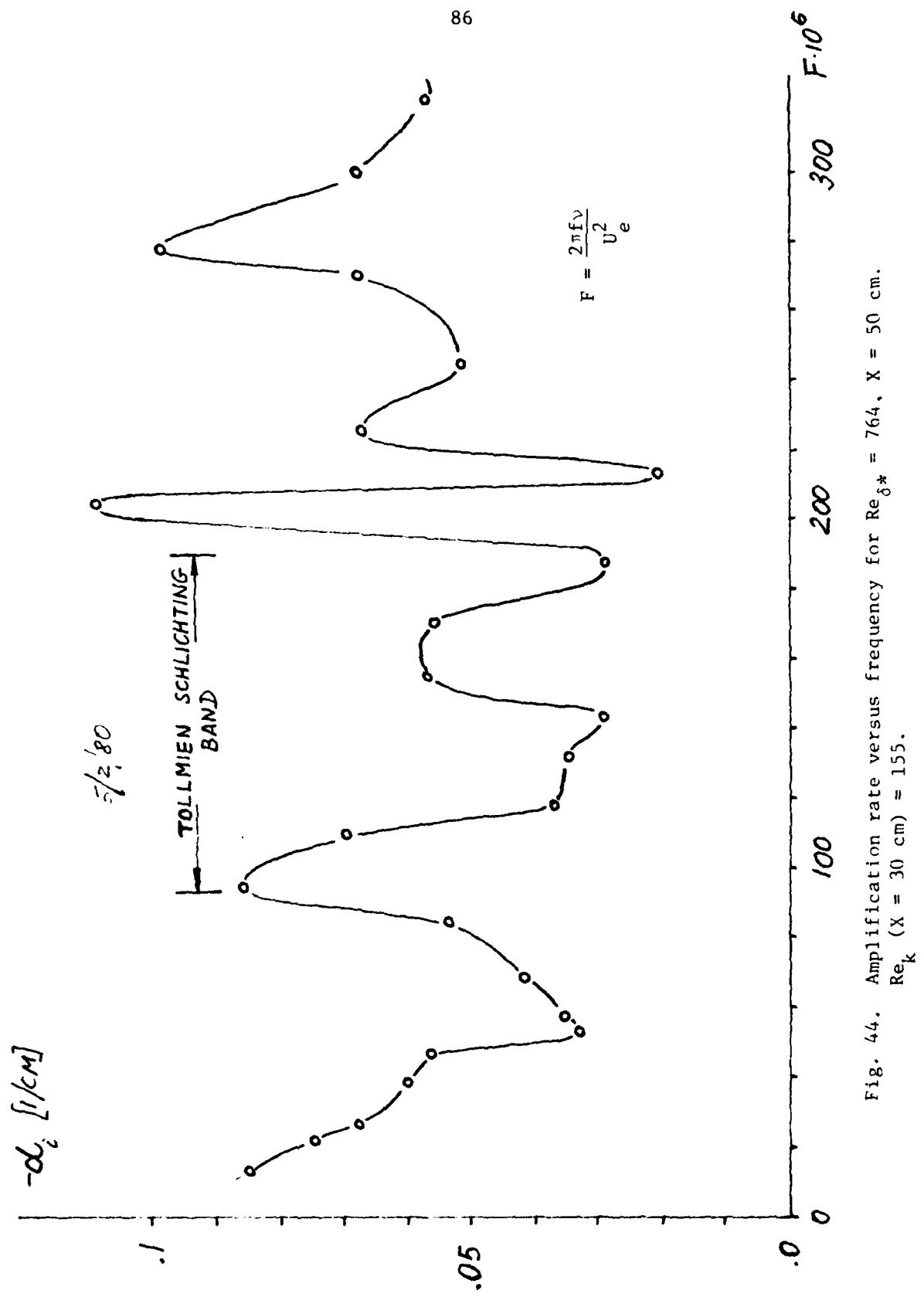


Fig. 44. Amplification rate versus frequency for $\text{Re}_{\delta^*} = 764$, $X = 50 \text{ cm}$.
 Re_k ($X = 30 \text{ cm}$) = 155.

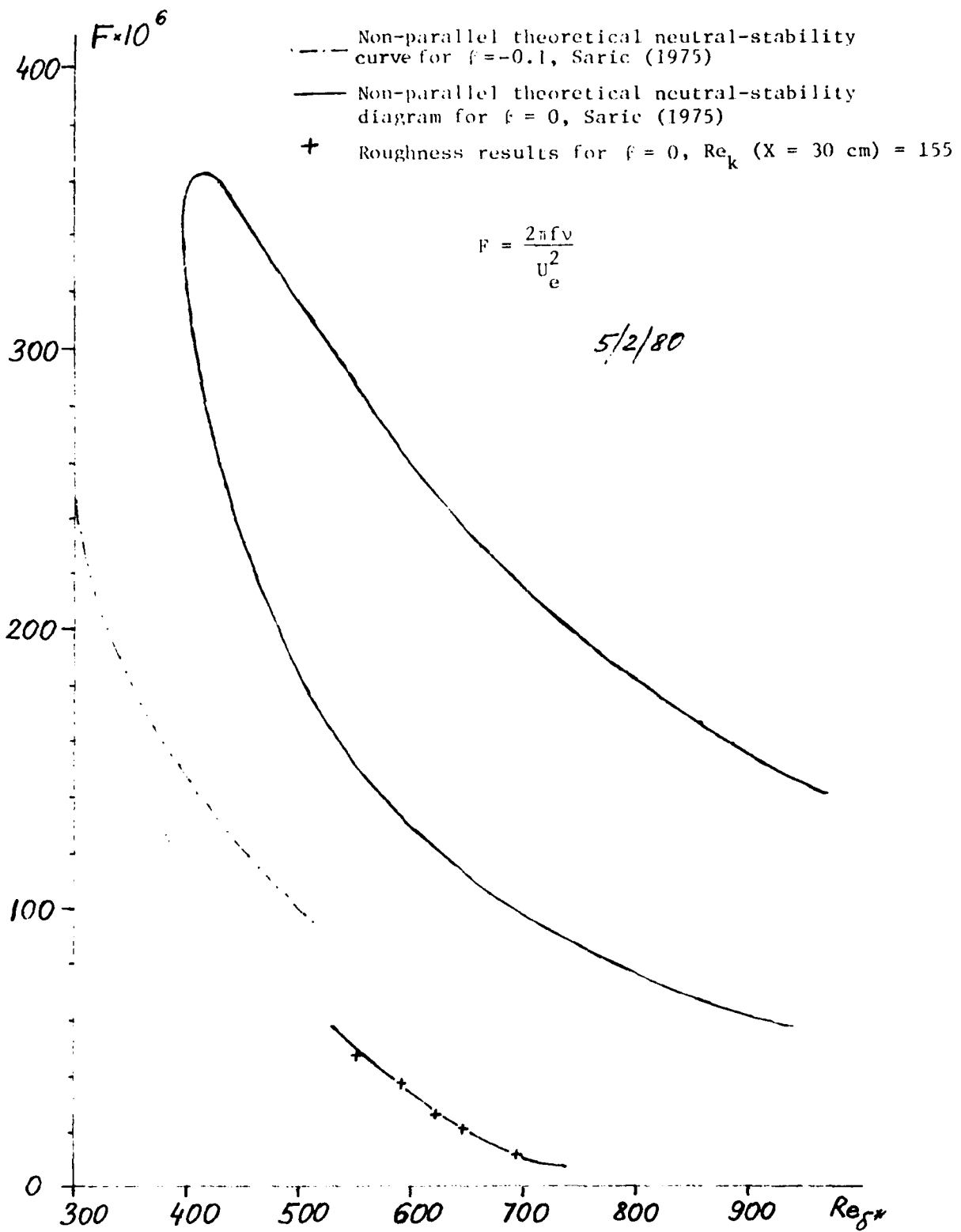
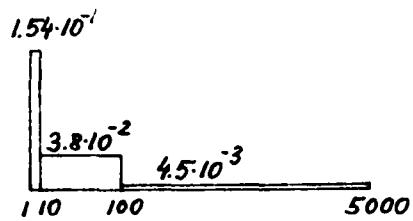
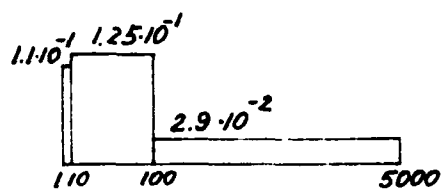


Fig. 45. Neutral stability results.

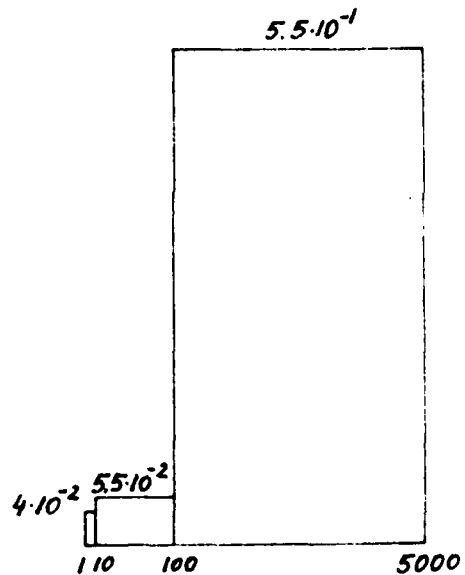
$X = 30 \text{ [cm]}, Re_k = 155$



$X = 40 \text{ [cm]}, Re_k = 136$



$X = 50 \text{ [cm]}, Re_k = 121$



$X = 60 \text{ [cm]}, Re_k = 110$

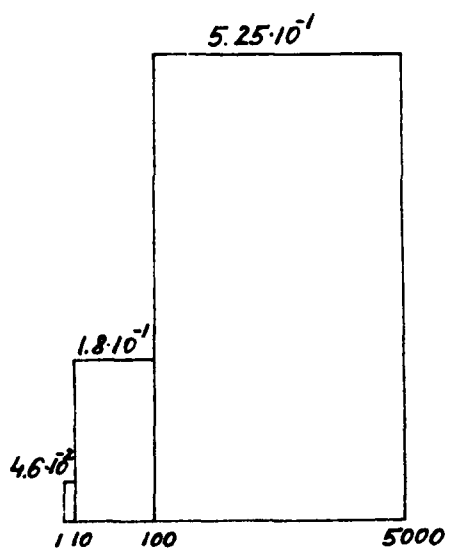


Fig. 46. Energy content for three frequency bands at the location of the maximum total energy, Re_k ($X = 30 \text{ cm}$) = 155.